Experimental and Numerical Investigation of Wire Waveguides for Therapeutic Ultrasound Angioplasty

Declan J. Noone (B.Eng.)

M.Eng.   2008

Experimental and Numerical Investigation of Wire Waveguides for Therapeutic Ultrasound Angioplasty

by

Declan J. Noone (*B.Eng.*)

Thesis presented to Dublin City University in fulfilment of the requirements for the degree of Masters of Engineering

Supervisors: Dr. Garrett B. McGuinness

Dr. Graham P. Gavin

School of Mechanical and Manufacturing Engineering,

Dublin City University,

Ireland

2008

Declaration

I hereby certify that this material, which I now submit for assessment on the programme of study leading to the award of M.Eng. is entirely my own work and has not been taken from the work of others save and to the extent that such work has been cited and acknowledged within the text of my work.

Signed: *Declan Noone*

I.D. No: **99036797**

Date: 04-01-08

Abstract

Title: **Experimental and Numerical Investigation of Wire Waveguides for Therapeutic Ultrasound Angioplasty**

by

Declan J. Noone (B.Eng.)

Therapeutic ultrasound angioplasty is an emerging minimally invasive cardiovascular procedure for disrupting atherosclerotic lesions using small diameter wire waveguides. The lesions are damaged through a combination of direct ablation, pressure waves, cavitation and acoustic streaming caused by distal-tip displacements at ultrasonic frequencies.

Numerical and experimental methods are used to investigate the outputs of the wire waveguides during ultrasonic activation. A commercially available generator and acoustic horn are used in combination with Nickel-Titanium (NiTi) wire waveguides in this study. A laser sensor is used to measure the frequency and amplitude output of the distal tip of the wire waveguide, and this is compared to amplitude estimations obtained using an optical microscope. Power is observed to affect both amplitude and frequency.

Clinical devices will require long, flexible waveguides with diameters small enough to access the coronary arteries. A finite element model is used to design tapered sections in long wire waveguides in order to achieve low profile distal geometry, and improve ultrasonic wave transmission. These tapered sections reduce the wire waveguide diameter in two stages, firstly from 1 to 0.35mm and then from 0.35 to 0.2, while increasing the amplitude of the ultrasonic wave by factors of 2.85 and 1.75, respectively. The numerical model also showed damping could potentially be a significant problem in long untapered wire waveguides (>1.5m).

Experimental ablation trials were conducted using the tapered long wire waveguides, including assessment of the effect of various combinations of bend radii and bend angles. The waveguide was found to perform well, but increased power levels were required to transmit ultrasound through tortuous waveguide configurations.

Acknowledgements

I would like to acknowledge the following people for their support, encouragement and advice during this research:

Table of Contents

List of Figures

List of Tables

IX

X

Nomenclature

u *harmonic displacement amplitude at any point in a uniform rod*

x *the distance of a point in a uniform from the proximal end*

t *time*

l *length of a uniform rod*

c *longitudinal speed of sound in a medium*

f *frequency (Hz)*

f_n *natural frequency*

ρ *density*

d *displacement amplitude*

E *Young's Modulus*

σ *Standard Deviation*

$[K]$ *stiffness matrix*

$[M]$ *mass matrix*

$(\ddot{u})$ *nodal acceleration vector*

$(\dot{\bar{u}})$ *nodal velocity vector*

$(\bar{u})$ *nodal displacement vector*

$(\bar{F}^{a})$ *applied force vector*

[C]   *damping matrix*

B_p *Diameter of the proximal end of the taper*

B_d *Diameter of the distal end of the taper*

I   *Percentage increase in the amplification of tapered section*

R   *Bend radii in single bend tests*

D   *Length from the first bend to the distal tip of the waveguide in single bend tests*

λ *Bend angle in single bend tests*

R_1 *First bend radius in double bend tests*

R_2 *Second bend radius in double bend tests*

D_1 *Length from the first bend to the distal tip of the waveguide in double bend tests*

D_2 *Distance between first and second bend radii in double bend tests*

θ *Bend angle related to R_1*

δ *Bend angle related to R_2*

Note: All displacements used are peak-to-peak displacements unless otherwise stated

List of Abbreviations

CVD   *Cardiovascular Disease*

CHD   *Coronary Heart Disease*

CTO   *Chronic Total Occlusions*

PTCA   *Percutaneous Transluminal Coronary Angioplasty*

NiTi   *Nickel Titanium*

p-p   *Peak to Peak*

FFT   *Fast Fourier Transform*

LVDT   *Linear Variable Differential Transformer*

KS/s   *Kilo Samples per second*

mm   *millimetres*

nm   *nanometres*

μm   *micrometres*

V   *Volts*

Chapter 1

Introduction

1.1 Cardiovascular Disease

Cardiovascular disease (CVD) is the leading cause of death in the western world, accounting for over 4 million deaths in Europe, which represents approximately 49% of all deaths [1]. It is estimated that approximately 16.7 million people die globally each year of CVD and it is predicted that this will rise to 25 million by 2020 [2]. The main forms of CVD are stroke and coronary heart disease (CHD). Over half of all deaths (53%) from CVD can be attributed to CHD [3]. Approximately 460,000 people in the US and 744,000 people in Europe died from coronary heart disease in 2004. The American Heart Association estimates that the cost of cardiovascular diseases to the American economy, in 2005, was approximately $393 billion including hospital, procedure and nursing costs. This is a significant economic impact for CVD on the American Healthcare system [4].

In 2003, 39% of deaths were related to cardiovascular disease in Ireland and of this coronary heart disease accounted for 20% of all those. For the under 65 years age group, 24% of all deaths in Ireland were as a result of CVD. This is one of the highest averages per population in the EU [5]. However, over the last few years in Ireland and globally deaths related to CVD have fallen significantly due to earlier diagnosis from diagnostic equipment, more interventional procedures being carried out and higher success rates.

Coronary heart disease is the narrowing or blocking of the coronary arteries, which results in a reduction of blood flow to the heart muscle. Atherosclerosis is defined as the development of blockages due to the presence of plaque. This is a gradual process starting with thickening of the arterial walls resulting in reduced

blood flow and possible rapid total occlusion due to clotting, known as thromboembolism [6]

1.2 Mechanically Based Minimally Invasive Interventional Procedures

The main aim of interventional procedures is to restore normal blood flow in the lumen of arteries that have full or partial blockages due to lesions. To re-canalise the lumen of these vessels, the blockage must be de-bulked, removed or, in the case of severe blockages, by-passed. By-pass surgery, the original solution for the treatment of lesions, is now only used in extreme cases. By-pass surgery is a fully invasive procedure, which is extremely severe on the patient. This involves a long recovery period and also requires a skilled surgeon to graft a vessel to either side of the lesion. However, with advances in the field of medicine, the necessity for by-pass surgery is reduced as diseases of the blood vessels can be detected earlier and can be dealt with by using minimally invasive treatments.

Minimally invasive mechanically based interventions concentrate on removing or de-bulking the lesion or blockage. Examples of these are balloon angioplasty, stenting, and rotational and directional atherectomy. These types of procedures have shorter recovery times and they also reduce the actual operating time, increasing the number of procedures that can be performed. Most of these devices have a similar surgical method. The device is inserted into an artery either in the upper leg close to the inner thigh or the upper forearm, which allows direct access to the Aorta and coronary arteries. A hollow tube, or catheter, is then manipulated to the location of the blockage, which acts as a conduit for the main device. Generally, these devices aim to reduce the blockage in the arterial lumen by loading and permanently deforming the plaque.

With the use of intervention methods such as coronary artery bypass, balloon angioplasty, stenting and atherectomy the death rates from 1992-2003 have fallen by 9.9% [3]. The three main complications of these procedures are

2

(a) Abrupt closure.

(b) Restenosis, which is a re-closing of the lumen believed to be related to the stretching of healthy and diseased arterial tissue and remodelling.

(c) Chronic total occlusions (CTO's), which are lesions that completely, block the arteries.

It has been shown that "abrupt closure typically results from thrombotic occlusion, obstruction by intimal or medial flaps or medial recoil". [7]. This will generally occur within the first few hours after the procedure. Damage to the arterial walls and denudation of the endothelial cells appears to be the main initiator of restenosis. This will generally occur within the first few months after the procedure. Restenosis rates for balloon angioplasty procedures alone can be as high as 60% after six months whereas for stented vessels restenosis is usually between 20-30% for a similar time period [8].

There are two main problems with these procedures. Firstly, the lesion must be capable of being crossed by a guidewire. This acts as a guiderail to direct the device into place. If the lesion cannot be crossed due to total occlusion success levels of the procedure are greatly reduced [9]. Secondly, the mechanical properties of lesions vary widely. A number of investigators have reported mechanical properties of plaque ranging from soft distensible material to a rigid plaque [10, 11]. The more rigid lesions, also known as calcified plaques, have a greater resistance to deformation from balloon pressure or stenting.

Finally, all of the above procedures have one major drawback, whether they are based on removal or deformation of the lesion. This is their inability to distinguish between healthy and diseased tissue. A device that could distinguish between the two and break up only rigid calcified plaque could increase success rates, reduce the damage to healthy tissue and reduce restenosis.

1.3 Therapeutic Ultrasound Angioplasty

Therapeutic ultrasound using low frequencies (in the 20-50 kHz range) has been used for a number of applications such as surgical instruments [12] and dentistry devices. This type of ultrasound is useful because of its physical and

3

chemical effects. Using focused ultrasound at higher frequencies it has been shown that the cellular effect of ultrasound is essentially non-thermal and that very little damage is produced during operations [13 cited in Parsons *et al* 12].

Work has been reported on high-power, low frequency ultrasound in removing, ablating or cracking these lesions during minimally invasive vascular surgery [14]. These ultrasound devices generally consist of an external ultrasound transducer, powered by an ultrasonic generator, delivering power to an acoustic horn and, via a wire waveguide with a ball tip, to the distal end of a catheter inserted into an artery. The operating principle of these types of device is based on the fact that ultrasound at the correct frequency and amplitude can disrupt inelastic rigid tissue while distensible healthy elastic tissue in the locality will remain largely unaffected [14,15].

A review of current literature has shown that this form of ultrasonic energy can be delivered via small diameter (<1mm) wire waveguides [16]. This has been used to disrupt thrombus and rigid plaques, *in vitro* and *in vivo* [17, 18].

1.4 Research Objectives and Methodology

A literature review examining arterial and lesion properties in cardiovascular disease is presented in Chapter 2 and the effect of using therapeutic ultrasound as a treatment for these is also reviewed. The operational settings and effect of this type of device on surrounding tissue and fluid published by other authors is also presented.

The first objective of this research is to fully characterise the output of a prototype waveguide apparatus. A fibre-optic laser sensor is used to measure these amplitudes and frequencies in the 0-100μm and 0-200 kHz ranges. Following this, a series of experiments will be performed to investigate the effect of power settings on the wire waveguide output.

The second objective of this research is to construct and demonstrate an ultrasound wire waveguide with characteristics suitable for minimally invasive procedures. The lengths required must be sufficient to traverse the arteries to reach the point of any blockage. The wire waveguide should also have small wire

4

waveguide diameter to allow access to coronary arteries, possibly in conjunction with other devices. A method for using numerical modelling to design tapered wire waveguides is presented. An overview of the layout of this research project is given in Figure 1.1

```
┌─────────────────────────────────────┐
│            Chapter 2:               │
│         Literature Survey           │
└─────────────────────────────────────┘
                  │
                  ▼
┌─────────────────────────────────────┐
│            Chapter 3:               │
│    Characterisation of wire waveguide│
│              output                 │
└─────────────────────────────────────┘
                  │
                  ▼
┌─────────────────────────────────────┐
│            Chapter 4:               │
│    Tapered wire analysis and design │
│            methodology              │
└─────────────────────────────────────┘
                  │
                  ▼
┌─────────────────────────────────────┐
│            Chapter 5:               │
│    Experimental measurements and    │
│           demonstrations            │
└─────────────────────────────────────┘
                  │
                  ▼
┌─────────────────────────────────────┐
│            Chapter 6:               │
│    Conclusions and Recommendations  │
└─────────────────────────────────────┘
```
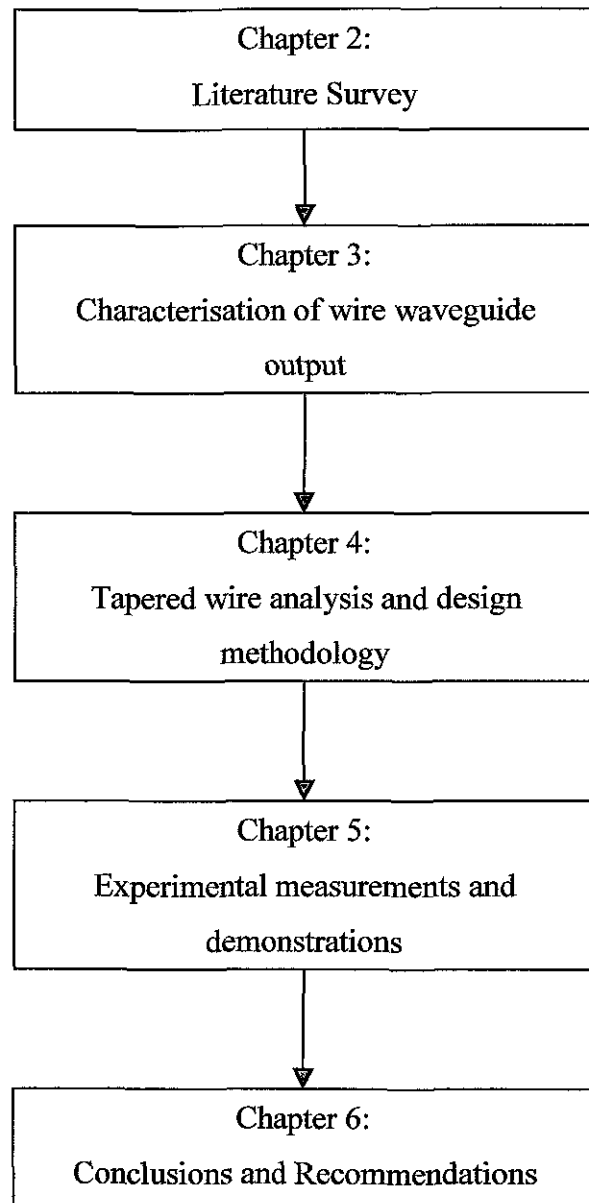
Figure 1.1: Layout and progression of research

Chapter 2

Literature Survey

2.1 The Cardiovascular System

In order to establish the design requirements for an ultrasound wire waveguide capable of accessing the coronary arteries in a minimally invasive procedure, an understanding of the cardiovascular system is necessary. A healthy artery is a complex structure with a number of different functions, depending on location within the vascular tree. It is important to understand the composition and functions of the artery. Arteries have two main functions:

1) Delivery of oxygen-enriched blood to both themselves and all the tissues and organs of the body.

2) Control of pressure and velocity of the blood in the system, which allows a steady

flow of blood to the organs and tissues of the body.

Blood is pumped from the left ventricle of the heart in to the Aorta which branches repeatedly to form progressively smaller arteries. This forms the arterial tree, and is shown in Figure 2.1. As the arteries become smaller, there is a gradual transition in the elastic tissue and smooth muscle content. There are usually considered to be two main types of arteries: elastic arteries or muscular arteries.

Elastic arteries are the largest diameter arteries and have the thickest walls. A greater proportion of their walls are composed of elastic tissue, which gives them greater compliance than muscular arteries. Elastic arteries are stretched when the heart pumps blood into them. The elastic recoil of the elastic arteries prevents blood pressure from falling rapidly and maintains blood flow while the ventricles are relaxed [19]. Elastic arteries are more commonly found in locations close to the heart, e.g. Aorta, pulmonary, common carotids and iliac arteries

6
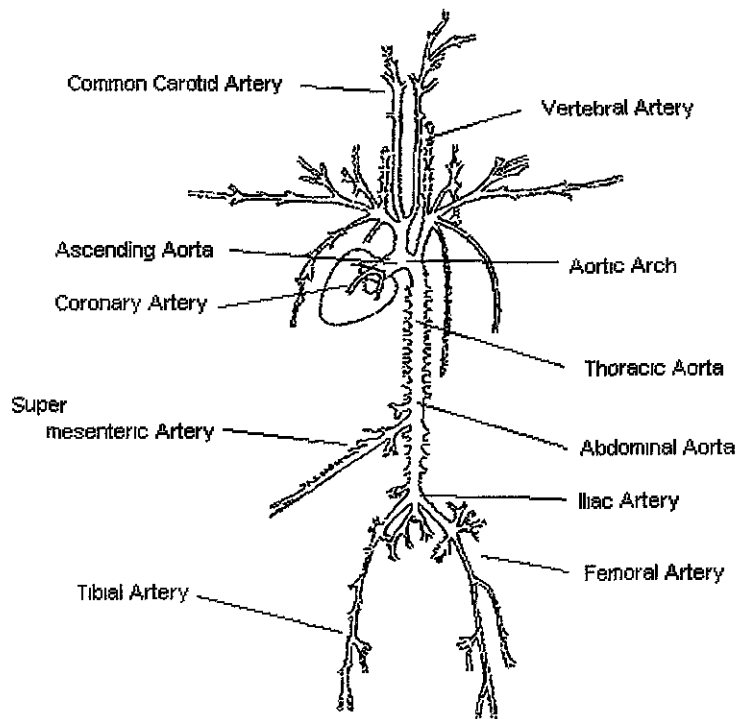
Figure 2.1: Systemic Arterial Tree [20]

Muscular arteries are relatively thick in comparison to their lumen diameter and most of this thickness is composed of smooth muscle. Muscular arteries include femoral, renal, coronary and cerebral arteries.

A healthy artery is composed of three main layers, the intima, the media and the adventia shown in Figure 2.2. Each of these layers is made up of the following components: endothelial lining, collagen fibres, elastin fibres, smooth muscle cells and ground substances [20]. Depending on the location of the arteries relative to the heart, the proportions of each of these components vary, which affects the mechanical properties of the vessels and hence specifies the functionality of each vessel, including its reaction to stimuli such as pressure.

For example, the amount of collagen to elastin increases the further the arteries are located from the heart. Although collagen and elastin are composed of similar proteins their mechanical properties are very different. Collagen is much stronger and stiffer than elastin. More collagen will be found in muscular arteries. Smooth muscle

7

cells have the ability to relax and contract and hence act as another means of controlling blood flow in the vessel.
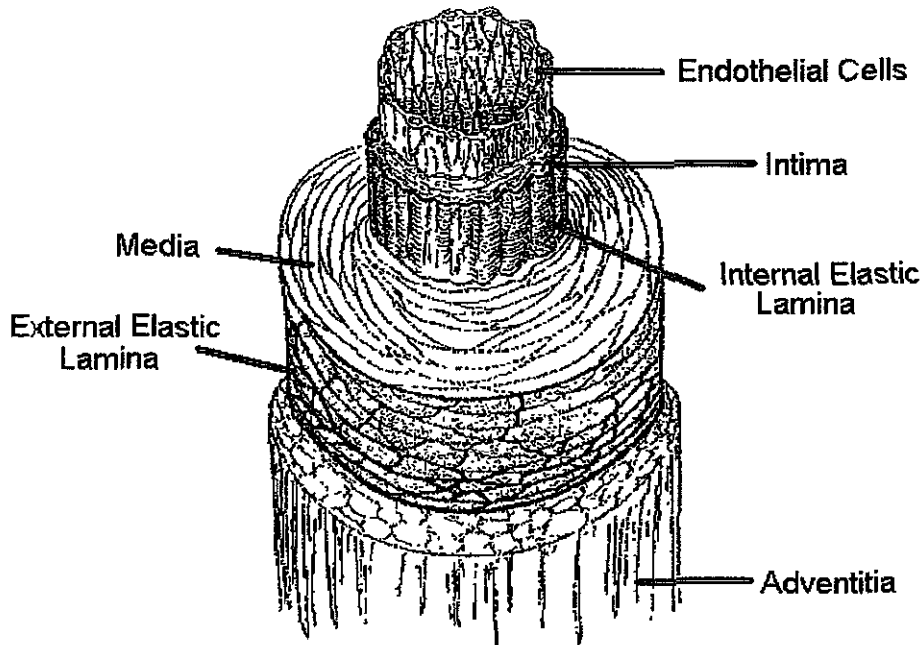
Figure 2.2: Model showing the major components of a healthy arterial wall [20]

2.2 Biomechanics of Vascular Disease

Atherosclerosis is a pathological condition that is an underlying cause of several important disorders including coronary artery disease, cerebrovascular disease and diseases of the Aorta and peripheral arterial circulation.

There are number of different hypotheses related to the incidence of atherosclerosis, such as the inflammatory hypothesis, the lipid hypothesis and the response to injury hypothesis. In general, atherosclerotic lesions are localised in the intima of the artery wall. In more advanced forms, these consist of fibrous caps and a combination of macrophages, lipids and smooth muscle cells. These can also become heavily calcified.
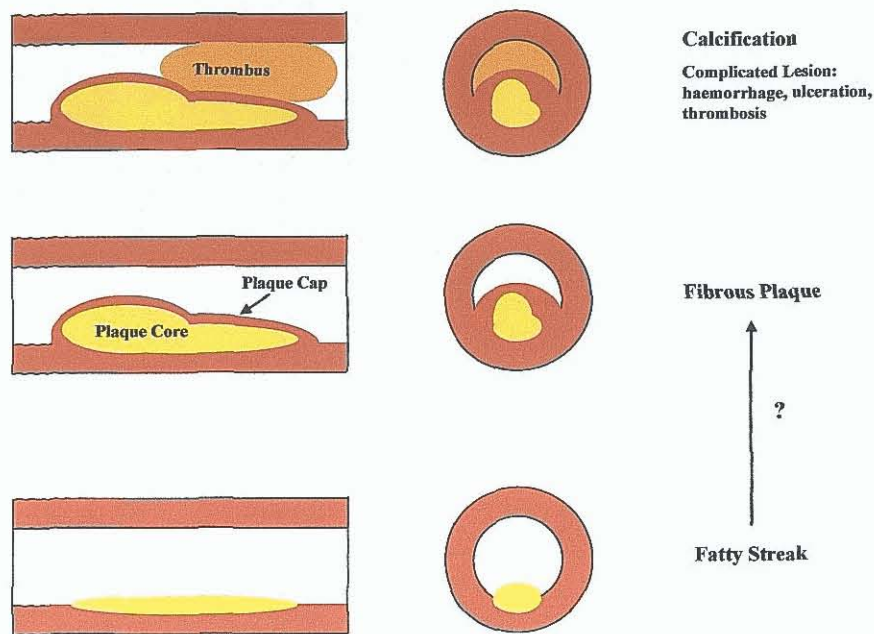
Figure 2.3: Natural history of atherosclerosis

The lesions vary from a fatty streak to advanced complicated lesions. The progression from one to the next is split into phases with specific morphologic characteristics. This is based on a classification study by Stary [21], shown in Figure 2.3, for the American Heart Foundation.

According to observations by Oh *et al* [22] the shapes of lesions can be divided into the following three categories.

1. Concentric and Circular
2. Eccentric and Circular
3. Eccentric and Non-Circular

When these shapes of lesions are combined with already complicated lesions, they will cause a larger set of problems for mechanical based intervention and procedures.

2.2.1 Percutaneous Transluminal Balloon Angioplasty

Balloon angioplasty or percutaneous transluminal coronary angioplasty (PTCA) was first performed in the late 1970s. The procedure matured rapidly and became the most widely accepted and used procedure. Its popularity stems from its high primary

9

success rate and low morbidity rates. The basic principle of the procedure is that a small balloon is moved across the lesion and inflated, applying a load to lesion walls and deforming it permanently, and hence increasing the diameter of the lumen of the artery and returning the blood flow closer to normal parameters [23]. In 2001, an estimated 571,000 balloon angioplasty procedures were performed in the United States, representing an increase of 266% since 1987 [4].

2.2.2 Cardiovascular Stents

Stenting is also a procedure that was developed as a result of balloon angioplasty. During balloon angioplasty when the balloon is deflated there can be some recoil, depending on the structure of the lesion. To reduce this, a wire mesh scaffold, known as a stent, is placed around the balloon and is deployed as the balloon is inflated. The balloon is then removed, with the stent remaining to reduce lesion recoil [24]. Other procedures such as rotational and directional atherectomy are based on removal rather than deformation of lesions. With the use of intervention methods such as coronary artery by-pass, balloon angioplasty, stenting and atherectomy, the death rates from 1992-2003 have fallen by 9.9% [3]

2.2.3 Chronic Total Occlusions

A major problem with mechanically based minimally invasive procedures is that it may be extremely difficult, if not impossible, to cross the lesion to reopen the blockage. These cases are known as chronic total occlusions (CTO's) and are caused by advanced plaques, haemorrhaging and thrombosis and result in total closure of the vessel. They can be found in small arteries such as those in the coronary artery tree. CTO's can account for 20% of angioplasty procedures [16]. Due to the difficulty in dealing with CTO's a number of patients with these types of lesions are referred to by-pass surgery. Success rates in CTO's have steadily increased over the last 15 years because of greater operator experience, improvements in equipment, and procedural techniques. However, minimally invasive procedures on these types of lesions are the most likely to fail. The majority of failures are due to the inability to successfully pass a guidewire across the lesion (89%) [16].

The content of calcification is a significant factor when examining the plaque cap or core. The increased presence of calcium in the plaque requires increased balloon pressure during the procedure, resulting in greater localised damage and higher restenosis rates [25].

These procedures work best with concentric lesions as the pressure is divided relatively evenly over the lesion. However, dilation of eccentric lesions can be problematic because the lesions are located to one side of the vessel. This results in overstretched less diseased walls, increased risk of necrosis of cells and tearing and increasing the risk of restenosis. These complications seriously affect the success rates of these interventional procedures.

2.2.4 Current Guidewire Technology

There are currently a number of different guidewires from different companies shown in Table 2.1, on the market, having various successes with crossing CTO's [26]. The majority of these have a main shaft diameter of 0.35mm or less. The tips vary from 0.2-0.35mm in diameter depending on the guidewire. Guidewires are also classified as soft, intermediate or stiff. Soft wires are normal used for advancement of the catheter and crossing occlusions with small lumens. Intermediate wires are used for recently occluded lesions or tortuous vessels and stiff wires are used for advancing through CTO's. The suggested method [26] used for crossing CTO's is to use a soft or intermediate wire to explore the area. A stiffer guidewire is then used to cross the proximal cap if needed. A stiffer wire can again be used, if necessary to cross the CTO and penetrate the distal cap. After the occlusion has been crossed the stiff guidewire is then replaced by a soft guidewire.

Research from Lefevre [27] found that, during a procedure involving CTO's it might take up to 35mins to cross the lesion and with the possibility of changing guidewires a total procedure time may take 1.5 hours. This has implications for the cost of the procedure and with success of crossover at between 26.2% and 58.7% for different guidewires, a new approach may be needed. A soft guidewire with the capability of crossing CTO's would be a major advantage in a procedure similar this reducing the need

11

for changing wires, reduce the time duration required for crossing a CTO and increasing the likelihood of success for the procedure.

Ideally a device would be capable of navigating vascular vessels, specifically target diseased tissue and reopening blockages while causing little damage to the surrounding structures. Therapeutic ultrasound transmitted via a wire waveguide appears to have the potential to disrupt these types of lesions by minimally invasive means.

Manufacturer	Wire	Shaft Diameter (mm)
Guidant	Whisper	0.35
	Pilot 50	0.35
	Pilot 150 & 200	0.35
	HT Intermediate	0.35
	HT Standard	0.35
	Cross-IT 100-400	0.35
Boston Scientific	Choice PT & PT2	0.35
	PT Graphix & P2	0.35
Cordis	Shinobi & Shinobi Plus	0.35
Medtronic Vascular	Persuader	0.35
	Persuader 9	0.35 (tip diameter 0.27)
Abbott Vascular Asahi	Confianza	0.35
	Confianza Pro (Conquest)	0.35 (tip diameter 0.22)
	Medium	0.35
	Miraclebros	0.35

Table 2.1: Variety of guidewires with shaft and tip diameters [26]

2.2.5 Intravascular Sonotherapy

Intravascular Sonotherapy is a prophylactic and therapeutic application of ultrasound, transmitted down a long wire waveguide. This type of procedure is a non-ablative, non-thermal form of therapeutic ultrasound with the aim of reduction of intimal hyperplasia after stent implantation. The hypothesis is that the acoustic cavitation

12

minimizes the release of specific chemical mediators in the adventitia [28]. The ultrasound delivered has an operating frequency currently between 0.7 -1.4 MHz. Once the stent is in place and expanded, the sonotherapy catheter is moved into place and ultrasound energy is emitted. The catheter is then moved slightly and ultrasound emission is repeated so the entire area of the stented lesion is covered.

Fitzgerald et al. [28] performed 48 *in vivo* balloon angioplasties on pig arteries. An over-sized balloon was deployed causing intimal damage and then a stent was implanted. An 8F over-the-wire catheter was used to deliver the ultrasound probe with a frequency of 700 kHz to the area. 28 of the stent implantations were treated with intravascular ultrasound and the rest were used as a control. The stented regions were assessed after 28 days and the results showed that there was an 8% reduction in stenosis and a 35% reduction in intimal thickening. However the assessment of the effect of the sonotherapy was carried out at 28 days so there is a possibility that the restenotic process is merely delayed.

One clinical study [29] with 93 patients received intravascular sonotherapy with stent implantation for de novo coronary stenosis. Baseline lesion characteristics were similar to temporary coronary stenting trials. Before the procedure the vessels were occluded by 70.3%± 14.9%. Immediately after the procedure this was reduced to 16.1%±12.6%. The vessels were checked with angiography after 6 months and these results showed the level of stenosis in stents treated with sonotherapy was 37.6%±19.5% in comparison to the untreated stent implantations, which was 35.3%± 21.3%. This result shows sonotherapy has very little effect on lumen diameter but the study suggests that using sonotherapy is still more favourable than restenosis without use of sonotherapy. A second study [30] had a sample of 403 patients. The results showed that treatment with sonotherapy after stenting reduced the re-intervention rate by 40% at seven months when compared to stenting alone. The re-intervention rate using sonotherapy was 10.4%, versus 17.4% in stenting alone. This reduced rate of re-intervention resulted in a 27% reduction in major cardiac events. Major cardiac event rate for the sonotherapy was 18.8%, versus 25.9% in stenting alone. It should be noted that these are preliminary results and a single company publishes all data on the sonotherapy device.

2.3 High Power, Low Frequency Therapeutic Ultrasound

Ultrasound has been used in medicine for years, both for diagnostics and as a therapy for various conditions. Therapeutic ultrasound usually involves the use of high-intensity, low frequency ultrasound [31].

The mechanical effect that ultrasound has on biological tissues was first noted in the 1940s [citied in 32]. Using the right combination of frequency and amplitude, the ultrasound vigorously disrupts inelastic tissue while healthy tissue in the same region remains undamaged [17]. It was conceived that this form of energy may be useful in disrupting cardiovascular lesions especially rigid calcified and fibrous plaques and would have advantages over standard procedures such as angioplasty or atherectomy.

Development and testing of experimental devices for the delivery of ultrasound was first attempted in the early 1970s by Sobbe and Trubenistein [33] as a means of concentrating ultrasound to the vasculature as a method of aiding drug delivery.

During the mid-1980s, two groups headed by Siegel and by Rosenschein respectively pursued the objective of producing an actual working prototype for initial clinical testing and use in trials. Both teams based their design efforts on the system developed by Sobbe *et al* [33] delivering the ultrasonic waves to the lesion via a wire waveguide. This sets up longitudinal stress waves and a longitudinal peak-to-peak displacement at the distal-tip of the wire waveguide with the potential to disrupt both lesions and clots.

2.3.1 Ultrasound Generation

In order to displace the distal-tip of a wire at the frequencies and high amplitude displacements required to cause disruption to lesions, a source capable of delivering these ultrasonic displacements was required. Both Siegel *et al* [15] and Rosenschein *et al* [14] describe the use of a piezoelectric transducer as a source for the ultrasound.

The piezoelectric effect is a property of certain classes of crystalline materials including natural crystals of quartz, rochelle salt and Tourmaline plus manufactured ceramics such as Barium Titanate and lead zirconate titanates (PZT). When a mechanical pressure is applied to these materials a voltage is produced proportional to the pressure

14

applied. Conversely, when a voltage is applied the structure changes shape; acting as an electromechanical transducer. These shape changes are usually very small, in the order of a few microns, and the voltage amplitudes required to produce them are large, of the order of 1000V [34].

Dynamic voltages can also be applied which result in a dynamic displacement or shape change in the material. In this arrangement the material behaves very similar to a mechanical system with resonant frequency characteristics. By placing these crystals in a stack arrangement, small mechanical displacements of 0–5μm peak-to-peak at frequencies up to 100 kHz can be achieved. An ultrasonic generator provides the electrical source to drive the transducer at the resonant frequency of the piezoelectric stack. These types of transducer are used for sonochemistry applications where agitation of chemical and biological samples is required. The frequencies and amplitudes discussed are chosen for their ability to cause cavitation, a desirable effect in processing chemical solutions. Prototype therapeutic ultrasound devices have been developed using the same transducers [35].

The displacements achieved from the transducers are still relatively small and too low for the intended application use, and therefore need to be amplified. This amplification is performed via an acoustic horn or a waveguide, which is attached to the end of the transducer.

Horns come in three main shapes, shown in Figure 2.4 below, but they are all based on the same principles. They are solid metal rods manufactured from materials with high dynamic fatigue, high strength and low acoustic loss properties, such as titanium alloys [35]. The amplification of displacement outputs from these materials is achieved by two methods. First, the surface area of the horn reduces from the output face of the transducer to the horn output face. This reduction in surface area compresses the input wave resulting in a larger displacement at the output. Secondly, horns can be manufactured to resonate at the frequency of the ultrasonic converter and are generally designed to be exactly half the wavelength of the frequency. With a horn attached to the converter output displacements greater than 150μm peak-to-peak can be achieved and at frequencies less than 100 kHz [35].

15
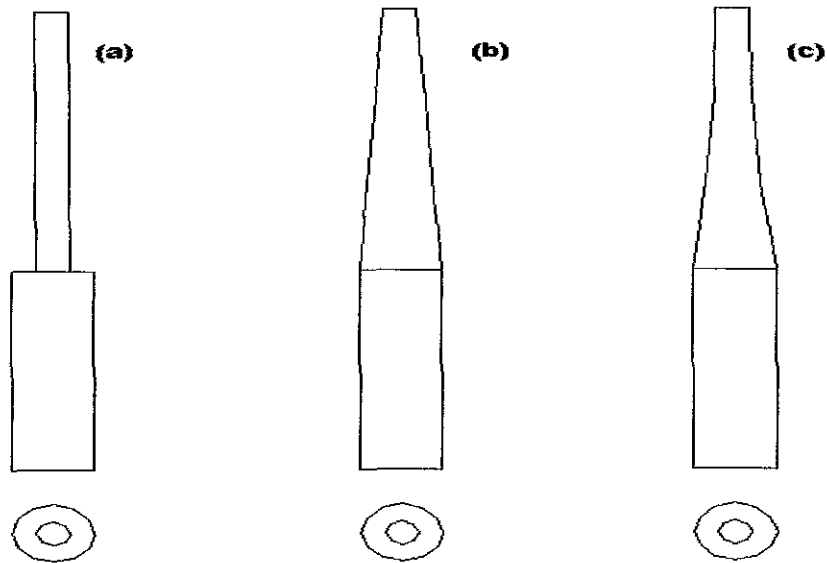
Figure 2.4: Main types of acoustic horns: (a) stepped, (b) tapered and (c) exponential horns

An acoustic horn is of great benefit in increasing the output displacement from the transducer. However due to its inflexibility, it is not possible to use them to traverse the tortuous vascular geometry. So another method of delivering the ultrasonic wave is necessary. Using ideas from minimally invasive surgery, wire waveguides were developed allowing sufficient length, size and flexibility to manoeuvre through the vascular system in order to deliver the ultrasonic displacements [6, 14].

2.3.2 Ultrasound Delivery

Current guidewires for minimally invasive surgeries range from 1.4-1.9m in length. They are very flexible and can be guided into coronary arteries with diameters less than 1mm using guidewires with diameters less than 0.4mm. If therapeutic ultrasound is to be used for intravascular minimally invasive surgery using wire waveguides, it is necessary to establish ultrasonic peak-to-peak longitudinal displacements over lengths up to 1.9m and diameters as low as 0.4mm based on the anatomy of the coronary arteries and the cardiovascular system. While the delivery of ultrasonic waves using wire waveguides is reported in the literature there is little published data on the design or construction of these waveguides.

16

Fischell *et al* describe the use of a solid 1.5F (≈ 0.5 mm diameter) titanium wire waveguide [36]. Others have also used titanium wires [6, 15]. Rosenschein *et al* [14] described a flexible aluminium wire mechanically attached to the acoustic horn to transmit the ultrasound wave. The use of enlarged tips by placing a ball-tip on the end to increase the area of contact between the wire and the lesion has also been described. Demer *et al* [37] describes the use of a 2.0 mm diameter ball-tip and Siegel *et al* [15] a 1.7 mm diameter ball-tip in conjunction with the wire waveguide.

2.3.3 Localized Effects at Wire Waveguide Tip due to Displacement

Four disruptive mechanisms have been observed, (i) direct contact ablation, (ii) acoustic pressure waves, (iii) cavitation and (iv) acoustic streaming. All these appear to be generated as a result of distal-tip displacement amplitude, frequency and geometry [38, 39, 40, 41].

Direct Contact Ablation

As the waveguides oscillating tip moves towards the lesion, it comes into direct contact with it. It has been observed that this results in fragmentation and ablation of the plaque [39].

Acoustic Pressure Waves and Cavitation

As a result of the direct contact between the oscillating distal-tip and a surrounding fluid, an oscillating acoustic pressure field is established around the distal-tip [39, 42]. If the pressure amplitudes are sufficiently high, cavitation may occur. Cavitation occurs, on the negative side of a pressure cycle, such as when the wire waveguide tip is retracting. Suspended gas bubbles in the fluid, in channels within the tissue or trapped at solid interfaces, expand and collapse. Cavitation has a potentially significant erosion effect, which may be undesirable in most acoustic applications but may contribute to the disruption of plaques and thrombi.

Acoustic Streaming

Around the tip there are two distinct regions of flow. A very narrow boundary region forms around the surface of the tip, which is an oscillatory fluid motion. The second is a region of unidirectional fluid motion as shown in Figure 2.5 [39, 40].
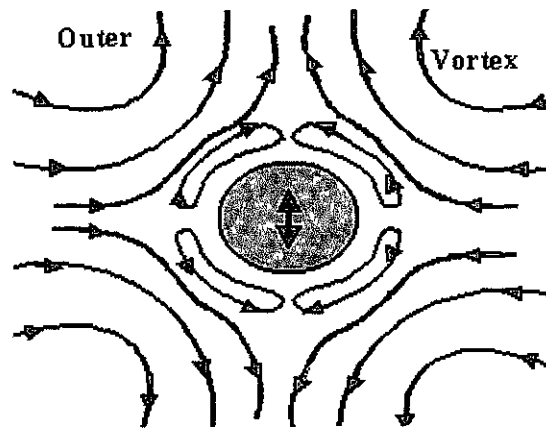
Figure 2.5 General features of acoustic microstreaming near a small vibrating sphere from Nyborg [39]

It is the combination of all of these disruptive mechanisms that led investigators to believe that delivering ultrasound via a wire waveguide could affect arterial lesions. All of these mechanisms are dependent on amplitudes and frequencies of the ultrasonic waves.

2.4 Testing of Ultrasound Delivered via Wire Waveguide

The literature concerning the use of therapeutic ultrasound delivered via wire waveguides can be divided into; (i) mechanical performance characteristics and (ii) pre-clinical and clinical studies.

2.4.1 Mechanical Performance

Ariani *et al* [6] describe the use of a 20 kHz converter delivering pulsed energy (50% duty cycle) to a 0.76 mm titanium wire waveguide with a 2.0 mm ball-tip and a length of 89 cm. Using this system for various acoustic horn distal-tip power inputs (8 − 25 Watts), the wire waveguide distal-tip displacements outputs were measured between 63.5 µm and 111 µm.

18

Makin and Everbach [42] reported experimental measurement of the acoustic pressure field in the region surrounding the distal-tip as a result of ultrasonic displacements at a frequency of 22.5 kHz. They used two different lengths of waveguide (445mm with a 1.98mm ball tip and 660mm with a 2.46mm ball tip). The authors showed that as the distance from the tip is increased, a decrease in pressure amplitudes is observed. However the authors were unable to acquire measurements at distances less than 12mm from the tip but suggested that the pressure inside this region was sufficiently high to achieve the cavitation that was observed.

Various authors describe therapeutic ultrasound waveguide performance over a wide range of powers, (0.7-50 Watts) [e.g.15]. Rosenschein *et al* [14] noted that a cavitation field was only observed above a certain threshold, and that below this threshold cavitation does not occur due to insufficient acoustic pressures. The amplitude threshold was reached at approximately 8 Watts [14].

Cimino and Bond [43, 44] used three devices with frequencies of 12, 23, and 36kHz, producing displacements between 25 and 165µm. Each device featured a hollow cylinder probe and was operated in conjunction with adjustable suction. Each device was then tested on porcine Aorta, kidney, liver, heart and brain. Results from their work have shown that the higher strength tissues, such as the Aorta, show more resistance to fragmentation. They also noted that it is the acceleration of the tip that is primarily responsible for the fragmentation rather than the velocity at the tip, or density or water percentage of the tissue.

2.4.2 Pre-clinical and Clinical Evaluation

Ariani *et al* [6] used an ultrasound waveguide to disrupt human thrombus *in vitro* and *in vivo*. This study showed an inverse relationship between acoustic horn distal-tip power and the time to dissolve the clots; higher powers and hence higher peak-to-peak tip displacements required shorter times to disrupt clots. Rosenschein also reported similar findings [14].

Siegel *et al* [17] carried out procedures on 50 lesions in 45 patients, 17 of which were classified as calcified. The system used was run at a frequency of 19.5 kHz with a

waveguide length of 145cm and 0.76mm diameter wire tapering to 0.25mm. No further details of the waveguide and taper design are provided. Using this system, the lumen of the arteries affected by lesions were recanalised reducing the occlusion by 38%. Subsequently the calcified arteries showed increased distensibility and required lower pressure to achieve dilation.

Using pressure-volume inflation curves from a standard dilation catheter Demer *et al* [37] found that after a specified dosage of ultrasound, the pressure-volume curve from the balloon catheter shifted, confirming the observation by Siegel *et al* [17] that the vessels showed increased distensibility and lower dilation pressures after exposure to ultrasound. Fischell [36] noticed that therapeutic ultrasound had an ability to induce local vasodilatation, or the relaxation of the muscle fibres in arteries, which may add to the distensibility of the arteries.

Flowcardia Inc. [45] has developed a monorail ultrasound angioplasty device for specific use on chronic total occlusions (CTO's). The system used is run at a frequency of approximately 20kHz with a working length of 146cm. The ultrasound is transmitted via a nitinol wire waveguide to a 1mm diameter stainless steel tip. Apart from the tip the ultrasound wire and guidewire are all housed in a 6F catheter, which acts as an irrigation system. The system works by moving a guidewire to the point of the lesion and then the stainless steel tip is advanced over the guidewire, fragmenting the lesion as it is pushed forward. The system was CE marked in January 2005 and received FDA approval in January 2007 after completing a number of feasibility clinical trials [42].

In one trial, 55 CTO's in 53 patients were treated using the system. The device showed a success rate of 76% with no major cardiac events or coronary perforation. In a second study with 30 lesions in 28 patients success was achieved on 63% of procedures. However there was one guidewire perforation with no serious adverse effects and one peri-procedural myocardial infarction. The main limitation of these studies however is the small sample size of the patients. Other feasibility studies are currently ongoing.

2.5 Wire Waveguide Distal Tip Peak-to-Peak Displacements

Gavin *et al* [46] measured distal-tip displacements for short 1.0 mm diameter wire waveguide optically using a microscope with a magnification of 40 (Figure 2.6). This was carried out over various power inputs setting of the generator.
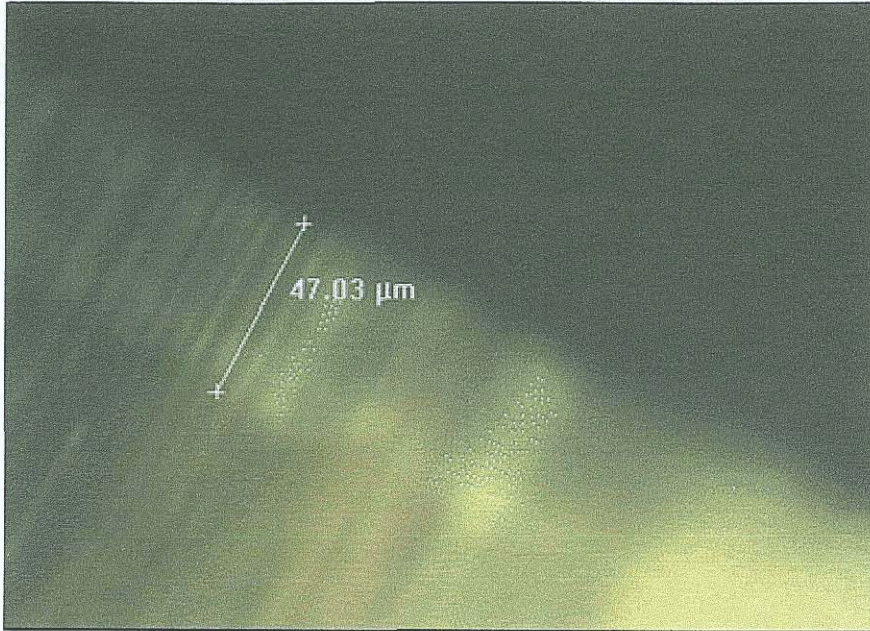
Figure 2.6: Image of vibrating wire waveguide distal-tip obtained by the optical microscope and image analysis software [47].

Gavin *et al* [47] examined the 1mm diameter wire waveguides over multiple lengths and each length was tested at various power level settings. It was found that as the power input is increased then the output peak-to-peak displacement is also increased as shown in Figure 2.7. This is not true for all wire waveguide lengths; some lengths result in poor or no transmission
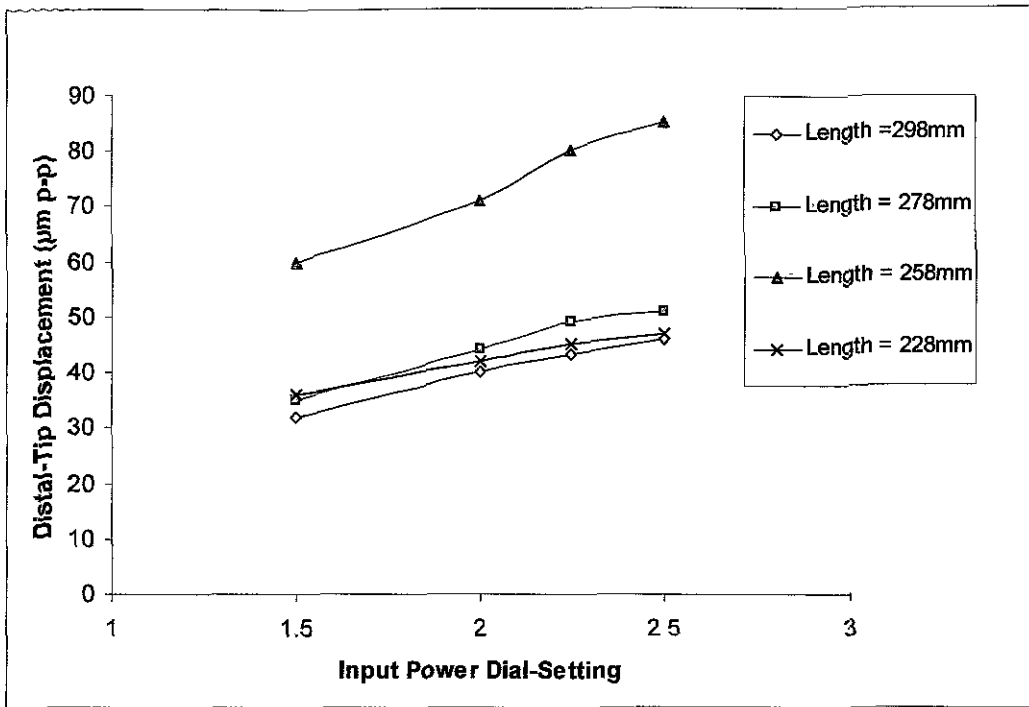
Figure 2.7: Distal-tip displacements for a 1.0mm diameter wire waveguide for generator input power dial settings of 1.5, 2, 2.25 and 2.5 [47]

The study suggests that the resonant length of the wires affects the transmission. Wire waveguide lengths were examined between 118 and 303mm at intervals of 5mm and again using the 1mm diameter wire waveguides at a constant power setting input.

The study shows that the wire waveguide has specific resonant and anti-resonant lengths. These results also showed stable ultrasound transmission was attained at anti-resonant lengths. The performance decreases as the wire length approaches resonant lengths, for the same power input.

Equation 2.1 can be applied to determine the frequency of the system. A frequency of 23.5kHz was inferred which would be consistent with the experimental findings.

$$f = \frac{nc}{4l_n} \qquad n = 0, 2, 4, 6...\qquad (2.1)$$

Using anti-resonant peak-to-peak wire waveguide distal displacements, two other important pieces of information were extrapolated, a damping coefficient for the wire

22

waveguide and input peak-to-peak displacements from the acoustic horn for specific power outputs. Measurements at resonance could not be made as the apparatus failed to transmit ultrasonic distal-tip displacements at these lengths. Input proximal displacements for power settings between 1.5-2.5 range from 32μm- 46μm, respectively [47].

The experimental results were further verified using measurements of the displacement amplitudes along the waveguide and comparing them with an analytical theory.

2.6 Finite Element Analysis of Ultrasound Transmission in Wire Waveguides

As all four damage mechanisms depend on frequency and the peak-to-peak displacements of the wire waveguide there is a need to fully understand the mechanics of the apparatus. Theoretical analysis provides an excellent basis for examining the fundamental mechanics of ultrasound transmission and output via a wire waveguide. However it is limited to use in the analysis of simple geometries. In an attempt to understand and further vary these geometries and conditions, it may be beneficial to employ the finite element method.

Based on the experimental results Gavin *et al* [47] showed that the wire waveguides exhibits a relatively complex behaviour that cannot be fully described by the steady-state analytical solution (Appendix A). The main reason for this is that the analytical solution does not account for damping. In reality there is damping due to the wire waveguides surroundings and material properties.

The study used a finite element model of the wire waveguide to investigate the behaviour of the waveguide in modal and harmonic analyses. The extrapolated values for frequency and acoustic horn distal tip peak-to-peak displacements were used as inputs for both models. These models should validate experimental data and hence determine points of maximum and minimum displacements and stresses in the waveguide.

2.6.1 Modal Analysis of Wire Waveguide

Gavin *et al* [47] used a modal analysis of the waveguide to determine optimum meshing and predict basic wire waveguide behaviour for resonant frequencies with less computational time.

A 2D axisymmetric model was used in the study with 4 node quadrilateral structural elements (Plane42). The model was constrained to allow zero displacement in the radial direction along the axial centre-line and is also constrained with a zero displacement in the axial direction at the proximal end nodes.

Mesh density analysis was performed on 0.35, 0.6 and 1mm wire waveguide models to determine the optimum mesh density. All material properties were constant for each of the models. For optimum mesh density, modal analysis results show that 4 elements per millimetre in the radial direction for all three wires are sufficient. The mesh density in the axial direction varies for each wire. It was found that for the 0.35, 0.6 and 1mm it was necessary to have 2, 3 and 4 elements per millimetre, respectively.

Using these mesh densities, the numerical model compares favourably with analytical results and, with a high degree of confidence, these results can be used further in performing the harmonic analyses.

2.6.2 Harmonic Response Analysis of Wire Waveguide

Gavin *et al* [47] also used a harmonic response analysis to determine the response of a structure under a sustained cyclic load. This is a steady-state analysis that requires sinusoidal input displacements or forces and will determine how a structure will react over a wide range of frequencies.

The analysis produced results comparable to the experimental measurements such as peak-to-peak tip displacements and also the internal structure of the wire waveguide. A 2D axisymmetric model with the same elements and mesh density as for modal analysis was used. Applying boundary conditions, the proximal end was subjected to a sinusoidal displacement similar to power settings and zero displacement in the radial direction along the axial centreline over a range of frequencies from 0-30kHz. Distal-tip and internal displacement and stress results at a frequency of 23.5 kHz (the operational frequency)

were predicted for each of the models. It is also important to determine an appropriate damping value to more accurately predict the behaviour of the wire waveguide. Using experimentally obtained results, models were created to test variation in damping values. It was determined that a damping value of 4.5% most accurately represents the experimental data obtained [46].

Including this value in the models produced some interesting results. With wire waveguide models of 288mm, there is a reduction of approximately 12.5% in peak-to-peak displacement. Results also showed increased stress levels at the connection point of the wire waveguide and the distal tip of the acoustic horn, where previously stress levels had been near zero, which is related to the losses in the wire waveguide. This increased stress level is cyclic in nature and results in a cyclic force all of which requires greater force from the converter and acoustic horn to maintain the output displacement from the acoustic horn. These cyclic forces increase as the wire waveguide length approaches a resonant length and may be the reason why the ultrasonic apparatus fails to operate at resonant lengths of wire waveguide.

2.7 Limitations of Current Studies

Only one published study, by Gavin *et al* [47], addresses design issues for ultrasonic wire waveguides for use in recanalisation of chronically occluded arteries. There are, however, some limitations to the clinical applicability of the device described in this study. The first limitation is the wire waveguide length. In order to gain access to coronary arteries wire waveguide lengths must be in the region of 1.6m. With this device limited to waveguide lengths of less than 0.3m, the device is not capable of reaching the coronary arteries. The second limitation of the device is the lack of flexibility of the wire waveguide and the connection to the acoustic horn. The ultrasonic device developed by Gavin *et al* [47] has a 1mm diameter wire waveguides, as smaller diameter wire waveguides result in immediate fracture at the connection point to the acoustic horn. However, 1mm diameter wire waveguides are not sufficiently flexible or of sufficiently low profile for the waveguide to transverse the arterial tree.

Finally, Gavin *et al* [47] do not directly measure the frequency of the device or guidewire. Therefore, this important characteristic, potentially affecting the interaction of the device with the tissues and fluids, is not adequately verified.

2.8 Contribution of Thesis

This thesis will make the following contributions.

1. An analysis of the design requirements associated with the development of safe and effective therapeutic ultrasound wire waveguides for interventional cardiology procedures is presented.

2. An experiment to measure the frequency output of a high power low frequency wire waveguide is developed and demonstrated.

3. A tapered wire waveguide concept is proposed in order to meet the engineering and clinical requirements associated with transmitting ultrasound to chronic total occlusions.

4. A design methodology for tapered wire waveguides, incorporating analytical and numerical methods, is proposed and applied to the present problem. This model accounts for the damping due to wire properties, as well as signal amplification due to the tapers.

5. A new device, incorporating a long, flexible, tapered wire waveguide is constructed. Its effectiveness in ablating model materials over long wire lengths and via tortuous pathways, is demonstrated.

Chapter 3

Frequency and Displacement Measurements with a Laser Sensor

3.1 Introduction

A limitation of the optical method of output measurement for ultrasound waveguides used by Gavin and other workers [47] is that no information on frequency can be determined. In this chapter a new laser based system is developed in order to obtain information on peak-to-peak tip displacements. The information obtained is processed with a Fast Fourier Transform (FFT) algorithm to determine frequency changes.

3.2 Ultrasound Apparatus Overview

A generator and wire waveguide system has previously been developed at Dublin City University. Gavin *et al* [46] describes the design and operation of this system. The apparatus consists of an ultrasonic generator, piezoelectric converter, acoustic horn, housing and small diameter wire waveguides. In this section each of these components will be discussed in detail.

3.2.1 Ultrasound Generator

The generator and converter are from Branson Ultrasonics™ (41 Eagle Road, Danbury, CT, USA), which produce tools for sonochemisrty applications. The generator produces a sinusoidal voltage output (950 Vrms$_{max}$) at 22.5 kHz ± 6% [48]. The generator is equipped with an auto-tuning function that sweeps for the resonant frequency of the converter as this may alter slightly during operation due to heat but also due to the addition of wire waveguides. The generator has an adjustable power setting that can vary the output from the acoustic horn.

3.2.2 Piezoelectric Converter

The converter is a piezoelectric transducer (lead zirconate titanate) that is designed using an internal stack structure of the piezoelectric crystals. The converter is specified to resonate at approximately 22.5 kHz. It is also designed to accommodate a range of acoustic horns that are also designed to resonate at the same frequency.

3.2.3 Acoustic Horn

The acoustic horn is also from Branson Ultrasonics™, as most manufacturers design specific acoustic horns to resonate at the same frequency as their converters. The acoustic horn is made from a titanium alloy with both step and linear tapers with a maximum output peak-to-peak displacement of approximately 100μm. The manufacturers recommend operating the converter and horn in a fluid as this cools and loads the acoustic horn.

3.2.4 Wire Properties

The wire waveguides used by Gavin *et al* [47] are made from a Nickel-Titanium (NiTi) alloy obtained from Fort Wayne Metals© (9609 Indianapolis Road, Fort Wayne, IN 46809). NiTi is commonly used in biomedical engineering for guidewire technology and also used as a shape memory alloy in stenting. The alloy consists of 56%Wt nickel, some trace elements and the balance consisting of titanium ($\approx$ 43%Wt). This material was chosen as it demonstrates superelastic behaviour, good sound transmission and low damping qualities while it is in its austenitic phase. The material is also biocompatible and is therefore considered suitable for contact with the vascular system.

Mechanical testing was performed by Gavin *et al* [47], on NiTi wires of sizes ranging from 0.35mm to 1mm in diameter in order to determine Young's Modulus, Ultimate Tensile Strength and ensures the wire is in its austenitic phase at room temperature. The Young's modulus was determined as approximately 75 GPa providing the strains are small and the wire remains in the austenitic phase. The ultimate tensile strength and density were determined as 1400 MPa and 6448 kg/m^3

respectively. These values for material properties in the austenitic phase compared closely with the supplier's data sheet for Nitinol [49].

3.2.5 Connection of Wire Waveguide to Acoustic Horn

In order to effectively transmit the ultrasonic waves from the distal tip of the acoustic horn to the proximal end of the waveguide, a rigid connection is required in order for the acoustic horn and waveguide to move together. By attaching a wire waveguide to the end of the acoustic horn, the mass of the system is changed. This may slightly change the natural resonant frequency of the system, which is expected to be approximately 22.5 kHz.

The generator has the ability to automatically sweep and tune the device to the resonant frequency within ± 6% of the natural frequency of the system. It is therefore important that the mass of the waveguide and connections be negligible in comparison to the mass of the acoustic horn.

Gavin *et al* [47] determined that a suitable connection method is an axial configuration as shown in Figure 3.1.
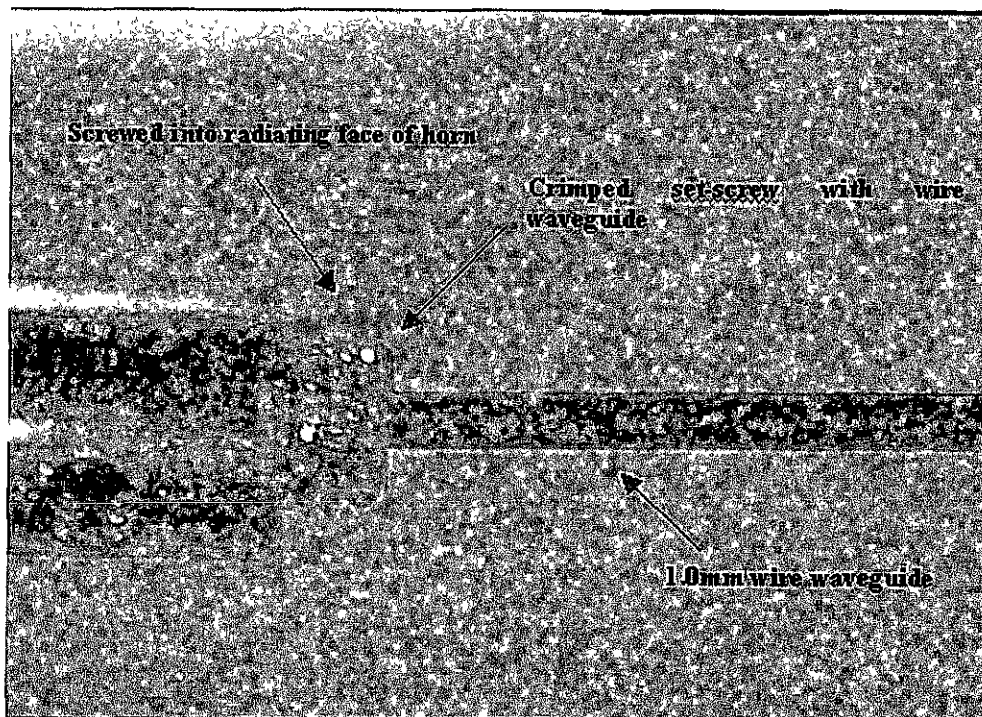
Figure 3.1: Image of axial crimped setscrew connection method from Gavin et al [47]

29

This configuration is similar to how the acoustic horn is attached to the converter. First, a hole with a tight tolerance is drilled in an M3 stainless setscrew to accommodate the wire waveguide. The wire is then inserted and the setscrew is then lightly crimped to prevent damage to the waveguide. A tapped hole was made in the distal tip of the acoustic horn so the setscrew can be inserted.

This method of connection has been shown to provide good transmission of ultrasonic energy to the distal tip of the waveguide. Three different wire waveguides were examined (0.35, 0.6 and 1mm diameter) with this connection method. Transmission with 1.0mm wire waveguides was successfully achieved but it may be considered that diameters of 0.6mm and 0.35mm failed prematurely at the connection point. The connection point undergoes high stresses during operation that eventually lead to fracture. The time to failure of each wire is increased from seconds to minutes as the diameter increases. Therefore, the work of Gavin *et al*[47] does not provide a technical solution to the problem of transmitting ultrasound into wire waveguides, which are below 1.0mm in diameter. This is one of the key objectives of the present thesis.

3.2.6 Housing

The housing unit has a number of functions such as cooling and loading the acoustic horn, protection for the user and allows the wire waveguide to emerge from it. It is also compact and lightweight.

The acoustic horn has a case, which fits around the acoustic horn and can be filled with fluid to act as a coolant and load the acoustic horn. A female connector is attached to the inner casing to allow the wire waveguide to emerge. This also has a second function as it supports the wire waveguide, reducing transverse waves and hence reducing stress at the connection point. The final portion of the Housing is an outer casing, which holds the inner casing and covers the acoustic horn and a portion of the converter. This prevents any unnecessary contact between the user and the device. The entire handheld unit is shown in Figure 3.2
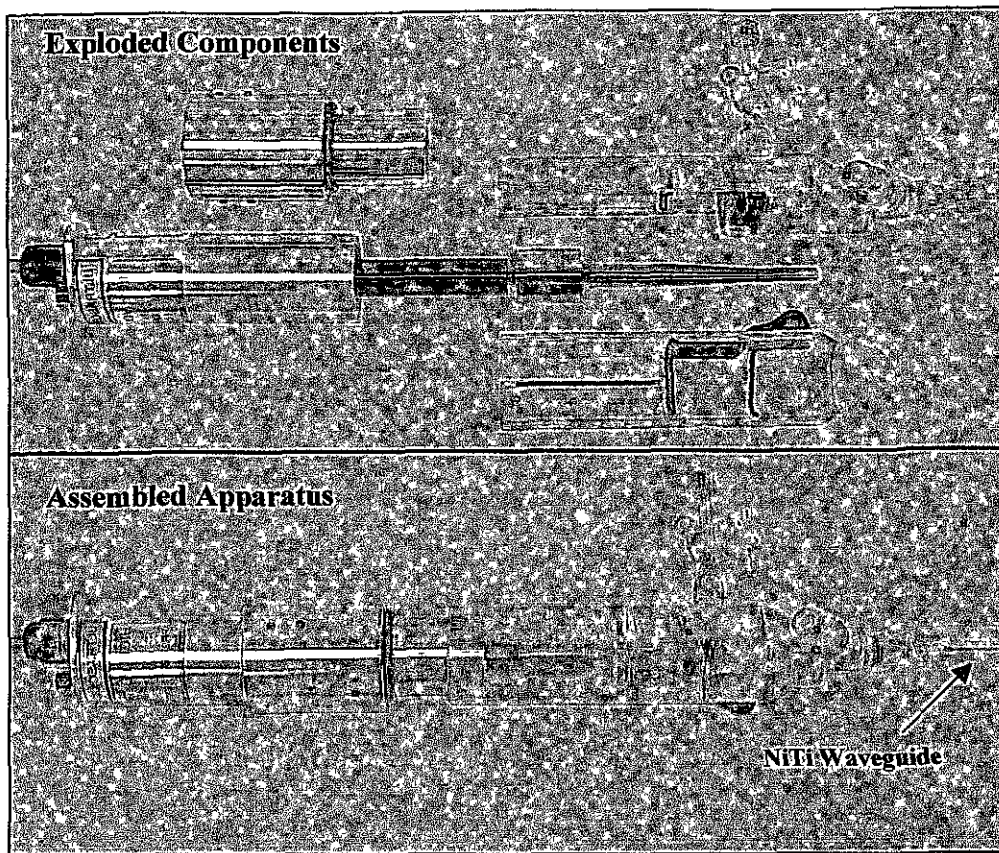
Figure 3.2: Image of ultrasonic wire waveguide apparatus in its housing with catheter emerging [47].

3.3 Optical Output Measurements

Optical measurements of the distal tip peak-to-peak displacements Gavin *et al* obtained by means of an optical microscope, digital camera and computer with image analysis [47] shown in Figure 3.3. The technique is based on focusing the microscope, with a magnification of 40X, on the distal tip of the wire waveguide. The power is then turned on causing the tip to oscillate rapidly creating streaks on the screen and an image is captured. Manually, the length of the streak is then measured using measurement software showing the extent of the peak-to-peak displacement shown in Figure 3.4.

The total peak-to-peak displacement is given by:

Total Displacement = Streak Length − Initial Length

31
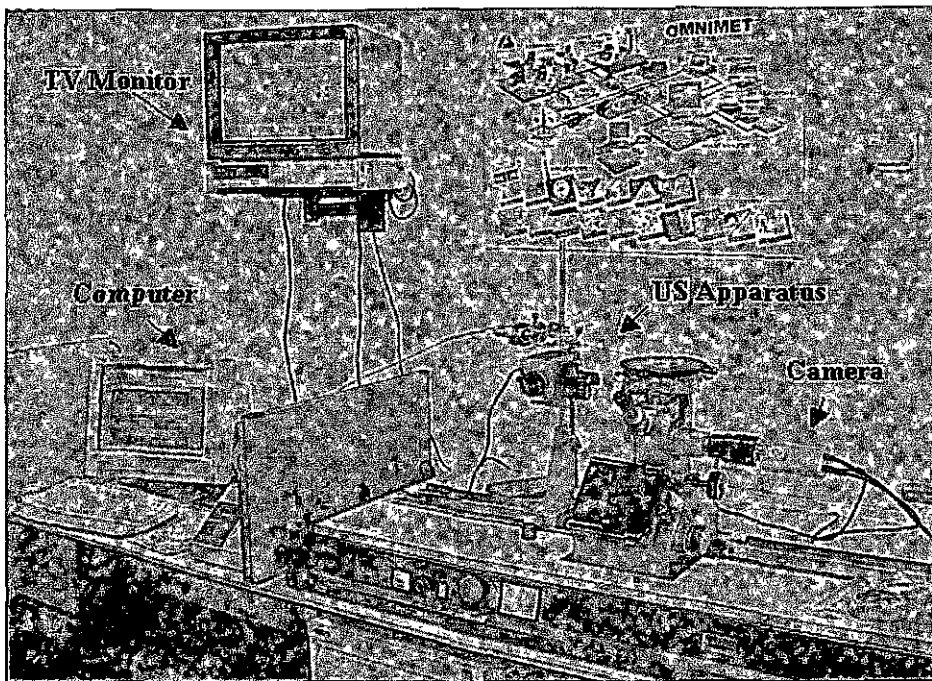
Figure 3.3: Image of wire waveguide displacement measurement system with optical microscope, camera and PC with image analysis software.
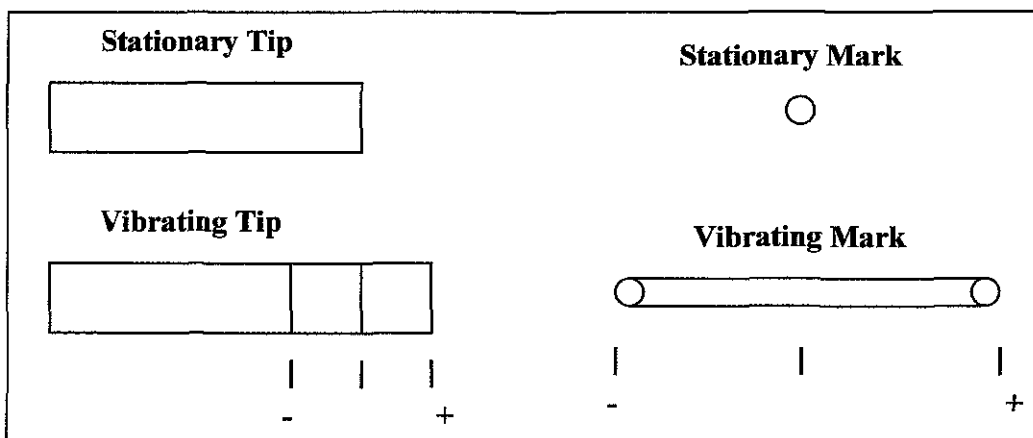
Figure 3.4: Schematic of peak-to-peak displacement measurement by optical means [47].

There are a number of limitations to using an optical method. Firstly, using the optical method the distal tip movement is assumed to oscillate from maximum peak of the streak to the minimum peak of the streak for all cycles of the ultrasonic wave. This assumption is believed valid for regions of the wire waveguide lengths close to anti-resonant length. As the waveguide length moves closer to the resonant lengths it becomes increasingly difficult to obtain a clear streak using the optical method. It is not possible to determine any pattern or measurement at resonant lengths of wire

32

waveguides as the distal tip oscillates with an irregular motion that cannot be captured using the optical method.

Secondly the optical method has an accuracy of approximately ±3-4 μm [47]. In low power inputs with peak-to-peak displacements of 20-40 μm, this represents a 10-20% possible error. It must also be noted that measurements in previous studies were taken from a short 1mm wire waveguide. Finally, the optical method captures an image of distal tip vibrations at single moment in time. However no information about frequency changes or other harmonics during apparatus operation can be determined. This is an extremely important aspect of the apparatus as the amplitudes and outputs from the device are a function of frequency. Also, the wire geometries are selected based on the frequency of the apparatus.

3.4 Development of Laser Sensor Measurement System

A method of measuring distal tip displacement is needed to overcome some of the short falls with the optical measurement method. The method also needs to be non-contact, obtain information from a small target surface size, have a micrometer measurement range and require a sample rate at a minimum of 75kS/s (kilo Samples per second) due to the frequency of operation of the device. This has not been achieved in any previous studies. The system used in the measurement of the wire waveguide displacements is shown in Figure 3.5.
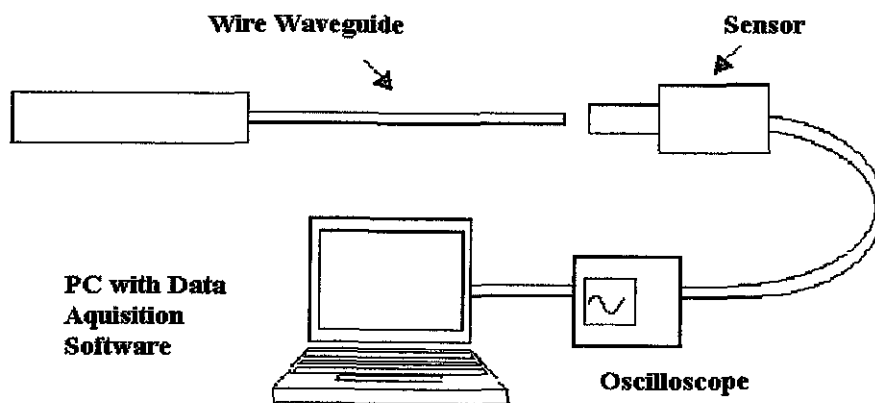
Figure 3.5: Wire waveguide displacement measurement set up with laser sensor, hardware low band pass filter and PC with data acquisition software

It consists of a Laser sensor, an Oscilloscope and a PC with Data acquisition card and software. A number of other sensors were examined such as LVDT, eddy current, capacitor and strain gauges. The design requirements for the sensor are non-contact, small spot size, high frequency and capable of micrometer sensitivity. Taking all of these into account the choice of sensor was quickly narrowed down to Laser sensors. It must also be noted that other authors [46] have used hydrophones to determine amplitude and the effects of frequency changes in a fluid. However due to cost this was not considered. Further investigation with laser sensor options with respect to the design requirements the sensor chosen is a D6-HiTi Type D reflectance dependent fibre optic displacement sensor from Philtec Inc. This is a reflectance dependent non-contact sensor with a target surface size of $0.16mm^2$. The sensor is capable of sampling up to 200kHz. The sensor has a 0-1mm measurement range, which is calibrated by the manufacturers to an output of 5V corresponding to a polished mirrored surface, as shown Figure 3.6.
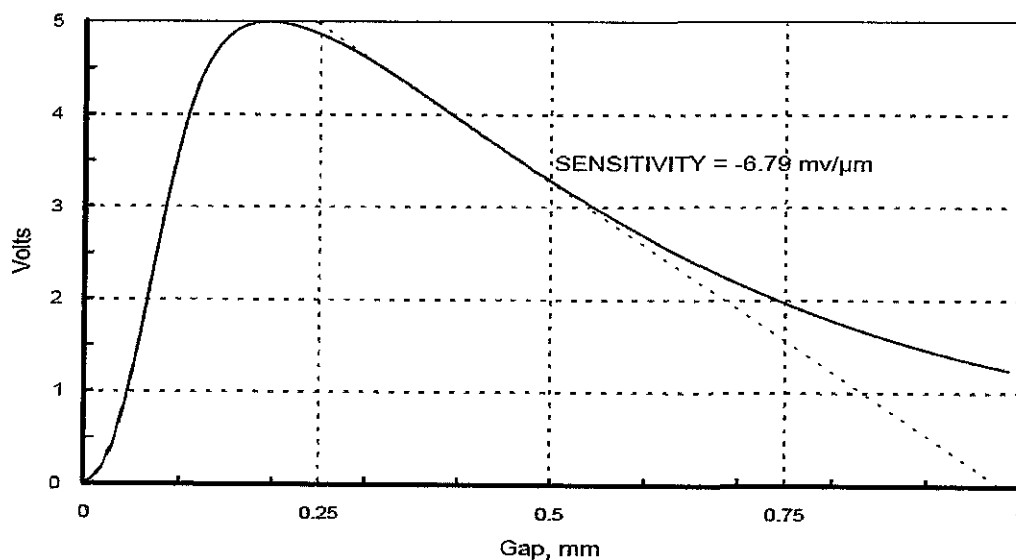
Figure 3.6: Original calibration curve of the Fibre Optic Laser Sensor

The sensor is restricted within the 0-1mm range to two linear regions known as the near side and far side. The near side is a linear range closer to the sensor tip measuring in the region between 60-90 nm. The far side is a linear range beyond the maximum output of the sensor tip measuring peak-to-peak displacements in the region between 0.21-0.49 mm. Due to the magnitude of the distal tip peak-to-peak displacements the device will be operating in the far side region.

34

3.4.1 Calibration for Polished NiTi

As the sensor was calibrated to a polished mirror surface an in house calibration was necessary. A jig shown in Figure 3.7 was designed (Appendix B) to rigidly hold the NiTi wire waveguide and the sensor tip in order to keep the wire waveguide and sensor tip on the same central axis during the experiments. The jig has guiding rails on either side that restricts the movement of the sensor tip along the central axis of both the sensor tip and the NiTi wire waveguide. The movement of the sensor tip is controlled by a micrometer, which has a minimum displacement of 0.01mm.

The sensor was calibrated to a polished mirror surface, which would return a maximum of 5V for a 0.18mm gap between sensor tip and measuring surface. However, the reflectance properties of polished NiTi are much less than that of a mirrored surface, returning a maximum of 2.5V, therefore the sensor had to be calibrated to account for the difference.
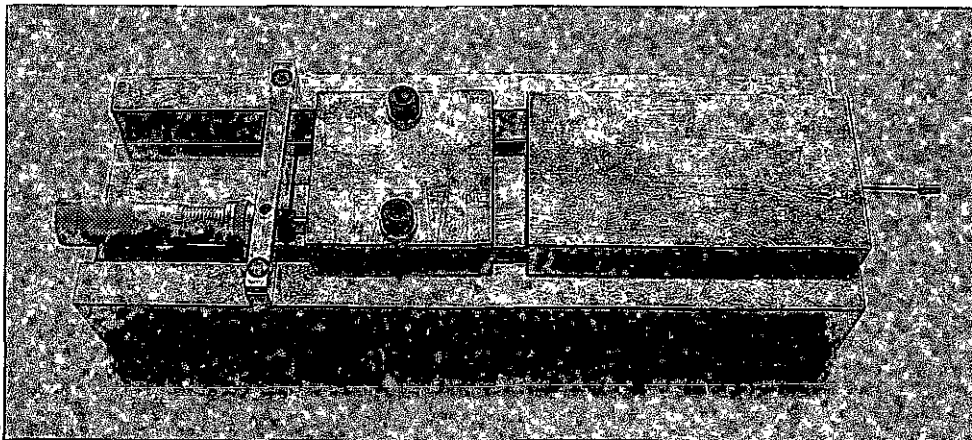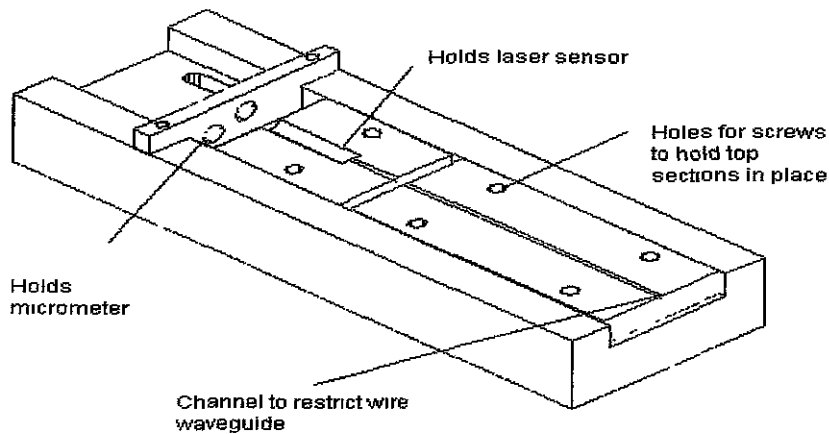
Figure 3.7: Sketch and picture of jig to hold laser sensor tip and wire waveguide with micrometer

To recalibrate the sensor, the output was connected to an ohmmeter and the sensor tip was placed directly in front of the distal tip of the polished NiTi wire waveguide with no gap between the two tips. The sensor tip was then retracted in increments of 0.01mm measured by micrometer over a 1 mm range to obtain a displacement-voltage curve that could be used to determine distal tip displacements. Figure 3.8 shows the recalibrated curve for the laser sensor for polished NiTi wire waveguides. The sensitivity of the far side linear range is $22.67\mu V/\mu m$
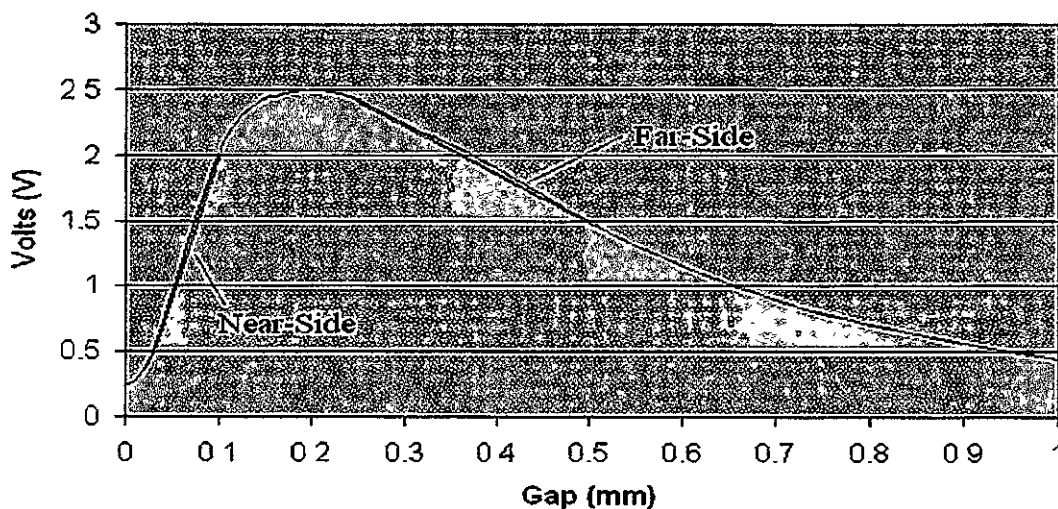
Figure 3.8: Calibrated graph for laser sensor for reflective output for polished NiTi wire waveguides

3.4.2 Laser Sensor Data Acquisition

The data acquisition is achieved using a PCI-6024E card from National Instruments Inc, which connects the sensor to the LabVIEW software. The sampling rate of the software is important. This card offers a 200 kS/s (kilo Sample per second) sampling rate. In general, the sampling rate should be as high as possible and with a minimum of 2.5 times the higher than the highest frequency component of the signal of interest. Based on this the minimum sampling rate for a 22.5kHz signal is approximately 56 kS/s. The sampling rate selected is 175 kS/s, which is expected to be more than sufficient to determine a good sample signal from the device through the sensor [50].

3.4.3 Signal Processing

Using LabVIEW 7.0, a program for processing the signal acquired from the laser sensor was developed (Appendix C). The two main steps in the program were the band-pass filter and the Fourier transform. The purpose of a Fourier transform is to take a waveform and decompose or separate a waveform into a sum of sinusoids of different frequencies (Appendix C).

Band-pass Filter

The aim of using digital processing filters in this application is to remove any external noise from the signal. Another reason for using a digital filter is to prevent aliasing. An aliased signal provides a poor representation of a signal as it causes a false lower frequency peaks to appear in sampled data of a signal due to reflection of other higher harmonic frequencies. With these false signals occurring at approximately f_n / 2, where f is the natural frequency of the device and n is 1,2,3... The band-pass filter can be used to remove these identified alias frequencies.

Classical linear filtering assumes that the signal content of interest is distinct from the remainder of the signal in the frequency domain. An infinite impulse response (IIR) band pass filter with a low and a high cut off frequencies of 21.5kHz and 23.7kHz, respectively, was used in the program. This narrow bandwidth removes any of the aliased sections of the signal.

For band-pass filters, which have two cut-off frequencies, high order filters are a more direct form of filter design than low order filter stages as the drop-off beyond the cut-off frequencies is rapid. A number of different filter types available in the LabVIEW program for digital signal processing. The program used to process the signal from the laser sensor is a Chebyshev filter design for a number of reasons. This type of filter achieves a sharper transition between the band pass with a lower order filter. The sharp transition of a Chebyshev filter produces smaller absolute errors and faster execution speeds than the other filters. Figure 3.9 shows schematically the frequency response of a band-pass Chebyshev filter.
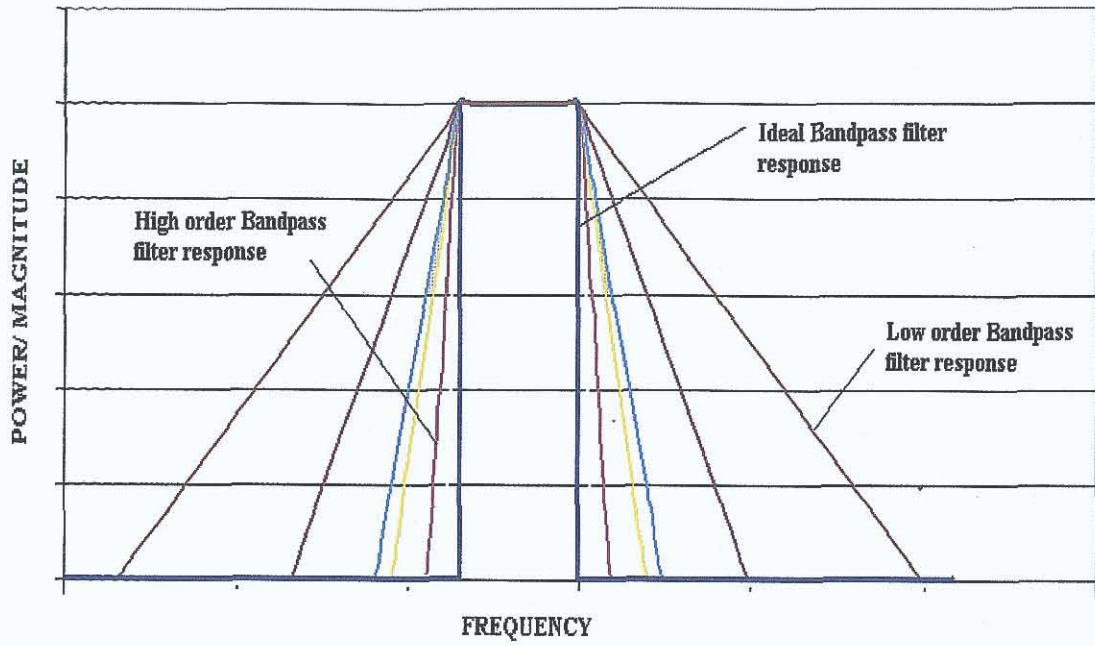
Figure 3.9: Sketch of frequency responses from low to high order band pass Chebyshev filters

3.5 Laser Sensor Measurement of Wire Waveguide Displacements

Using the displacement laser sensor, the wire waveguide apparatus was oriented and held to allow the wire waveguide distal-tip to be positioned in front of the tip of the sensor as shown in Figure 3.10.
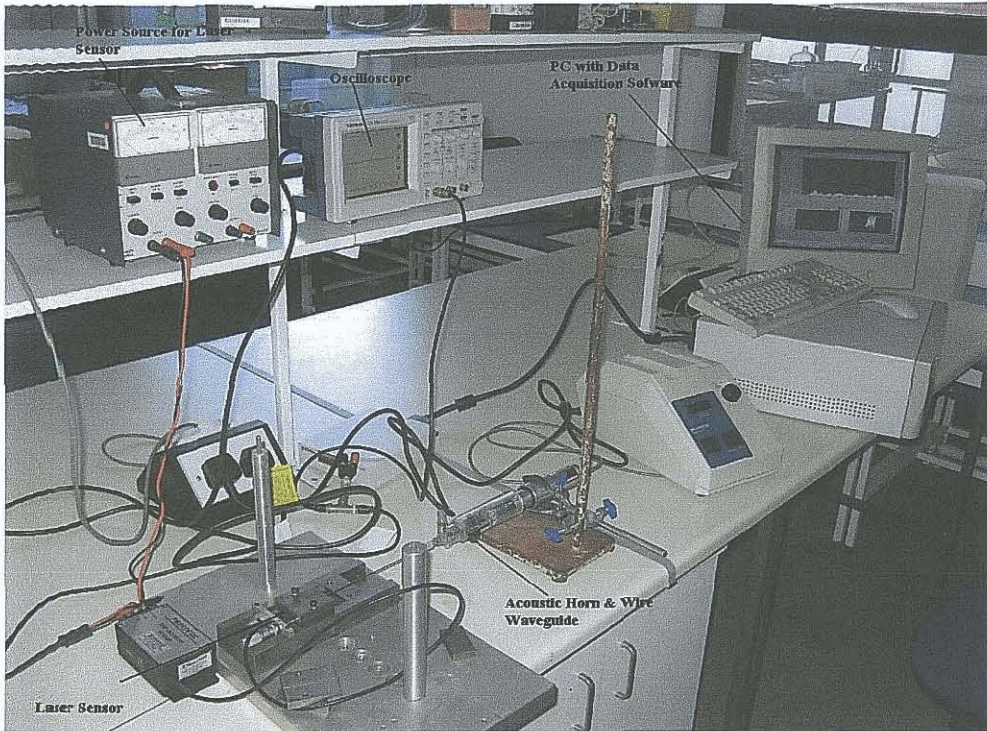
Figure 3.10: Image of wire waveguide displacement laser sensor measurement system with power supply, oscilloscope, laser sensor and PC with data acquisition software.

The wire waveguide is placed in a lubricated channel in order to minimise transverse vibrations and ensure that the waveguide tip is parallel to the lens tip. Figure 3.11 shows an enlarged image of the distal-tip of the wire waveguide located in front of the laser sensor tip. Measurements of the distal tip displacements are carried out on wire waveguide with a diameter 1.0mm and a length of 278mm. Measurements from the laser sensor were made by recording 0.1 seconds of data. Due to the band pass filter properties the first 0.05miliseconds are unusable so this time portion is removed from the overall data. Using root mean square method on the remaining data the average of over 3000 peak values is determined. Although wire waveguides with smaller diameters function, the tips of these wires have proved difficult to polish to a flat surface in order to attain enough reflectivity for the laser

sensor. Figure 3.12 shows typical screen readouts from the laser sensor at a power dial setting of 1.5. This shows a snapshot of the real time graphs of amplitude against time and amplitude against frequency during a test.

Figure 3.11: Wire waveguide in front of laser sensor tip for measurement
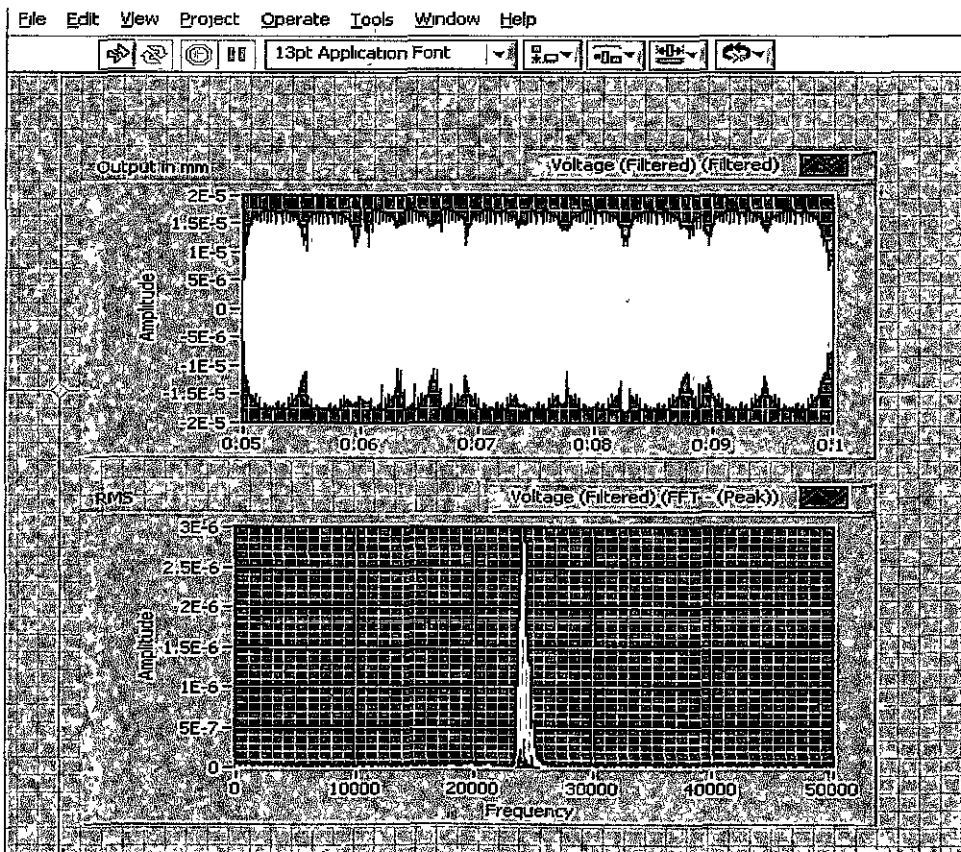
Figure 3.12: Real time snap-shot of amplitude against time and amplitude against frequency graphs from the Labview interface

3.5.1 Comparison between Optical Microscope and Laser Sensor Techniques

For a wire waveguide with a length of 278mm and 1.0 mm diameter the distal tip displacement measurements for increasing input power dial settings, obtained experimentally with the optical microscope and laser methods, are shown in Figure 3.15. Both sets of data show that as the power delivered from the generator is increased the wire waveguide distal-tip displacements are also increased. It should be noted that this is not a linear correlation. As the power settings are increased the increase in distal tip displacements start to reduce slightly. As the value for the microscope is taken from a still image only a small number points can be measured. Compared with this, the laser sensor gives an averaged value of 3000 peak measurements. The results for the laser sensor has a maximum standard deviation of 7% for each input power setting.

From the results in Figure 3.13 the power dial settings can be related to acoustic horn inputs to the wire waveguide. This is achieved by using a harmonic analysis method described in Gavin *et al* [47]. This method uses an iterative process to determine the required acoustic horn peak-to-peak displacement input to the wire waveguide in order to produce the measured distal tip peak-to-peak displacements. These are shown in Table 3.1.
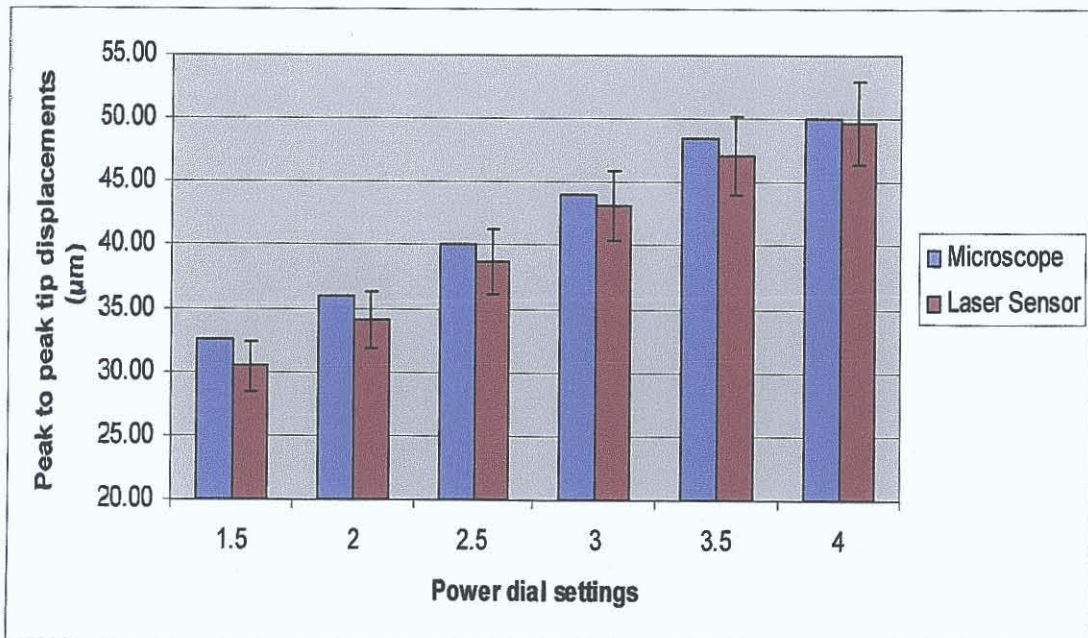
Figure 3.13: Comparison of optical microscope and laser sensor for tip displacements with varying power dial settings

Power Input	Laser Measurements (μm)	Acousitc Horn Input (μm)
1.5	30.39	32
2	34.08	36
2.5	38.4	41
3	43.14	45
3.5	47.13	49
4	49.65	52

Table 3.1: Power dial settings for the ultrasonic device and the associated acoustic horn peak-to-peak displacement outputs into the wire waveguide

3.5.2 Transient Frequency Measurements

Using the same wire waveguide of length 278mm and 1.0 mm diameter as above a time verses frequency plot is shown in Figure 3.14.
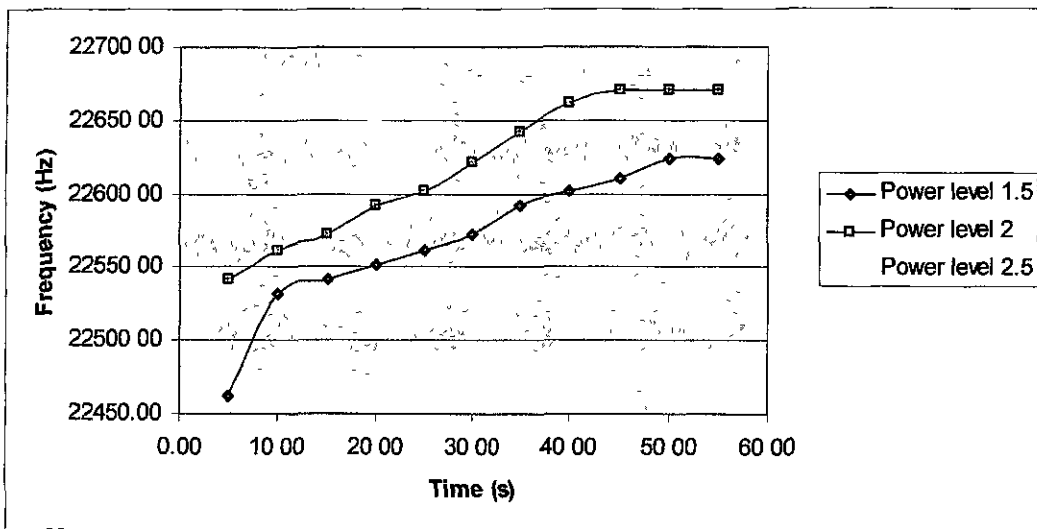
Figure 3.14: Change in frequencies of the distal tip displacements with respect to time

The results show that for low power settings, it can take approximately one minute for the device to settle at a specific frequency. However as the power input from the generator increases this settling time is decreased.

The decrease in settling time may be due to the material characteristics of NiTi waveguides. Researchers have examined the effects of temperature, frequencies,

42

amplitude, dynamic modulus, hysteresis and stress levels in this material. It has been shown for NiTi materials in their martenstic state, that for low frequencies (2-400Hz) there are small changes in the dynamic modulus [51]. If this is directly applied to Equation 2.1 then we can expect changes in frequency of the system until an equilibrium state is reached. However, the guidewires used in this research are in their austenitic phase in temperatures greater than 18°C [49]. At the same low frequencies, very little change was found for NiTi materials in their austenitic state but research states that this is frequency dependent and this could affect the settling time [51]. However, research has also shown that when loading and unloading of NiTi materials with high frequencies, the resultant stresses can force the material back into the martenstic phase which would allow a greater dynamic modulus and hence effect the frequency [52, 53].

It can also be noted that there is a greater frequency change between the power settings from 1.5-2 and 2-2.5 of 46Hz and 12Hz respectively. Overall this translates as a 0.2% and 0.05% change in frequency respectively. This may also be attributed the effects of changes of the dynamic modulus and properties of the material. The increased strains and stresses due to the increase power may reach a slightly higher equilibrium state. It may also be due to the changes in the acoustic horn properties due to the addition of the wire waveguide.

3.5.3 Frequency Measurements of Different Power Settings

Figure 3.15 shows an increase in frequency as the power dial settings is increased. Figure 3.16 shows that as peak-to-peak tip displacements are increased, the frequencies are also increased for a specific wire length. The gap between increasing frequencies remains reasonably constant beyond a power setting of 2. However with increased power input being used to adjust for frequency changes of the wire waveguide, it may be possible that this is the reason that the increase in distal tip displacements are not increasing linearly. The changes in frequency with increasing power inputs could also be due to changes in the dynamic modulus of the NiTi material.
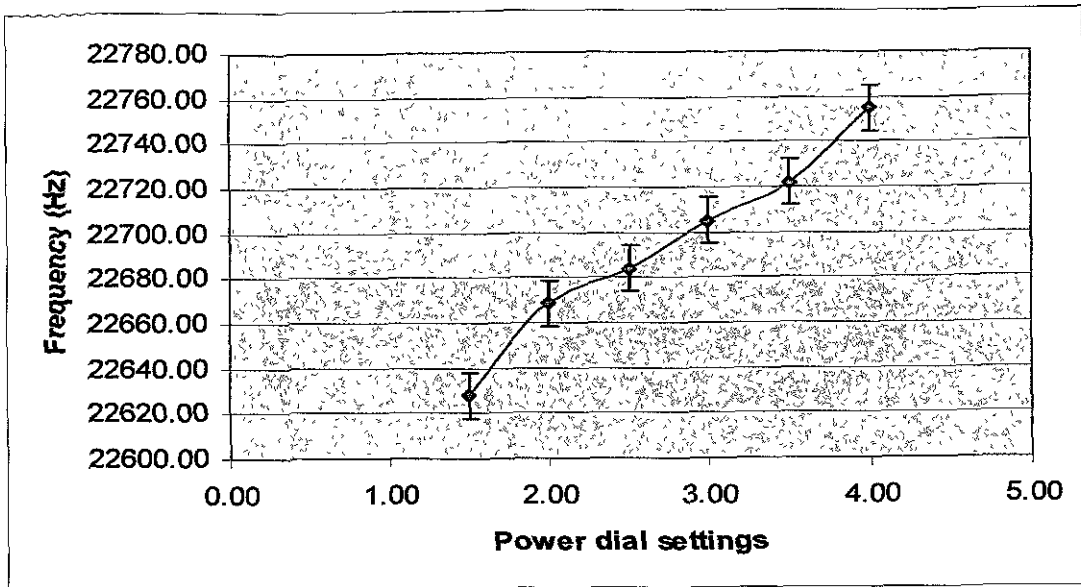
Figure 3.15: Graph of increase in frequency as the power dial settings are increased
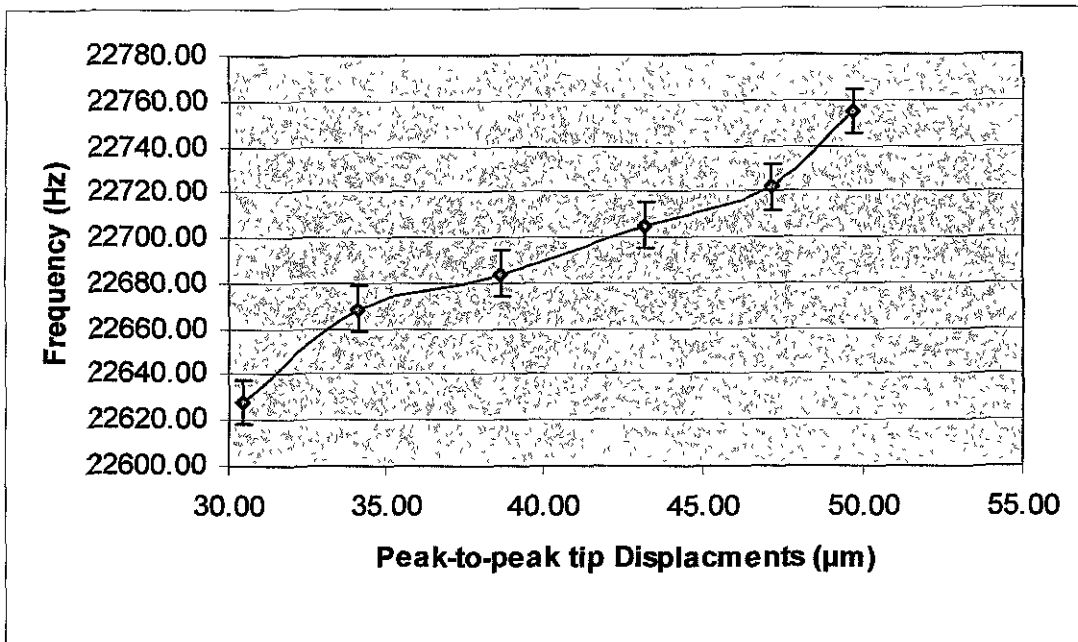
Figure 3.16: Graph of increase in frequency as the power dial settings are increased for 278mm wire

44

Chapter 4

Design and Development of Tapered Ultrasonic Wire Waveguides

4.1 Introduction

An experimental prototype suitable for short wire waveguides (up to 330mm) has previously been developed [46]. However, lengths and diameters of approximately >1600mm and <0.35 mm respectively are required to access the coronary arteries. The original apparatus delivers ultrasonic waves over lengths shorter than 330mm and fails at the connection point for diameters less than 1mm. This is not sufficient for a clinical device.

The high frequency oscillations in wire waveguides result in high stresses and failure at the connection point of the wire waveguide to the acoustic horn. It has been observed that any wire waveguide diameter less than 1mm results in failure after a few seconds [47]. As a result of the increased mass associated with longer wire waveguides, the acoustic horn requires more cyclic force to drive the wire waveguide at a given frequency, which can lead to the generator stalling. The mass of longer lengths of the 1mm wire waveguide may no longer be negligible with respect to the mass of the acoustic horn. For these reasons, it is necessary to develop a waveguide that can sustain the stresses at the connection point, transmit over long lengths and keep the overall mass of the system relatively unchanged.

The proposed solution is to use tapers to reduce wire diameter and mass. There are a number of factors that need to be considered in the design of a tapered wire waveguide, such as the number, diameter and length of the uniform and tapered sections. The finite element method will be used to design of a tapered wire waveguide based on the uniform diameter models of Gavin *et al* [47].

45

4.2 Design of the Tapered Wire Waveguide

The published literature does not contain an assessment of the design specifications or pre-clinical tests required to demonstrate the safety and effectiveness of ultrasound angioplasty devices, or similar devices. Therefore, as part of this thesis, an analysis of the design inputs, design outputs, and proposed verification and validation protocols, has been conducted. This is presented in Table 4.1. The design and analysis for the tapered wire waveguide is shown in Figure 4.1.

Design Inputs

↓

Design Specifications

↓

Material, Amplification
Length, Flexibility

↓

Numerical Analysis

↓

Individual Section Design

↓

Assembled Sections

↓

Manufacturing & testing of
concept
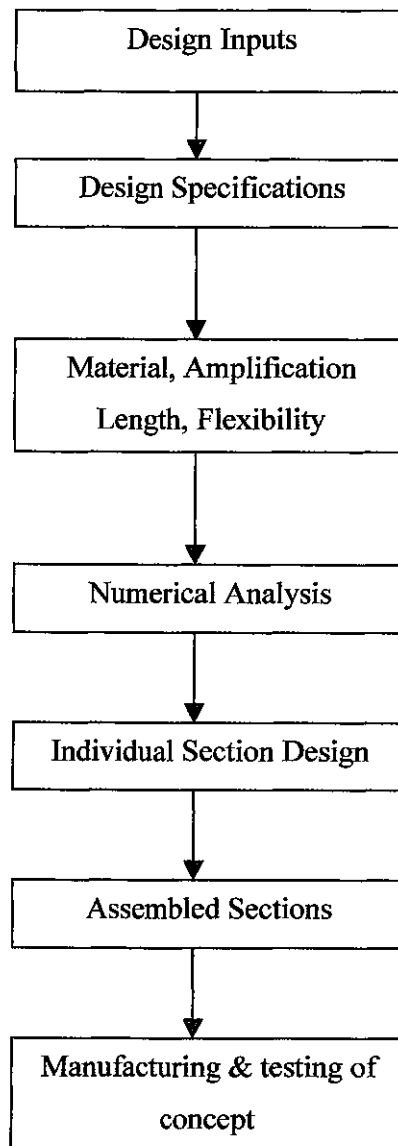
Figure 4.1: Layout and progression of full length tapered wire waveguides

		Design Input	Design Output (with acceptance criteria)	Verification	Validation
1		**Geometric**			
1.1		Wire waveguide must be of sufficient length to reach coronary arteries when introduced via the femoral artery.	Wire must be >1.4 m in length.	Wire length to be verified using measuring tape to show conformance with manufacturing specifications.	Device to be navigated through catheter configured to simulate the clinical over-the-arch configuration.
1.2		Wire waveguide must be sufficiently low profile to traverse arterial system in combination with a standard guidewire and catheter arrangement.	Wire profile must be ≤ 0.35 mm at the distal end (coronary arteries), and ≤ 15 mm for the main shaft (femoral and aortic arteries).	Wire diameters to be verified using a micrometer.	-
2		**Mechanical**			
2.1		Wire waveguide must be sufficiently flexible to permit navigation of the arterial system.	Specification of a maximum 1mm diameter. Specification of superelastic material (NiTi).	Wire diameters to be verified using a micrometer.	Device to be navigated through catheter configured to simulate the clinical over-the-arch configuration.
2.2		Wire waveguide must operate at ultrasonic frequency and set up standing waves in the wire.	22.7±0.5kHz generator specified.	Wire waveguide distal tip measured by laser sensor over the full operating range of power settings.	Frequency and amplitude testing.
2.3		Must operate reliably (specifically at connection point).	Specification of wire diameter at connection of ≥1mm.	Proximal wire diameters to be verified using a micrometer.	Demonstrate reliable operation at peak operating power levels (7) for durations of 5 minutes.

		Design Input	Design Output (with acceptance criteria)	Verification	Validation
2.4		Wire waveguide must not damage catheter or other peripherals during ultrasonic activation.	Wire waveguide must not exceed 40°C during normal operation.	Wire waveguide must not exceed 40°C during normal operation. Inspection of friction or heat damage after operation of wire in catheter.	Visible inspection and mechanical testing of catheter after being used in conjunction with wire for 5 minutes at a maximum power setting.
3	**Biological Interaction**				
3.1		Wire material must not initiate any adverse biological reaction.	Biocompatible NiTi by Fort Wayne Metals 56% Nickel 43.14% Titanium 0.033% Carbon 0.028% Oxygen 0.025% Hydrogen.	ASTM F1058.	Monitoring for clinical evidence of adverse biological reaction to product biomaterials.
3.2		Ultrasonic energy must not initiate any adverse biological or cellular reaction.	Cells exposed to ultrasonic energy at operating power levels (1-7) for 10 minutes duration should exhibit normal morphology, proliferation and apoptosis with respect to a control.	Application of ultrasound (35 μm p-p) to bovine aortic endothelial and smooth muscle cells using submerged wire waveguide suspended 5mm from base of polystyrene culture dishes. Fluorescent Activated Cell Sorter (FACS) used to determine cell proliferation and apoptosis.	Monitoring for clinical evidence of adverse reaction to biological activation.

48

	Design Input	Design Output (with acceptance criteria)	Verification	Validation
3.3	Must ablate calcified arterial plaque.	Must ablate a model plaque material (calcium carbonate) at a rate of 1.4mm per second.	Testing wire waveguide on materials chosen for their properties which are similar to rigid calcified biological material.	Clinical evidence of recanalisation of chronically occluded arteries in clinical trials and post market surveillance.
3.4	Must leave healthy arterial tissue undamaged.	Excised arterial tissue exposed to ultrasonic energy *in vitro* at power levels (1-7) for 10 minutes duration should exhibit normal morphology, with respect to a control.	Testing of ultrasonic wire on healthy arterial tissue to identify evidence of damage. Histological examination of tissue damage or necrosis.	Monitoring for clinical blood vessel perforation events in clinical trials and via vigilance systems and post market surveillance (per MDD 93/42/EEC).

Table 4.1: Design criteria for tapered wire waveguides

4.2.1 Material Selection

NiTi was chosen for the tapered wire waveguide due to its flexibility, superelastic properties and good ultrasound transmission in its austenitic phase.

4.2.2 Uniform Diameter Sections

The second aspect of the design is the proximal wire waveguide connection to the acoustic horn. As previously discussed, 0.35 and 0.6 mm diameter wires, using the axial screw connection, rapidly failed after the apparatus was turned on. The performance of the 1.0mm wire waveguide was substantially more reliable. Increased bending stiffness may also reduce unwanted transverse vibration. A 1.0mm proximal wire diameter was selected. For 1mm diameter NiTi wire waveguides, experiments have shown that ultrasound is not transmitted over lengths greater then 330mm (which correspond to a weight of 1.67grams). To minimise weight, it is desirable that this section is as light and hence as short as possible.

The next aspect is the distal-tip of the wire waveguide. The distal tip needs to be flexible in order to be manoeuvred easily through arterial lumen. Upon reviewing of guidewires currently available capable of accessing coronary arteries, the distal tip diameters range from 0.2-0.4mm. Taking the above specifications into account, the tapered wire waveguide is a one-piece wire, as it reduces the risk of fracture, with five distinct sections as shown in Figure 4.2.
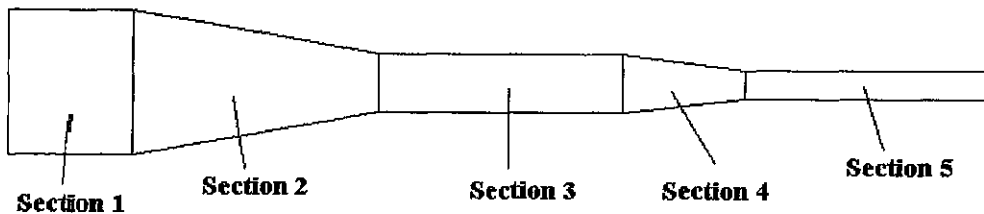

Figure 4.2: Sketch of proposed concept

There are three sections of uniform cross sectional area and two tapered sections. To reduce failure at the connection point the first section was chosen to have a 1.0mm diameter. It was desirable to keep this section as short as possible to reduce the mass of the wire waveguide. However, the length of each of the uniform cross sectional

area sections is critical in order to maximise the ultrasound transmission. From experimental testing, by Gavin *et al* [47], it was determined that the apparatus works with more stability at anti-resonant than at resonant lengths. Using this knowledge and the analytical solution of motion for an undamped longitudinally vibrating rod, the optimum anti-resonant length can be determined using, Equation 4.1 where, l are the anti-resonant lengths of the wire waveguide, f_n is the frequency of the system and c the speed of sound of the material (3410m/s).

$$l = \frac{nc}{4 f_n} \qquad n = 2, 4, 6...$$ (4.1)

The speed of sound (c) of the material is defined in Equation 4.2

$$c = \sqrt{\frac{E}{\rho}}$$ (4.2)

where E is the Young's Modulus (E) and the material density (ρ).

To keep the mass of the 1.0mm diameter section to a minimum, the anti-resonant length of 75.1mm (1/2 wavelength) was chosen for this section. This corresponds to a frequency of 22.7kHz as determined using the laser sensor. At this length the peak-to-peak displacement output from the initial section wire is a maximum, which ensures that as the standing wave enters the tapered section it attains the maximum amplification possible.

The next uniform cross sectional area (Section 3 in Figure 4.2) is the main length of the tapered wire waveguide. It is the longest sectional length of the wire waveguide. The diameter of this section is 0.35mm, as it requires a balance between sufficient flexibility to manoeuvre through the arterial lumens and still retain a level of rigidity to aid in the pushability of the wire waveguide. Also from discussions with medical device company this diameter size or smaller is preferable for access to coronary arteries. Using the smaller cross sectional area also reduces the overall mass of the wire waveguide. The length of this section was chosen so that overall length of the first three sections would be less than 1.4m. The reason for this is that the last two sections would be the sections entering the coronary arteries and do not need to be more than 0.20mm. Also it is an anti-resonant length, which maximises amplitude

transmission. The length using the analytical solution worked out as 1.05m (7 wavelengths).

The final uniform cross sectional area (Section 5 in Figure 4.2) has a diameter of 0.20mm and a length of 0.601m (4 wavelengths), which was chosen to allow a choice of overall wire length. This section is the tip section of the tapered wire waveguide and the diameter size is chosen to further improve manoeuvrability of the wire waveguide tip and reduce the mass of the wire waveguide. All of the lengths for uniform cross sectional area were analytically calculated.

4.2.3 Tapered Sections

While an analytical solution for steady-state undamped longitudinally vibrating rod exists, it is only valid for a rod of uniform cross sectional area. As the cross sectional area reduces along the section from proximal to distal end in the tapered sections, it is necessary to find another method of finding anti-resonant lengths of the tapered sections. Harmonic analysis has verified experimental standing wave and distal tip displacements in wires with uniform cross section of short wire waveguides; hence it can be used to determine the length of the tapered sections with a high degree of confidence [47].

A harmonic response analysis solves the general equation of motion for a structural system given by Equation 4.3 for the problem, Figure 4.3:

$$[M](\ddot{\vec{u}}) + [C](\dot{\vec{u}}) + [K](\vec{u}) = (\vec{F}^a)$$ (4.3)

where $[M]$ = mass matrix

$[K]$ = stiffness matrix

$(\vec{F}^a)$ = applied load vector

$[C]$ = damping matrix

$(\ddot{\vec{u}})$, $(\dot{\vec{u}})$ and $(\vec{u})$ = the nodal acceleration vector, nodal velocity vector and nodal displacement vector, respectively.

52

$u(0, y, t) = b \sin 2\pi f t$

$u(x, 0, t) = 0$
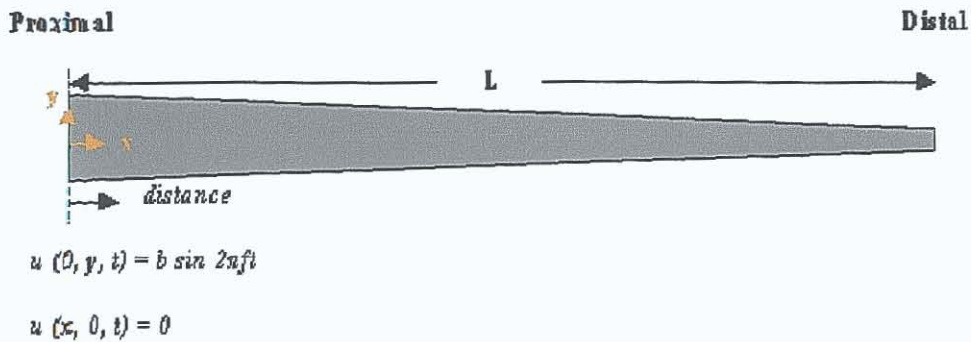
Figure 4.3: Problem sketch of wire waveguide with fixed-free boundary conditions

In ANSYS, the model uses is a 2D axisymmetric model using 4 node quadrilateral structural elements (Plane42). The model is used to determine the tapered sections lengths in order for them to be one wavelength. It was constrained to allow zero displacement in the radial direction along the axial centreline and is also constrained with a zero displacement in the axial direction at the proximal end nodes as shown in Figure 4.4.
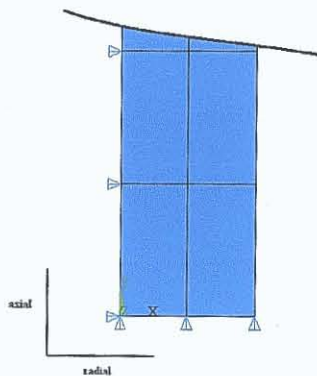
Figure 4.4: Proximal end of finite element model of wire waveguide

The mesh density is the number of elements in the radial direction multiplied by the number of elements in the axial direction. Insufficient element numbers in the axial direction will result in the internal mode shape being poorly resolved while the number of elements used in radial direction is to ensure good element aspect ratios. It is important to determine the optimum mesh density to ensure accurate solution and minimal computational time.

After all five sections are assembled together into one long wire waveguide the analytical solution is not sufficient to determine the response of the overall tapered wire waveguide. A finite element analysis of the full tapered wire is then modelled.

4.2.4 Harmonic Response Analysis for Tapers

The two tapered sections are discussed here. The first tapered section reduces from 1.0mm diameter to 0.35mm. This is the second portion of the tapered wire waveguide. The second tapered section is a reduction from 0.35mm diameter to 0.20mm.

Each of the tapered sections is to be one wavelength long, based on a frequency of 22.7 kHz as determined using the laser sensor. However, as the wavelength is based on the geometry, an iterative process must be used. Lengths are varied in the numerical model to determine the exact length of one wavelength in a tapered section. The mesh density changed after each iteration. All models were designed to have a mesh with an appropriate aspect ratio for each element based on the study of Gavin *et al* [47], and the program manual [54]. This method was used for both tapered sections.

Figure 4.5(a) and 4.5(b) shows the predicted distal-tip peak-to-peak displacement harmonic response for both tapered sections for a frequency range of 0 – 30 kHz and an input axial peak-to-peak displacement of 100 μm. A 4.5% damping value was used for all models [47]. Using the resonant frequency results predicted in the harmonic response, models of varying lengths were solved in order to shift these graphs left or right so that an anti-resonant frequency response corresponds with the frequency of operation of the system. The length for the 1.0 to 0.35mm and the 0.35-0.20mm one wavelength tapered section respectively were determined to be 156.0mm and 153.5mm. It must be noted that both tapers are of similar length. The overall tapered wire waveguide design is shown in Figure 4.6. It must be noted the 1.0mm section was increased to 120mm in order to allow for some adjustments, if necessary during experimentation.
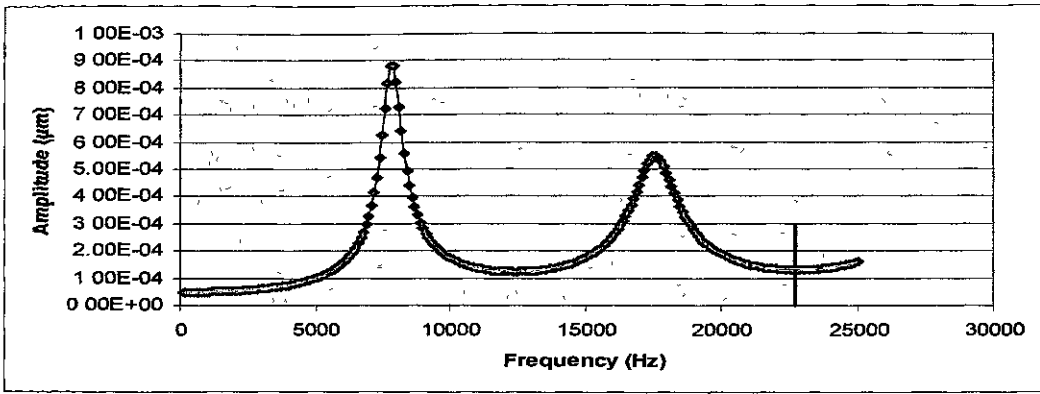
54

Figure 4.5 (a): Harmonic response for distal-tip peak-to-peak displacement of 1mm to 0.35mm tapered section.
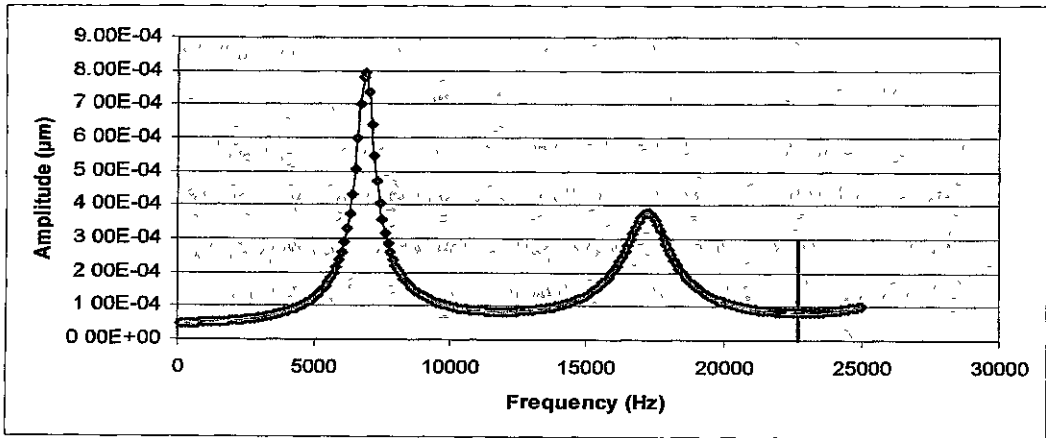
Figure 4.5 (b): Harmonic response for distal-tip peak-to-peak displacement of 0.35mm to 0.20mm tapered section.
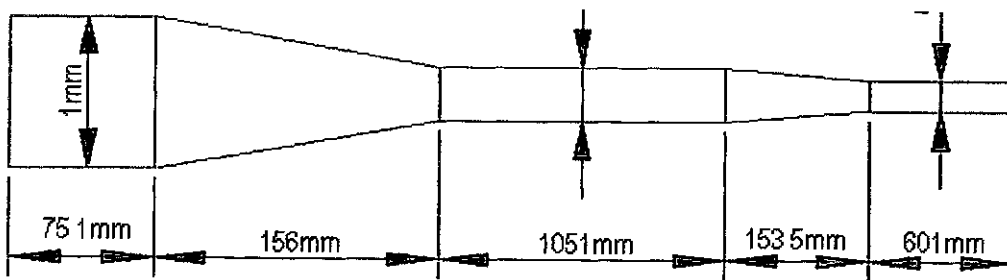
Figure 4.6: Dimensions for full tapered wire waveguide

55

Figures 4.7 (a) and 4.7 (b) show the predicted amplification of the distal tip peak-to-peak displacements as the wave passes through the optimum tapered sections at a frequency of 22.7 kHz. The main purpose of the tapered sections is to reduce the size of the wire waveguides. As can be seen from the graphs there are the added bonus of amplification, which is directly related to the difference in cross sectional area between the proximal and distal ends. Assuming no damping, the relationship is theoretically given by Equation 4.4 where B_p is the diameter of the proximal end, B_d is the diameter of the distal end and I is the percentage increase in amplification of peak-to-peak displacements. For the 1-0.35 mm and the 0.35-0.20 mm tapered sections, the resulting amplification was 285% and 175% respectively.

$$\frac{B_p}{B_d} \times 100 = I \qquad (4.4)$$

Figure 4.7 (a): Distal tip peak-to-peak amplification of 1mm to 0.35mm tapered section

56

Amplification Tapered 0.35mm-0.2mm Section

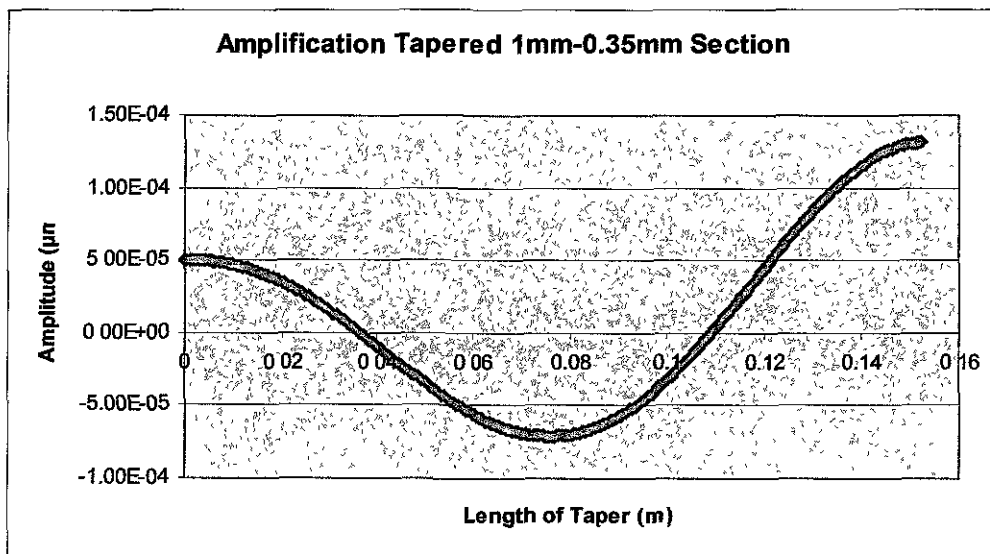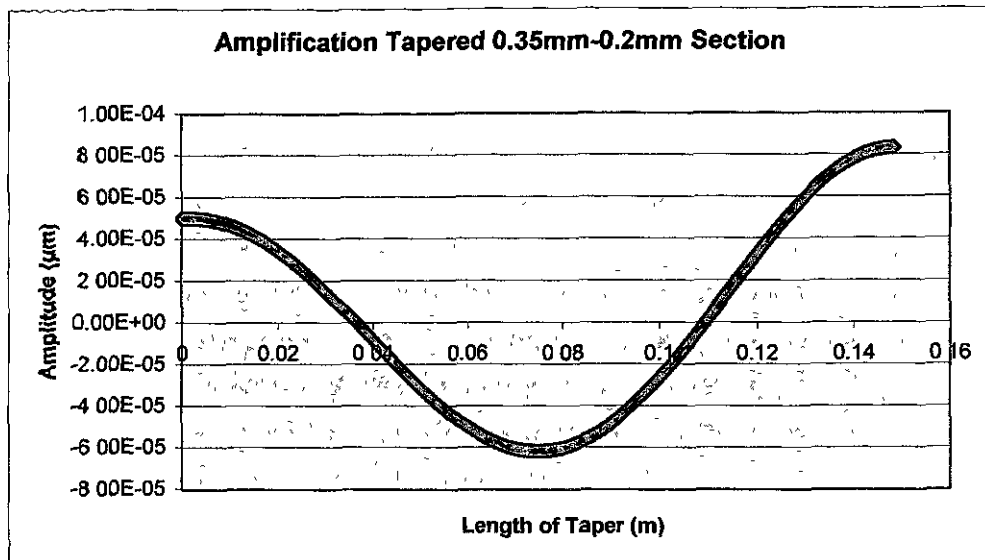Figure 4.7 (b): Distal tip peak-to-peak amplification of 0.35mm to 0.2mm tapered section

4.2.5 Sensitivity of Tapered Sections

Mesh density, Young's modulus and material density analyses were performed by Gavin [47] using modal and harmonic analysis to establish sufficient meshing pattern criteria and determine the effects of minor changes in material properties of the wire waveguide. This was to understand model sensitivity to changes in properties.

During the design of the tapered sections it was important to determine the effect of variations in length of the tapered sections due to manufacturing processes. In order determine the effect changes values of length were varied by ± 5% of the correct length of the tapered wire sections. There are two properties affected by a change in length of the tapered sections, the non-resonant frequency of the tapered section and the amplitude of the output. If the frequency changes by more than ± 6% of operating the frequency of the acoustic horn, then the generator will not be able to operate and no ultrasonic wave will be transmitted. If the length of the taper is altered sufficiently it will move towards a resonant length and increase the amplitude of the output. However previous research [47] has shown that the device does not operate when the wire waveguide reaches resonant lengths.

Figure 4.8 (a) and 4.8 (b) shows the effects of changing the length on frequency. These results show that as the tapered section length increases the non-resonant frequencies decrease for both tapered sections. For the tapered sections, 1-

0.35mm and 0.35-0.2mm at the +5% of the length of the tapered sections the non-resonant frequencies are 21.8kHz and 21.7kHz respectively. These values are higher than the minimum cut-off frequency of 21.2kHz in order for the generator to operate. However as the length decreases towards the –5% region, the frequency moves beyond the maximum cut-off frequency for the generator, which may result in the device not functioning. It must be noted that within ± 2% of the length there is not a large change in frequency, which translates as ±3mm before there is any significant effect on the operation of the device.

Figure 4.9(a) and 4.9(b) shows the effects of changing the length on the output amplitude from the tapered sections. Both of these show increases in the output amplitude of the tapered sections by 12µm and 5.5µm for the 1-0.35mm and 0.35-0.2mm tapered sections respectively. This increase may appear to be advantageous however these changes in length of the tapered section alter the resonant and non-resonant frequencies. So these amplitudes may be occurring closer to a resonant region of wire waveguide. Previous work [47] carried out on the device has shown that close to these regions there is no ultrasonic wave created and hence the device does not function. It is suggested that the tapered sections stay as close to the non-resonant frequency of 22.7kHz, which will be minimum consistent amplitude. Again staying within the ± 2% value of length should be sufficient.
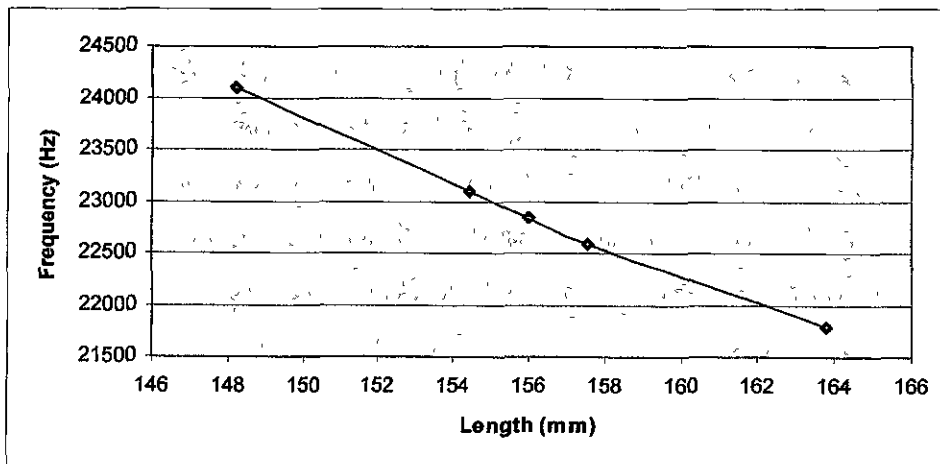
Figure 4.8(a): Change in frequency as the length of the 1-0.35mm tapered section varies from ±5%
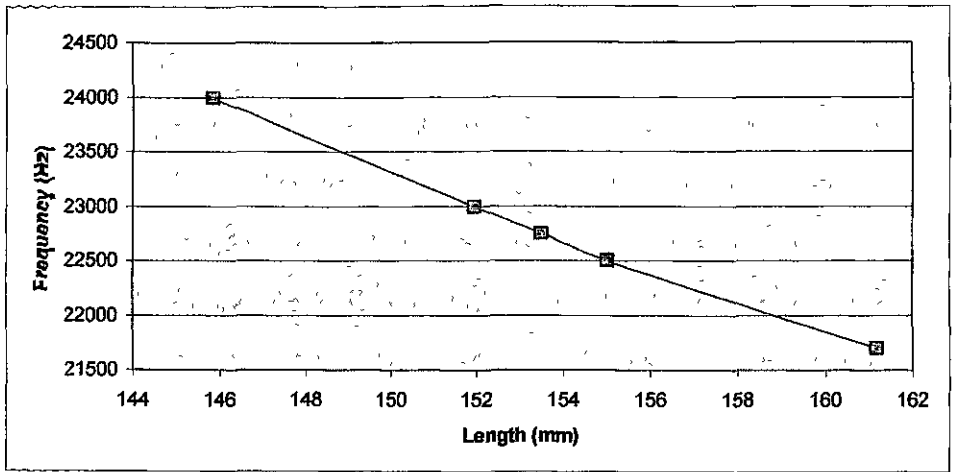
Figure 4.8(b): Change in frequency as the length of the 0.35-0.2mm tapered section varies from ±5%
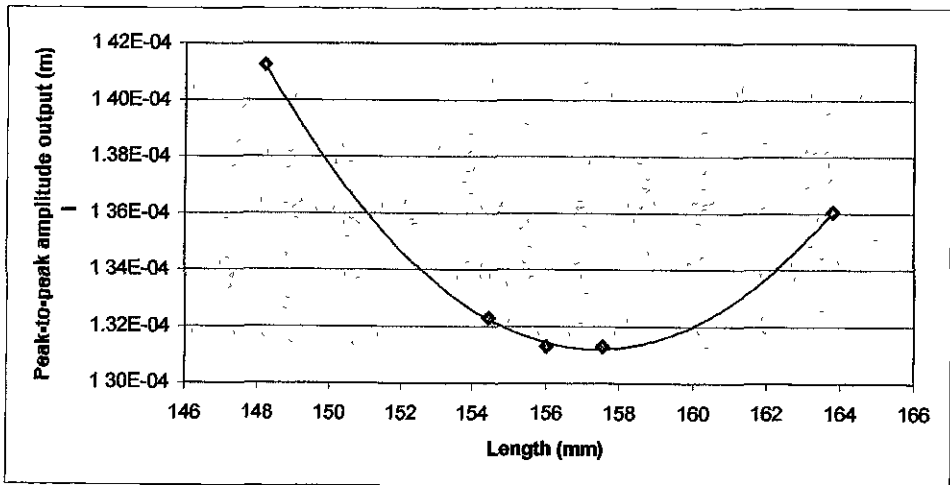
Figure 4.9(a): Change on peak-to-peak amplitude as the length of the 1-0.35mm tapered section varies from ±5%
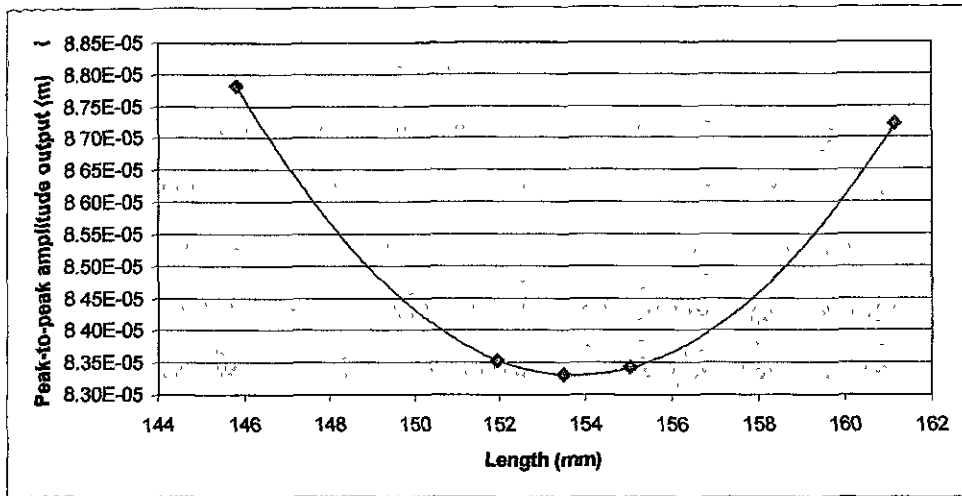
Figure 4.9(b): Change on peak-to-peak amplitude as the length of the 1-0.35mm tapered section varies from ±5%

4.3 Results of Harmonic Response of Long Tapered Wire Waveguide

The tapered wire waveguide consists of five sections in total, three uniform cross sectional area sections and two tapered sections (Figure 4.6). Due to the length and size of the whole waveguide it is very important to obtain a good mesh density. The lengths of each section are shown in Table 4.2

Section Piece	Length (mm)
1mm Uniform C.S A Section	75.1
1 to 0.35mm Diameter Tapered Section	156
0 35 mm Uniform C S.A Section	1,051
0.35 to 0.20mm Diameter Tapered Section	153.5
0.20mm Uniform C.S A Section	606

Table 4.2: Tapered wire waveguide section lengths

For the tapered sections mesh density an appropriate aspect ratio for each element was used in a similar method to harmonic analysis of the tapered sections

60

alone. Mesh density analysis was performed on 0.20, 0.35 and 1mm wire waveguide models to determine the optimum mesh density. All material properties were constant for each of the models. For optimum mesh density, modal analysis results show that 4 elements per millimetre in the radial direction for all three wires are sufficient. The mesh density in the axial direction varies for each wire. It was found that for the 0.20, 0.35 and 1mm it was necessary to have 1, 2 and 4 elements per millimetre, respectively.

Figure 4.10 shows the predicted standing wave internal displacements for a transient response for full tapered wire waveguide for a frequency range of 18 – 30 kHz and a proximal input axial peak-to-peak displacement of 50μm. A 4.5% damping value was used for all models. Over long lengths (>1.5m) of wire waveguide with a damping ratio of 4.5% the predicted peak-to-peak distal tip displacements reduced from 50μm of 17μm. This problem is very evident in Figure 4.11 as peak to peak tip displacements reduced significantly as the damping percentage is increased in the waveguide.
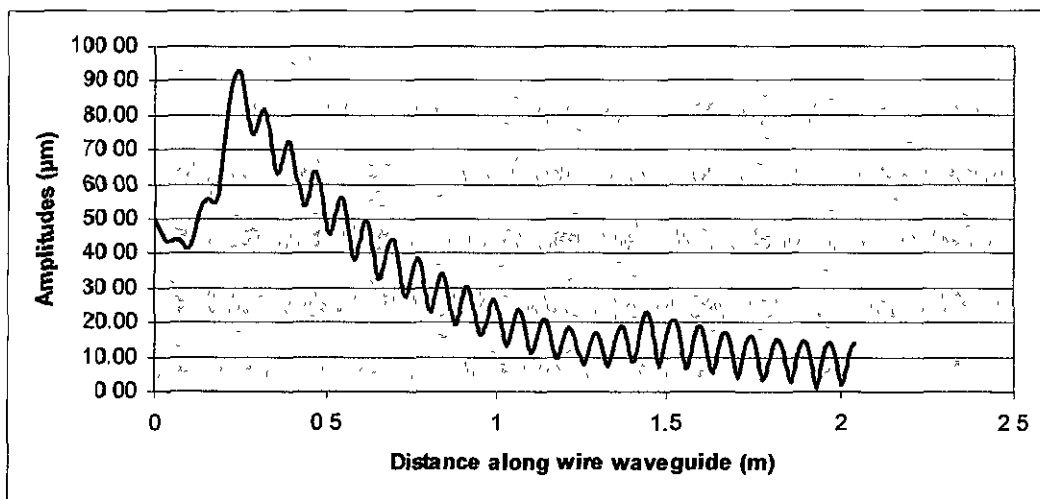
Figure 4.10: Reduction in distal tip displacement predictions due to 4.5% damping

It can also be seen that for a 1mm solid wire with the same input with no tapering and hence no amplification, the total distal tip displacements at the tip are reduced to less than 2.5μm. This may be a problem but as discussed in the next chapter, if the power is increased this may be overcome. When comparing both wires, the tapered wire waveguide produces distal tip displacements almost 7 times greater

61

than a uniform cross sectional area wire waveguide. From this the benefits of a tapered wire waveguide are evident.
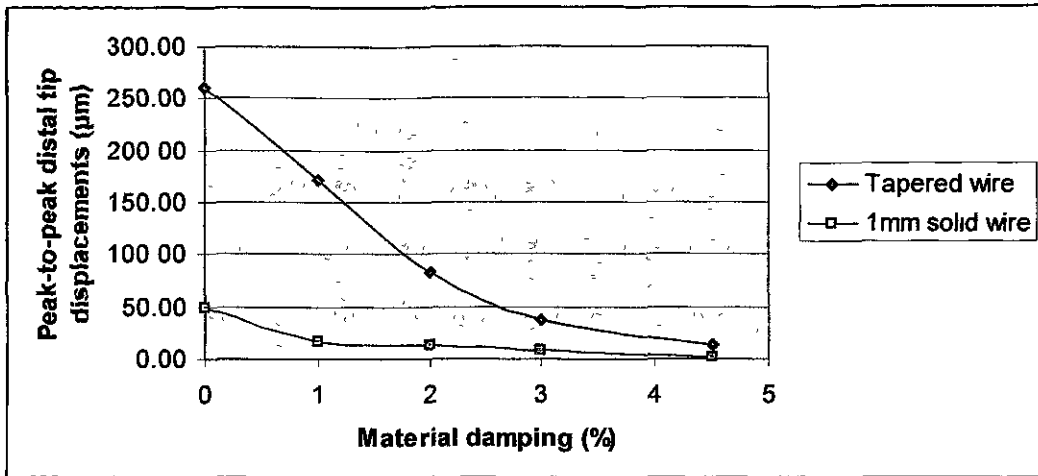
Figure 4.11: Reduction in distal tip displacements with increased damping percentage over 2m

Chapter 5

Observations and Measurements Using Wire Waveguides

5.1 Introduction

This chapter will describe the measurement and evaluation of distal tip displacement outputs for tapered wire waveguides.

5.2 Displacements of Short Tapered Wire Waveguides

Experimental measurements of displacement along the length of a tapered wire waveguide of length 506mm made using the optical microscope, method described in chapter 3 (Figure 5.1) as this represents an anti-resonant length. A standing wave structure would be expected from this type of measurement. All displacement measurements were made for an input power dial setting of 1 corresponding to 20μm input displacement to the proximal end of the waveguide. This is discussed later in this chapter.

Due to the flexibility of the 0.35mm wire, measurements near the tip of the wire waveguide could not be made.
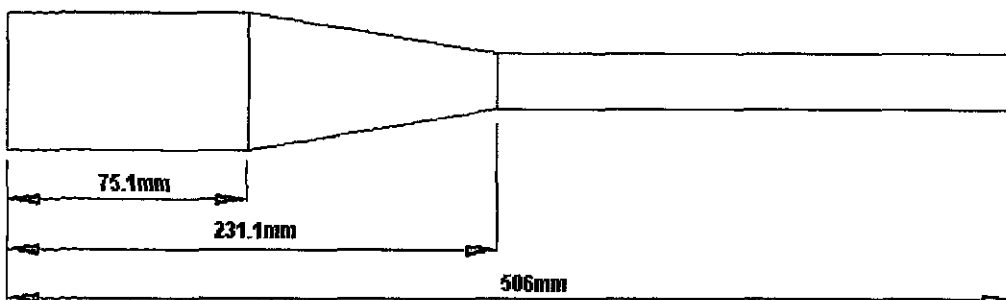
Figure 5.1: Sketch of 506mm tapered wire waveguide used for short wire measurements

The experimental results for the 506 mm tapered wire waveguide are shown in Figure 5.2 and indicate experimental values show a standing wave structure similar to that previously found by Gavin *et al* [47]. These results indicate that there is a standing wave with a series of displacement maxima and minima.
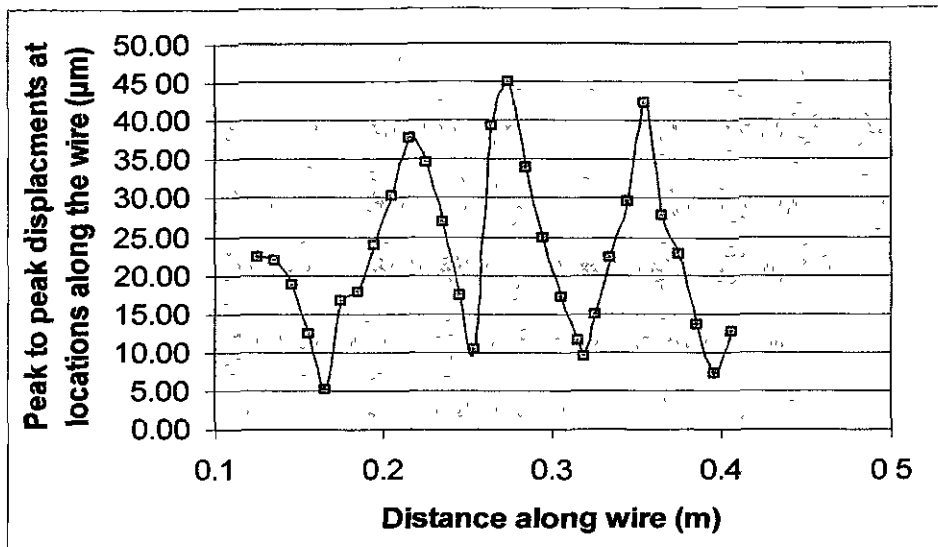
Figure 5.2: Experimental values for short tapered wires

The gain in amplification due to the taper is proportional to the ratio of the entry and exit diameters. The ratio of these diameters is 2.8. Experimentation showed a gain due to the taper is 2.4. Hence the taper is producing amplitudes 15% less than predicted by the numerical model. The reason for the loss may be due to damping.

5.3 Long Tapered Wire Waveguides

5.3.1 Optical Microscope Measurements

Experiments were carried out with a power level setting of 1 and a peak-to-peak input displacement of approximately 20μm. Wire lengths between 1.57m and 1.85m were tested in 5-10mm intervals with peak-to-peak displacements ranging from 62 to 197μm. Experimental values of peak-to-peak displacements for long tapered wire waveguides were examined using the optical microscope methodology. The wire waveguides are placed in a 1.6mm diameter catheter, which is fixed straight (Figure 5.3) to restrict the movement of the wire waveguide to one direction. The reason for this is when the wire is not restricted the wire tends to whip in a transverse as well as longitudinal motion. It must also be noted that the optical microscope

64

method is usually used to capture an image at a magnification of 40X. The wire is too flexible to obtain a repeatable measurement at this magnification due to transverse whipping even though the wire is held straight as possible with out restricting it, so a magnification of 16X was used.
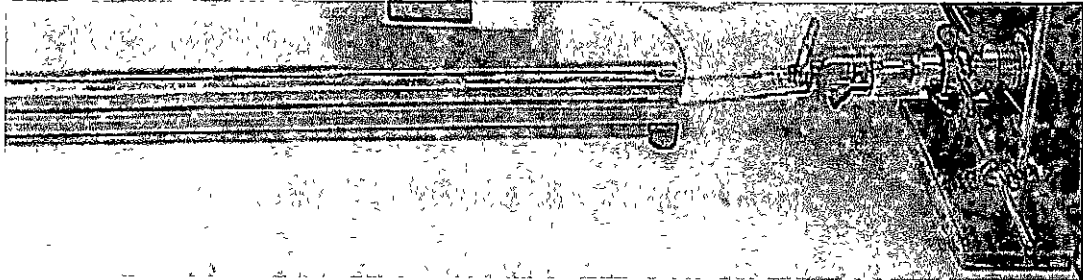
Figure 5.3: Long tapered wire waveguide restricted by catheter and fixed straight

For lengths of wire waveguide between 1.75m and 1.85m the device did not operate. It is possible that excess mass of the wire waveguide in addition to the acoustic horn prevented the system from working efficiently. Comparing the mass of a tapered wire waveguide and a 1mm diameter, shown in Figure 5.4, it can be seen that the mass of the tapered wire waveguide with a length greater than 1.75m is similar to the mass of a1mm diameter wire waveguide 0.33m in length. Experiments have shown that ultrasound is not transmitted over lengths greater than 0.33m (which correspond to a weight of 1.67grams).
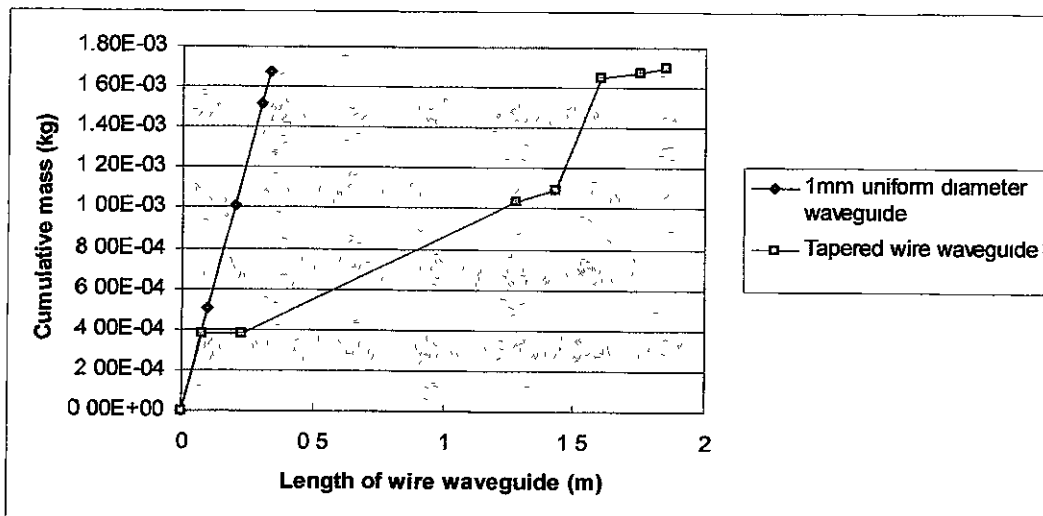
Figure 5.4: Mass comparison of uniform 1mm diameter and tapered wire waveguides

65

Table 5.1 summarises experiments conduced with a range of wire lenghs, diameters and distal outputs and records of the ablation characteristics observed. This is graphed in Figure 5.5. Distal tip displacements did not form a regular cyclic pattern as observed by Gavin *et al* [47]. The distal tip displacements magnitudes are also higher than previous observations of short wire waveguides.

According to the analytical equation (Appendix A) and modal analysis there should be three anti-resonant lengths at 1.59m, 1.66m and 1.74m, respectively. As can be seen on the graph and Table 5.2, there are peaks, which correspond to these lengths. However, the magnitudes of the peak-to-peak displacements are much higher than expected.

| Length of wire (mm)	Diameter of wire (mm)	Peak-to -peak tip displacements (µm)	Observed ablation characteristics
1750	0.205	108.8	Hammer action, Scraping Action, Causes damage to chalk
1741	0.205	167.2	Hammer action, Scraping Action, Causes damage to chalk
1733	0.203	70.8	Small scraping action
1722	0.204	192.7	Further reduced scraping action with no drilling
1709	0.208	102.2	Large amount of scraping with some drilling
1697	0.207	103 3	Slightly reduced scraping action
1688	0.204	97.8	Further slight decreased scraping action from previous measurement
1679	0.207	73.73	Reasonably good scraping with small amount of drilling
1673	0.204	86.86	Drilling, Large amount of scraping, Causes damage to chalk
1666	0.200	91.97	Drilling, Large amount of scraping, Causes damage to chalk
1654	0.202	125.5	Scraping and Causes some damage to chalk
1644	0.202	75.91	Scrapes well with some drilling
1634	0.205	78.85	Scrapes well with some drilling
1624	0.203	65.59	Scrapes with some drilling
1612	0.200	62.65	Scrapes well with some drilling
1600	0.202	135	Scraping well with some drilling
1587	0.193	83.94	Drilling, Large amount of scraping, causes damage to chalk
1577	0.203	80.30	Drilling, Large amount of scraping, causes damage to chalk

Table 5.1: Lengths, diameters, average peak-to-peak displacements for varying lengths of tapered wire waveguide including observed ablation characteristics during testing

Based on the finite element model, with an input of 20µm and a constant damping value of 4.5%, the displacement at the tip over 1.5m should be reduced to less than 10µm in the longitudinal direction. However over lengths between 1.57-1.75m distal tip peak-to-peak displacements between 62-197 µm were determined. The reason for these high amplitudes may be due to the wire waveguide diameter size and hence the flexibility of the wire waveguide.

With short wire waveguides, the main action of direct contact is in the longitudinal direction. However, the damage exhibited by long wires has a slightly different effect. The long wire waveguides moves longitudinally but also due to their flexibility transversely.
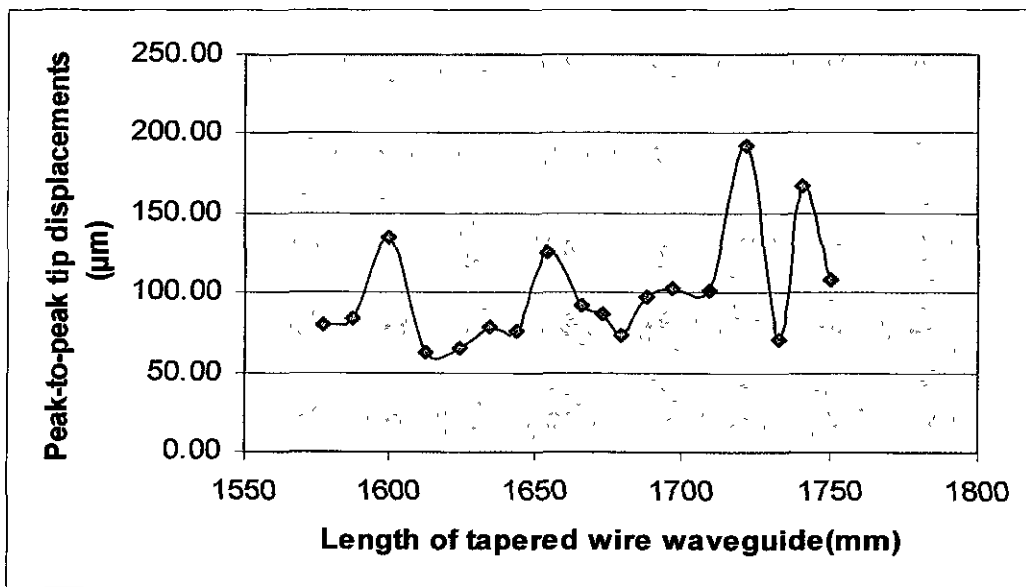

Figure 5.5: Amplitudes of peak-to-peak tip displacements for varying lengths of 0.2mm wire waveguide

Modal Analysis (m)	Optical Measurement Peaks (m)
1.59	1.60
1.66	1.65
1.74	1.73

Table 5.2: Comparison of modal analysis anti-resonant lengths and peak values obtained for long wire waveguides

Although the long tapered wire waveguide is restricted from transverse movement by the catheter, the difference in diameters between the wire waveguide and the catheter allows some transverse motion, which over a long length increased the peak-to-peak displacements. It is believed that a whipping motion starts shortly after the first taper.

With the short wire waveguides, the longitudinal motion acts directly into the material and with the long wires there appears to be a combination of an axial motion and a transverse whipping action that causes the tip to ablate through the material. This is illustrated in the Figure 5.6.

For long, low profile wires it is not possible to make distal output measurements by either laser sensor or optical microscope methods. Therefore, a qualitative method of assessing output or ablation performance is required
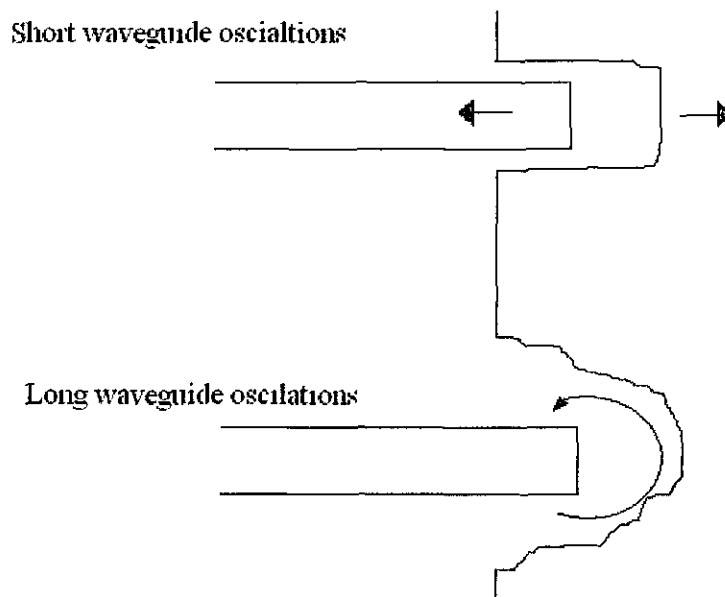
Figure 5.6: Comparative motion of long and short tapered wire waveguides

5.3.2 Proof of Concept –Ablation of Model Material

As the wire waveguides were reduced in length, they were examined visually for damage on calcium carbonate (blackboard chalk). In order to quantify the damage done to the calcium carbonate by the wire waveguide a scale from *No Transmission* to *Steady Damage* shown below has been devised (Table 5.3). Ideally the device should be operated in the highest region (*Steady Damage*) in order to achieve maximal

damage but operating the device in lower regions will cause some damage to the material.

Scale	Damage caused by Ultrasonic Device on Calcium Carbonate
No Transmission	No ultrasonic wave transmission at waveguide tip, No waveguide tip movement, No drilling action, No damage caused calcium carbonate
No Damage	Waveguide tip starts to move but no apparent ultrasonic wave transmission, No drilling action, No damage caused to calcium carbonate
Minimal Damage	Waveguide tip movement with intermittent ultrasonic wave transmission, No drilling action but minimal damage to calcium carbonate by a scraping action
Slow Damage	Waveguide tip movement with a build up and breakdown response of ultrasonic wave transmission, Slight drilling action, Obvious material removal of calcium carbonate but requires time for significant damage to be attained
Steady Damage	Clear and constant Ultrasonic wave, Consistent-drilling action with maximum damage caused by tip of ultrasonic waveguide device by drilling through material easily. Cause ablation at an approximate speed of 1.4mm/s

Table 5.3: Scale of damage to calcium carbonate

For a number of wire waveguide lengths (1.57-1.75m), the tapered wire waveguide was placed into a catheter, which held the wire waveguide straight reducing any whipping or bending. A calcium carbonate specimen was then placed at the distal tip of the tapered wire waveguide and the wire waveguide was moved forward into the calcium carbonate and any damage caused was noted which can be seen in Table 5.1. All of the lengths were tested to examine the ability of the wire waveguide to ablate model materials at a power dial setting of 1. For wire lengths in between 1587-1624mm and 1666-1697mm the results showed that *Steady Damage* was achieved. This corresponds well with a previous study [47] showing that *Steady Damage* occurs at anti-resonant lengths.

As the wire lengths moved away from these regions the amount of damage done to model materials was reduced, corresponding to a damage scale of *Minimal Damage*. Results showed that the tapered wire waveguide produced damage to model materials at all lengths. This is not the case in uniform cross section wires showing no damage to materials at lengths close to anti-nodes. It showed be noted that this scale is based on observation and a more sophisticated measurable damage criteria if further testing is carried out.

5.4 Effect of Bending on Tapered Wire Waveguide Performance

Some preliminary experiments were conducted to evaluate the performance of tapered wire waveguides in transverse bends and curves to represent *in vivo* configurations as it passes through the arterial lumen to the location of an atherosclerotic lesion.

A test rig was constructed to hold the waveguide and create specified positions that would allow the effect of bending on the waveguide to be examined, and eventually simulate the path of the wire through the vasculature to the location of the blockage. The test rig was designed to be modular using aluminium bars with profiles that allowed the test rig to be collapsible as well as adjustable, (Figure 5.7).

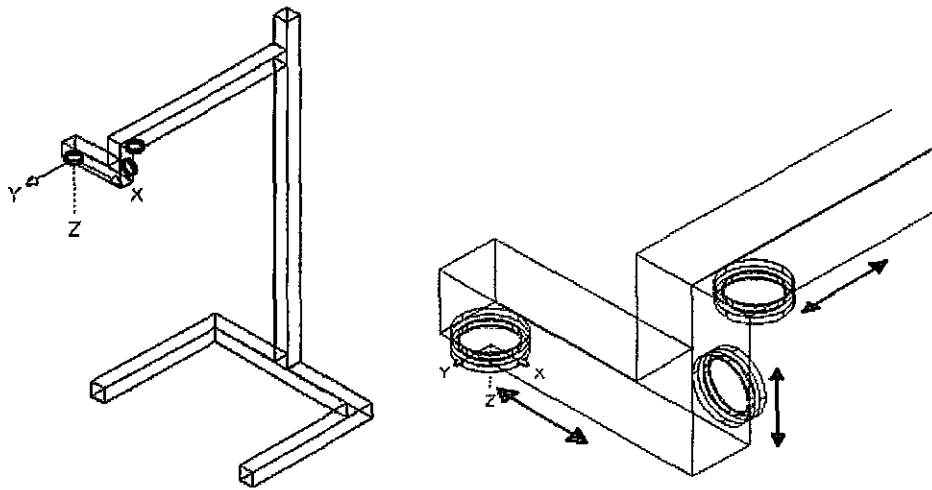Figure 5.7: Sketch of rig designed to test bend in wire waveguides

The rig can be adjusted to examine three main bending scenarios:

    a. A single bend with various radii in the X-Y plane (Figure 5.8a)

    b. A double bend with various radii in the X-Y and Y-Z planes respectively (Figure 5.8b)

    c. A model that is similar to the bends that the waveguide would encounter in the human body

70
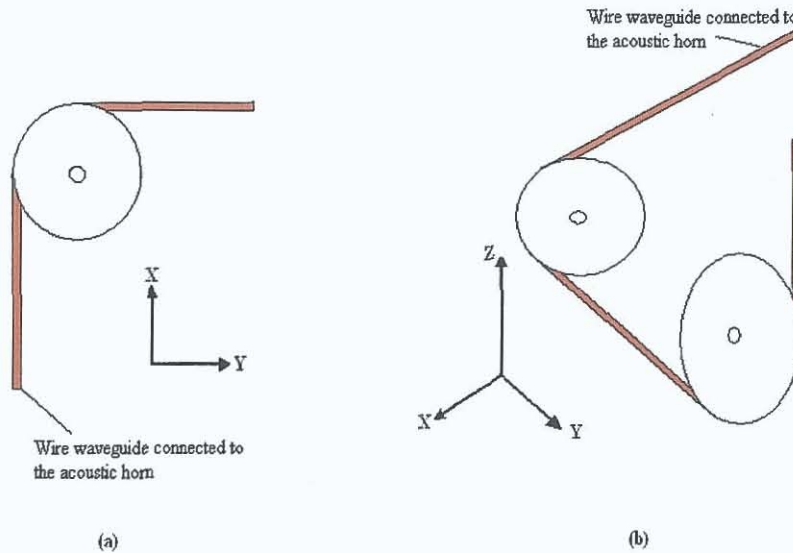
Figure 5.8 (a) and (b): Bend testing scenarios

5.4.1 Effect of Single Bends

All experiments were carried out using a tapered wire waveguide of 1577mm in length. The length from the bend to the wire waveguide distal tip (D) was varied. The radii (R) used for the experiments were 20mm and 40mm, which are similar to the radius or curvature in the arterial tree. The distance between bend angle and distal tip (D) was set at 30 mm, 70mm, 150 mm, 250 mm, 500 mm, 750 mm. Bend angles (λ) were measured from 0-180° (Figure 5.9). For all experiments bends power dial settings ranged from 1-7. The power dial settings and corresponding acoustic horn peak-to-peak inputs from Chapter 3 are shown in Table 5.4. Experimental observations indicate that the location of the bend in the waveguide does not significantly affect the ablation performance.

Power dial settings	Acoustic horn Inputs (μm)
1.5	32
2	36
2.5	41
3	45
3.5	49
4	52

Table 5.4: Power dial settings for the ultrasonic device and the associated acoustic horn peak-to-peak displacement outputs into the wire waveguide
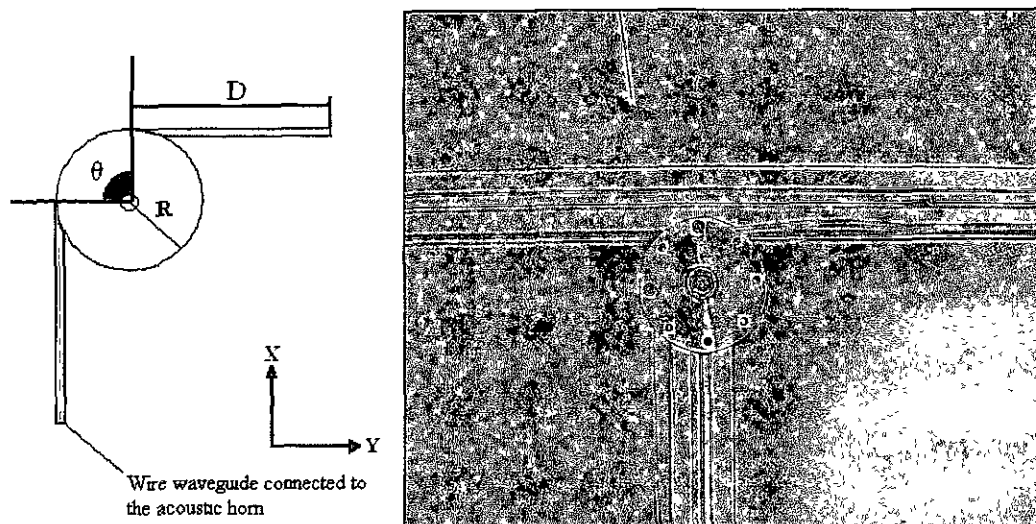
Figure 5.9: Schematic of single bend experiments set up

Table 5.5 shows that 90°-180° bends reduce the ability of the device to cause *Steady Damage* at the original power dial setting and requires a power dial setting increase to cause *Steady Damage* in the same manner as prior to bending. The associated acoustic horn peak-to-peak displacement inputs delivered to the wire waveguide are shown in Table 5.3. It was also noted that smaller radii had a greater effect on the reduction in transmission than the larger radii.

Bend Radius (R)	λ 0° (Straight)		λ 45°		λ 90°		λ 180°	
	Power Dial Setting	Damage	Power Dial Setting	Damage	Power Dial Setting	Damage	Power Dial Setting	Damage
20	1	*Steady*	1	*Steady*	2	*Steady*	2.5	*Steady*
40	1	*Steady*	1	*Steady*	2	*Steady*	2	*Steady*

Table 5.5: Power dial settings required to cause *Steady Damage* of calcium carbonate with a long waveguide around a single bend.

5.4.2 Effect of Double Bends

These experiments consist of a wire waveguide curving around two bend radii (Figure 5.10). The tapered wire waveguide used was 1577mm in length. From Figure 5.10, the first bend radius is denoted by R_1 with a bend angle θ and the second bend, which is closest to the distal tip of the wire waveguide, is R_2 with a bend angle δ. The distance between the first and second bend is denoted by D_1 and the distance between the second bend to the distal tip of the wire waveguide is denoted by D_2. There are two different bend radii, 20mm and 40mm. Three configurations were examined, using the notation R_1/R_2, these were 40/20, 20/ 40, 20/20.

In the first set of experiments the first bend with a radius of 40mm (R_1), the bend angle remained fixed at $90°$ (θ) and the second bend 20mm (R_2), varied from $45°$-$135°$ (δ) for each measurement over varying distances from the tip. The distance between the bends (D_1) is constant and the distance from the distal tip of the wire waveguide to the second bend (D_2) is varied from 50-300mm in 50mm intervals. Experiments were then repeated fixing δ and D_2. For all experiments power dial settings ranged from1-7 in order to determine the required power dial setting increase to cause *Steady Damage* in the same manner as prior to bending.

This process was repeated for the other two configurations. The power dial settings required in order to cause *Steady Damage* to the calcium carbonate for all configurations in each set of experiments are summarized in Tables 5.6- 5.9. These power dial settings correspond with acoustic horn inputs shown in Table 5.4.

From these Tables and Figure 5.11 it can be seen that the location of the bends does not significantly impact the ablative abilities of the wire waveguide. The size of the bend radius and the bend angles do have an impact, requiring a power input increase for each time the radius of the bend decreased and the bend angle increased. The power dial setting required to cause *Slow Damage* to calcium carbonate with a straight wire was 1. The power dial setting was increased to a maximum of 3.5 for the most tortuous of the experiments over two 20mm bend radii with one bend angle at $90°$ and the other at $135°$. This represents an increased displacement input from the acoustic horn of $20\mu m$ peak-to-peak. It can also be noted that these experiments shows a similar result to the single bend experiments that an increase in power will result in increased ability of the ultrasonic wave to be transmitted around a variety of bends.
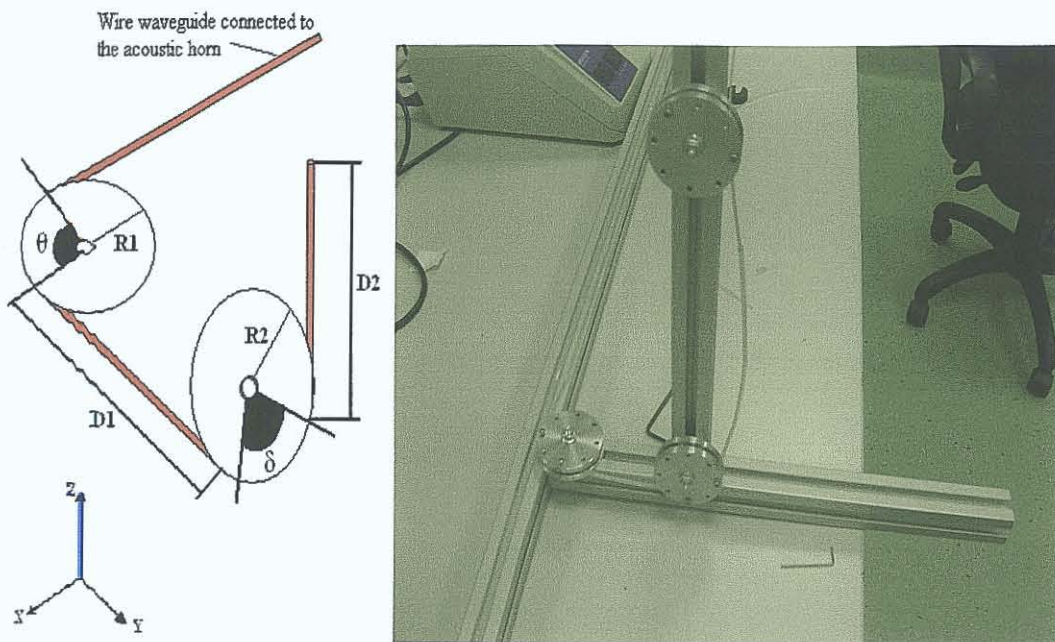
Figure 5.10: Schematic of double bend experiments set up

Configuration	θ - 45°		θ - 90°		θ -180°	
	Power Dial Setting	Damage	Power Dial Setting	Damage	Power Dial Setting	Damage
D_1 fixed / D_2 varying from 5-30cm	2	*Steady*	2.5	*Steady*	3	*Steady*
D_2 fixed / D_1 varying from 5-30cm	2	*Steady*	2.5	*Steady*	3	*Steady*

Table 5.6: Power dial settings required to cause *Steady Damage* of calcium carbonate with a long waveguide around both 40/20mm and 20/40mm configurations with the first bend angle (θ) fixed at 90°.

Configuration	δ - 45°		δ - 90°		δ - 135°	
	Power Dial Setting	Damage	Power Dial Setting	Damage	Power Dial Setting	Damage
D_1 fixed / D_2 varying from 5-30cm	2	Steady	2.5	Steady	3	Steady
D_2 fixed / D_1 varying from 5-30cm	2	Steady	2 5	Steady	3	Steady

Table 5.7: Power dial settings required to cause *Steady Damage* of calcium carbonate with a long waveguide around both 40/20mm and 20/40mm configurations with the second bend angle (δ) fixed at 90°.

Configuration	*θ - 45°*		*θ - 90°*		*θ - 135°*	
	Power Dial Setting	Damage	Power Dial Setting	Damage	Power Dial Setting	Damage
D_1 fixed / D_2 varying from 5-30cm	2 5	Steady	3	Steady	3 5	Steady
D_2 fixed / D_1 varying from 5-30cm	2 5	Steady	3	Steady	3 5	Steady

Table 5.8: Power dial settings required to cause *Steady Damage* of calcium carbonate with a long waveguide around a 20mm/20mm configuration with the first bend angle (θ) fixed at 90°.

Configuration	δ - 45°		δ - 90°		δ - 135°	
	Power Dial Setting	Damage	Power Dial Setting	Damage	Power Dial Setting	Damage
D_1 fixed / D_2 varying from 5-30cm	2 5	Steady	3	Steady	3 5	Steady
D_2 fixed / D_1 varying from 5-30cm	2.5	Steady	3	Steady	3.5	Steady

Table 5.9: Power dial settings required to cause *Steady Damage* of calcium carbonate with a long waveguide around a 20mm/20mm configuration with the second bend angle (δ) fixed at 90°.
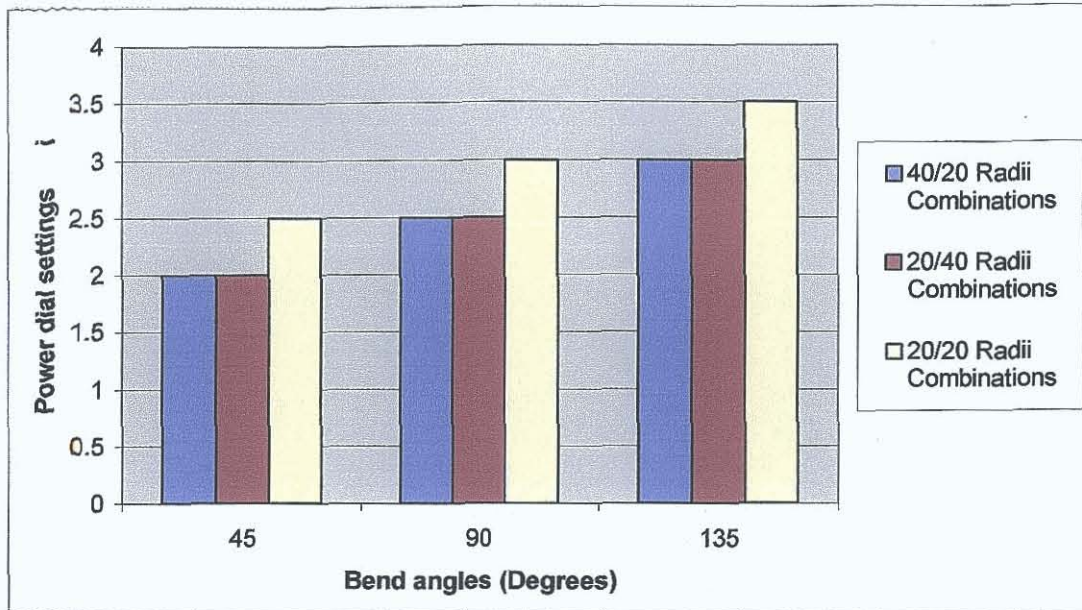
Figure 5.11: Increasing bend angles requires increased power dial settings in order to maintain *Steady Damage* for all double bend configurations

5.4.3 *In vivo* Configuration

For the *in vivo* "over the arch" configuration shown in Figure 5.12, a wheel with a radius of 40mm was used, as this is a close approximation to the adult human aortic arch. Three other wheels of radius 20mm were used to represent various bends of the coronary arteries. The wire passes through a 135° angle over Wheel 1, in order to simulate the configuration of a catheter in an *over-the-arch* position. Wheel 2 bends the wire through approximately 22.5° and Wheels 3 and 4 cause 90° curvatures. This is a similar structure to devices for testing the force to push catheters through the system. The *in vivo* configuration required a further increase (power dial setting 7) to produce *Steady Damage* of the model material. This shows that the ultrasound energy can be transmitted via NiTi wires through long, tortuous paths similar those encountered in minimally invasive cardiology procedures.
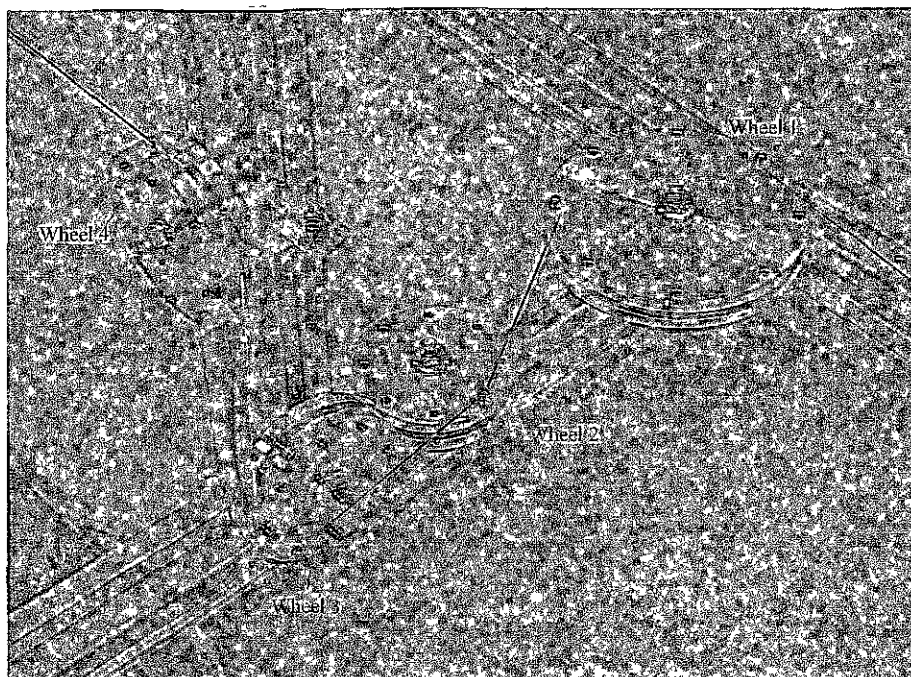
Figure 5.12: Rig set up to test bending in wire waveguides around a similar path to clinical configuration

5.5 Conclusions and Discussion

In straight wires, transmission and steady damage can be achieved at the lowest power setting. The transmission of ultrasound of ultrasound in wire waveguides is affected by:

- Small bend radii (i.e. increased curvature)
- Increased bend angles

It is believed that introducing bends to the wire waveguides increases stresses in the material reducing the ability of the wire to transmit the ultrasonic wave as discussed in Chapter 3. Increasing the curvature and angle increases the stresses in the wire further and hence requiring increased input from the ultrasonic horn to compensate for these changes. Transmission through complex pathways can be achieved by increasing the power setting to achieve a suitable output.

After the design and experimentation using low-profile long tapered wire waveguides in numerous straight and tortuous configurations the design inputs and requirements of ultrasonic waveguides are re-examined. Table 5.10 shows an evaluation of results against the design criteria. From this comparison it is believed that the device constructed has potential for clinical use, and has been brought to the stage of being suitable for use in further pre-clinical and then animal trials.

77

	Design Input	Design Output (with acceptance criteria)	Verification	Validation
1	**Geometric**			
1.1	Wire waveguide must be of sufficient length to reach coronary arteries when introduced via the femoral artery.	Wire must be >1.4 m in length.	Prototypes up to 1.75 m developed (Chapter 5)	Prototypes navigated through over-the-arch configuration (Chapter 5).
1.2	Wire waveguide must be sufficiently low profile to traverse arterial system in combination with a standard guidewire and catheter arrangement.	Wire profile must be ≤ 0.35 mm at the distal end (coronary arteries), and ≤ 15 mm for the main shaft (femoral and aortic arteries).	Wire diameters of 1.0mm, 0.35 and 0.2 mm measured, and within tolerance.	Prototypes navigated through over-the-arch configuration (Chapter 5).
2	**Mechanical**			
2.1	Wire waveguide must be sufficiently flexible to permit navigation of the arterial system.	Specification of a maximum 1mm diameter. Specification of superelastic material (NiTi).	Distal diameters of 0.35 and 0.2 mm measured, and within tolerance. NiTi #1, Fort Wayne Metals used.	Prototypes navigated through over-the-arch configuration (Chapter 5).
2.2	Wire waveguide must operate at ultrasonic frequency and set up standing waves in the wire.	22.7±0.5kHz generator specified.	Wire waveguide distal tip measured by laser sensor over full power range, and shown within tolerance.	Steady damage shown for wire waveguides up to 1.75 m in length.
2.3	Must operate reliably (specifically at connection point).	Specification of wire diameter at connection of ≥1mm.	Proximal dire diameter of 1.0mm measured within tolerance.	Reliable operation of the device at power level 7 for a duration of 5 minutes with no fracture of wire waveguides.

	Design Input	Design Output (with acceptance criteria)	Verification	Validation
2.4	Wire waveguide must not damage catheter or other peripherals during ultrasonic activation.	Wire waveguide must not exceed 40°C during normal operation.	Wire waveguide was inspected for friction or heat damage after operation of wire in catheter for 5 minutes with a variety of power levels.	After operation of the wire waveguide in a catheter visible inspection showed minor friction and heat damage at points along the catheter however this did not appear to significantly affect the catheter.
3	**Biological Interaction**			
3.1	Wire material must not initiate any adverse biological reaction.	Biocompatible NiTi by Fort Wayne Metals 56% Nickel 43.14% Titanium 0.033% Carbon 0.028% Oxygen 0.025% Hydrogen.	Fort Wayne Metals produce all documents from FDA and ISO standards demonstrating biocompatibility of their NiTi #1.	
3.2	Ultrasonic energy must not initiate any adverse biological or cellular reaction.	Cells exposed to ultrasonic energy at operating power levels (1-7) for 10 minutes duration should exhibit normal morphology, proliferation and apoptosis with respect to a control.	Examination of bovine aortic endothelial and smooth muscle cell proliferation after application of a 1mm ultrasonic wire waveguide at a acoustic horn input of 35µm peak-to-peak carried out in Vascular Research Center at DCU.	Unpublished data from these studies shows no significant difference of the proliferation between control cells and cells after the application of ultrasonic wire waveguide. (This testing was outside the scope of this project)

79

	Design Input	Design Output (with acceptance criteria)	Verification	Validation
3.3	Must ablate calcified arterial plaque.	Must ablate a model plaque material (calcium carbonate) at a rate of 1.4mm per minute.	0.2 and 0.35mm wire waveguide used to ablate through a rigid calcium carbonate specimen.	Wire waveguide ablated through a 10mm thick specimen repeatedly, taking between 7 to 10 seconds each time.
3.4	Must leave healthy arterial tissue undamaged.	Excised arterial tissue exposed to ultrasonic energy *in vitro* at power levels (1-7) for 10 minutes duration should exhibit normal morphology, with respect to a control.	This is beyond the scope of this project.	Other devices have been shown to ablate material but no clinical trails have been produced to examine arterial tissue damage.

Table 5.10: Comparison of design criteria for tapered wire waveguides against experimental results.

Chapter 6

Conclusions and Proposed Future Work

6.1 Conclusions from this Work

The concept that ultrasonic displacements capable of ablating model materials can be transmitted through tortuous configurations via long, flexible, low profile tapered wires has been proven. An experimental approach for measuring the frequency output of NiTi wire waveguide has been developed. A design methodology for tapered wire waveguides for the ultrasound angioplasty application has also been introduced.

6.2 Summary of Results

- The frequency output of ultrasonic wire waveguides has been directly measured using a laser sensor. The sensor showed good agreement with the earlier optical microscope measurement method, producing results that are within ±5μm. During testing the laser sensor measurements show that it can take up to a minute before the wire waveguide settles at a specific frequency and as the power dial settings are increased the frequency is also increased. It was also noted during ablation testing that the device required time before ablating material effectively. Information on frequency changes and settling time is important as it may take some time before full ablation ability is reach for the device in clinical practice.

- A wire waveguide with a combination of a small proximal diameter, reliable connection method and capable of transmitting ultrasonic waves over a large distance in order to access coronary arteries is capable of ablating material.

81

With that in mind a tapered wire waveguide was designed using finite element analysis and produced a full-length (2m) wire with a 1mm diameter proximal end, a 0.35mm diameter mid section, a 0.2mm diameter distal end and two tapered sections reducing the diameters.

● For peak-to-peak input displacements of 50μm, a uniform cross section wire waveguide with a length greater than 1.5m would theoretically result in output peak-to-peak displacements of 2.5μm. However tapered wire waveguides can theoretically result in output peak-to-peak displacements 7 times larger than uniform cross section wire waveguides. This would be a significant difference when trying to keep the output peak-to-peak displacements at a sufficient level to ablate occluded coronary arteries. In practice, even greater displacements are seen due to a whipping motion in slender wire waveguides. This may be a potential problem but if controlled effectively it may be turned to advantage.

● Smaller bending radii and larger bend angles had a greater effect on the transmission of ultrasonic waves in long wire waveguides than the larger bend radii or smaller bend angle. For the approximate *in vivo* configuration, the long tapered wire waveguide performed well causing damage to calcium carbonate model materials. However the input power needed to cause observable damage was much greater than for the straight wire scenario. The wire configuration can therefore be expected to affect distal outputs in clinical situations (e.g. difference between coronary and femoral arteries).

6.3 Future Work

Tapered wire waveguides were designed, increasing the reliability and operational lengths. The waveguides have been shown to cause damage to rigid material over lengths up to 1.75m and around various bend radii and angles. A new system is needed to more accurately characterise the distal tip displacements of long tapered wire waveguides. Future work is needed in order to fully understand

82

the effects of long wire waveguides and its effects on plaque and other biological material. Possible future work in this area may be:

- Experimental investigations, using the laser sensor, of distal tip displacements for tapered wire waveguides over lengths greater than 1.4m, determination of the distal tip displacements as wire waveguide lengths approach resonant lengths and the associated effects on ultrasound transmission.

- Numerical modelling and experimental investigation of tapered wire waveguides with bending to more thoroughly determine all mechanisms occurring.

- Testing of the ultrasonic wire waveguide apparatus on biological tissue and fluids to identify mechanism of ablation and disruption.

References

[1]   National Center for Chronic Disease Prevention and Health Promotion. (Homepage). [Online]. Available from: [Accessed 10 September 2006]. http://www.cdc.gov/nccdphp/aag/aag_cvd.htm

[2]   World Health Organisation. Publications, World Health Report, 2005

[3]   American Heart Association. Publications, International Cardiovascular Disease Statistics, 2004

[4]   American Heart Association. Publications, Heart Disease and Stroke Statistics-Update, 2003

[5]   Irish Heart Foundation, Reports and Position Statements: Mortality from Cardiovascular Disease (CVD), 2005

[6]   Ariani M, Fishbein M, Chae JS, Sadeghi H, Don Michael TA. Dubin SB and Siegel RJ. Dissolution of Peripheral Arterial Thrombi by Ultrasound, *Circulation*, 84, pp 1680- 1688, 1991

[7]   Huber KC, Kirk GN, Schwartz RS, Edwards WD. Chapter 7: Pathology of Post-interventional Coronary Restenosis. In: Coronary Restenosis Philadelphia, 1996.

[8]   Bauters C, and Isner JM,. The biology of restenosis. In: E.J. Topol, Editor, *Textbook of Cardiovascular Medicine*, Lippincott-Raven, Philadelphia, Pennsylvania, pp. 2465–2490, 1998

[9]   Harmann A and Kaltenbach M. Chapter 2: Approaches to Total Coronary Occlusions. In: Topol EJ and Serruys PW (eds.). *Current Review of Interventional Cardiology*, Philadelphia, 1994

[10] Loree HM, Grodzinsky AJ, Park SY, Gibsom LJ and Lee RT. Static Circumferential Tangential Modulus of Human Atherosclerotic Tissue. *J. Biomech.*, 27(2), pp 195-204, 1994

[11] Topoleski LDT, Salunke NV, Humphrey JD and Mergner WJ. Composition and history-dependent radial compressive behaviour of human atherosclerotic plaque. J. Biomed. Mater. Res., 35, pp 117- 127, 1997

[12] Parsons JE, Cain CA, Abrams GD, And Fowkles JB. Pulsed Cavitational Ultrasound Therapy for Controlled Tissue Homogenization, Ultrasound in Med.& Biol. Vol 32, (1), pp115-129, 2006

[13] Damianou C, Hynynen K. Focal spacing and near-field heating during pulsed high temperature ultrasound therapy. Ultrasound Med Biol, Vol.83, Issue 6, pp777-787, 1988

[14] Rosenschein U, Rozenszajn LA, Kraus L, Marboe CC, Watkins JF, Rose EA, Cannon PJ and Weinstein JS. Ultrasonic Angioplasty in Totally Occluded Peripheral Arteries, *Circulation*, Vol. 83, Issue 6, pp 1976 1985, 1991

[15] Siegel RJ, Fishbein MC, Forrester J, Moore K, DeCastro E, Daykhovsky Z and Don Michael TA. Ultrasonic Plaque Ablation: a new method for recanalisation of partially or totally occluded arteries. *Circulation*, 78, pp 1443- 1448, 1988

[16] Stone GW, Nicolaus RJ, Issam I, Hoye A, Cox DA, Colombo A, Baim DS, Teirstein PS, Strauss BH, Selmon M. Percutaneous Recanalization of Chronically Occluded Coronary Arteries: A Consensus Document: Part II, Circulation, 112, pp2530-2537, 2005

[17] Siegel RJ, Gaines P, Crew JR and Cumberland DC. Clinical Trial of Percuntaneous Peripheral Ultrasound Angioplasty. *JACC*, 22, (2), pp 480-488, 1993

[18] Steffen W, Fishbein MC, Luo H, Lee DY, Nita H, Cumberland DC, Tabak SW, Carbonne M, Maurer G and Seigel RJ. High Intensity, Low Frequency catheter-delivered ultrasound dissolution of occlusive coronary artery thrombi: An *in vitro* and *in vivo* study. *J. Am Coll Cardiol*, 24, pp 1571-1579, 1994

[19] Seeley RR, Stephens TD, Tate P, Chapter 21: Cardiovascular System: peripheral circulation and regulation, In: Essentials of anatomy & physiology, 4th edition, Boston, 2005

[20] Hayashi K. Mechanical Properties of Arterial Wall. In: *Biomechanics of Soft Tissue in Cardiovascular Systems International.* (eds) Holzapfel GA and Ogden RW. New York, Springer-Verlag Wien, 2003

[21] Stary HC. Chapter 26: The histological classification of atherosclerotic lesions in Human Coronary Arteries. In: Fuster V, Ross R and Topol EJ (eds.). Atherosclerosis and Coronary Artery Disease, Lippincott- Raven Publishers, Philadelphia, 1996

[22] Oh S, Kleinberger M and McElhaney JH. Finite element analysis of balloon angioplasty. *Med. Biol. Eng. Comput.*, 32, pp 108- 114, 1994

[23] Folland ED. Chapter 1: Balloon Angioplasty. In: Topol EJ and Serruys PW (Eds.). *Current Review of Interventional Cardiology*, Philadelphia, 1994

[24] De Jaegere PPT, De Feyter PJ and Serruys PW. Chapter 8: Intracoronary Stenting. In: Topol EJ and Serruys PW (eds.). Current Review of Interventional Cardiology, Philadelphia, 1994

[25]   Lee RT, Loree HM, Cheng GC, Lieberman EH, Jaramillo N and Schoen FJ. Computational structural analysis based on intravascular ultrasound imaging before *in vitro* angioplasty: prediction of plaque fracture location, J. Am. Coll. Cardiol., 21(3), pp 777-782, 1993

[26]   Cardiovascular Research Foundation. (Homepage). [Online]. Available from: [Accessed 10 December 2007] http://www.cvrf.org/conference/cto2007/factoid/02.pdf

[27]   Lefèvre T, Louvard Y, Loubeyre C, Dumas P, Piéchaud J.F, Krol M, Benslimane A, Premchand R.K and Morice M.C. A randomized study comparing two guidewire strategies for angioplasty of chronic total coronary occlusion. The American Journal of Cardiology, Vol. 85, Issue. 9, 1144-1147, 2000

[28]   Fitzgerald PJ, Takagi A, Moore P, Hayase M, Kolodgie FD, Corl D, Nassi M, Virmani R and Yock PG. Intravascular Sonotherapy Decreases Neointimal Hyperplasia After Stent Implentation in Swine, Circulation, Vol.14, Issue. 103 1828-1831, 2001

[29]   Kuntz RE, Cox N, Ho K, Fitzpatrick M, Girl S, Cutlip DE, and Popma, JJ. Late Angiographic Assessment of the Edge Effect and Restenosis Associated with Intraluminal Sonotherapy: Results from the SILENT (Sonotherapy for In-Lesion Elimination of Neointimal Tissue) Trial, JACC, 2002

[30]   Results of EuroSPAH Intravascular Sonotherapy(R)* Trial Presented at European Society of Cardiology (ESC) Meeting; 40% Reduction in Revascularization Reported (Homepage) [Online]. Available from: [Accessed 15 January 2007]. http://goliath.ecnext.com/coms2/gi_0199-2032446/Results-of-EuroSPAH-Intravascular-Sonotherapy.html#abstract

[31]   Yock PG and Fitzgerald PJ. Catheter-based Ultrasound Thrombolysis: Shake, rattle and reperfuse. Circulation, 95: pp 1360-1362, 1997

[32]   Atar S, Luo H, Nagai T and Siegel RJ. Ultrasonic Thrombolysis: catheter-delivered and transcutaneous applications. *European Journal of Ultrasound*, 9, pp 39-54, 1999

[33]   Sobbe A, Trubenstein G, Stumpff U, Figge H and Kozuschek W. Die Ultraschall Auflosung von Thromben. *Klin Wochenschr*, 52, pp 1117-1121, 1974

[34]   Perkins JP. Power Ultrasonic Equipment: Practice and Application. (Based on a paper presented at the Sonochemistry Symposium, Annual Chemical Congress, Warwick University, UK, 8-11 April 1986

[35]   Belford J.F. Morgan Electroceramics Ltd. The Stepped Horn. Technical Publication paper TP-214. 2004

[36]   Fischell TA, Abbas MA, Grant GW, Siegel RJ. Ultrasonic Energy: Effects on vascular function and integrity, *Circulation*, 84, pp 1783-1795, 1991

[37]   Demer LL, Mehrdad A and Seigel RJ. High Intensity Ultrasound Increases Distensibility of Calcific Atherosclerotic Arteries. *JACC*, 18 (5), pp 1259-1262, 1991

[38]   Burdic WS. Underwater Acoustic System Analysis. 2nd Edition Prentice Hall. 1991

[39]   Nyborg WL. Chapter 1. Basic Physics of Low Frequency Therapuetic Ultrasound. In: Ultrasound Angioplasty. Developments in Cardiovascular Medicine. (Ed. by Siegel RJ). Kluwer Academic Publishers, 1996

[40]   Lee CP and Wang TG. Outer acoustic streaming. Journal of the Acoustical Society of America, Vol.40, pp 1363-1370. 1990

[41]   Morse PM. 1981. Acoustical Society of America, Vibration and Sound, New York, Section 27, 311-326, 1981

[42]   Makin RS and Everbach EC. *J. Acoust. Soc. Am.*, Vol. 100(3), pp 1855-64, 1996

[43]   Cimino WW and Bond LJ. Physics of Ultrasonic Surgery Using Tissue Fragmentation: Part I, Ultrasound in Med.& Biol. Vol. 22, (1), pp89-100, 1996

[44]   Cimino WW and Bond LJ. Physics of Ultrasonic Surgery Using Tissue Fragmentation: Part II, Ultrasound in Med.& Biol. Vol. 22, (1), pp101-117, 1996

[45]   Flowcardia, Inc (Homepage). [Online]. Available from: [Accessed 23 March 2007]. http://www.flowcardia.com/index.htm

[46]   Gavin GP, McGuinness GB, Dolan F, Hashmi MSJ. Performance characteristics of a therapeutic ultrasound wire waveguide apparatus, International Journal of Mechanical Sciences, 49, *pp* 298-305, 2007

[47]   Gavin G. Experimental and numerical in investigation of therapeutic ultrasound angioplasty, PhD Thesis, Dublin City University. Retrieved 10th February 2006, from Dublin City University Library

[48]   Branson Ultrasonics Corporation©, Instruction Manual: Sonifier 150: Ultrasonic Cell Disrupter and Homogiser, Branson Ultrasonics Corporation, 41 Eagle Road, Danbury, CT, USA, 1999

[49]   Fort Wayne Metals©, *Nitinol General Data Specification Sheet*, 9609 Indianapolis Road, Fort Wayne, IN, USA, 2005

[50]   National Instruments: Products (Homepage). Available from: [Accessed 17 January 2007] http://sine.ni.com/nips/cds/view/p/lang/en/nid/202300

[51]   De Santis S, Trochu F, Ostiguy G. Stress-strain hystersis and damping in MnCu and NiTi alloys, Metallurgical and Materials Transactions, 32A, pp 2489-2498

[52]   Nemat-Nasser S and Guo WG. Superelastic and cyclic response of NiTi SMA at various strain rates and temperatures, Mechanics of Materials, 38, pp463-474, 2006

[53]   Van Humbeeck J. Damping capacity of thermoelastic martensite in shape memory alloys, Journal of Alloys and Compounds, 355, pp 58–64, 2003

[54]   ANSYS© Multiphysics 8.1: Structural Guide, *Chapters 4: Harmonic Response Analysis*. 2004

Appendix A

$$u(x,t) = (A \cos w_n t + B \sin w_n t)(C \cos \frac{w_n x}{c} + D \sin \frac{w_n x}{c})$$

If driven at constant frequency

$$u(x,t) = (A \cos wt + B \sin wt)(C \cos \frac{wx}{c} + D \sin \frac{wx}{c})$$

Need to find A,B,C,D from initial conditions, for a fixed-free bar

$$u(0,t) \rightarrow u = b \sin wt = (A \cos wt + B \sin wt).C$$

True if

$\rightarrow A \cos wt = 0$

$\rightarrow b \sin wt = CB \sin wt$

$\rightarrow b = CB$

@ x=l, EA du/dx =0

$$\overset{\bullet}{u}(l,t) = 0 = -\frac{CBw}{t} \sin wt \sin \frac{wx}{c} + \frac{DBw}{c} \sin wt \cos \frac{wx}{c}$$

$$@ x = l \rightarrow D = C \tan \frac{wl}{c}$$

Put back into overall eqn. 1.1

$$u(x,t) = b(\cos \frac{wx}{c} + \tan \frac{wl}{c} \sin \frac{wx}{c}) \sin wt$$

Resonant frequencies occur when $\tan \dfrac{w_n l}{c} = \infty$

At $\dfrac{w_n l}{c} = \dfrac{\pi}{2}$

Resonant Frequencies occur at Fn = nc/4l, n=1, 3,5,7,9...
Non-Resonant Frequencies occur at Fn = nc/4l, n=2, 4, 6, 8...

$$fn = \frac{nc}{4l} \quad \text{or} \quad l = \frac{nc}{4fn}$$

Appendix B

6

30

10

220

75

4.5

5.5

4

2

2

75

15

15

50

Ø4
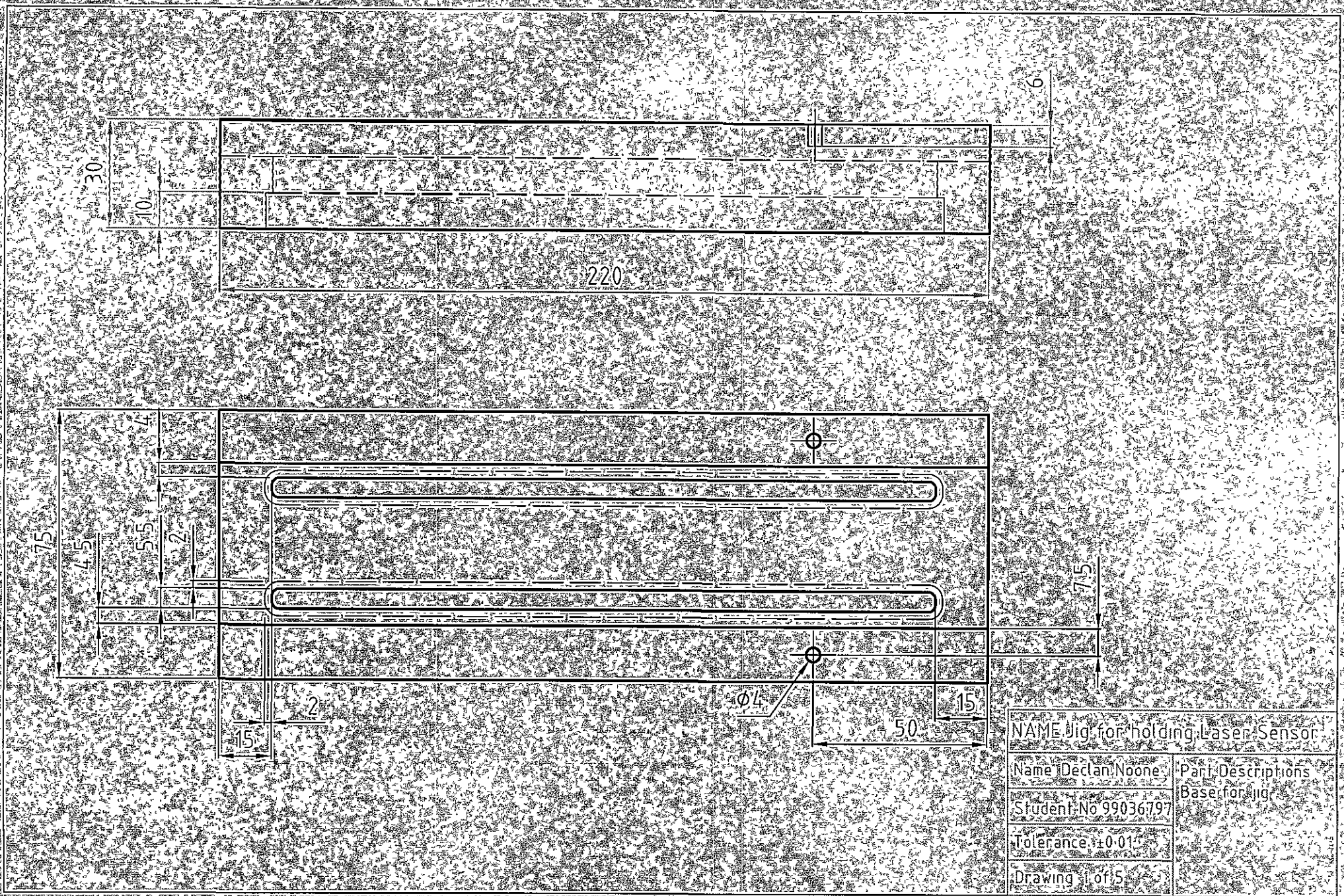
NAME Jig for holding Laser Sensor

Name Declan Noone	Part Descriptions
Student No 99036797	Base for jig
Tolerance ±0·01	
Drawing 1 of 5	
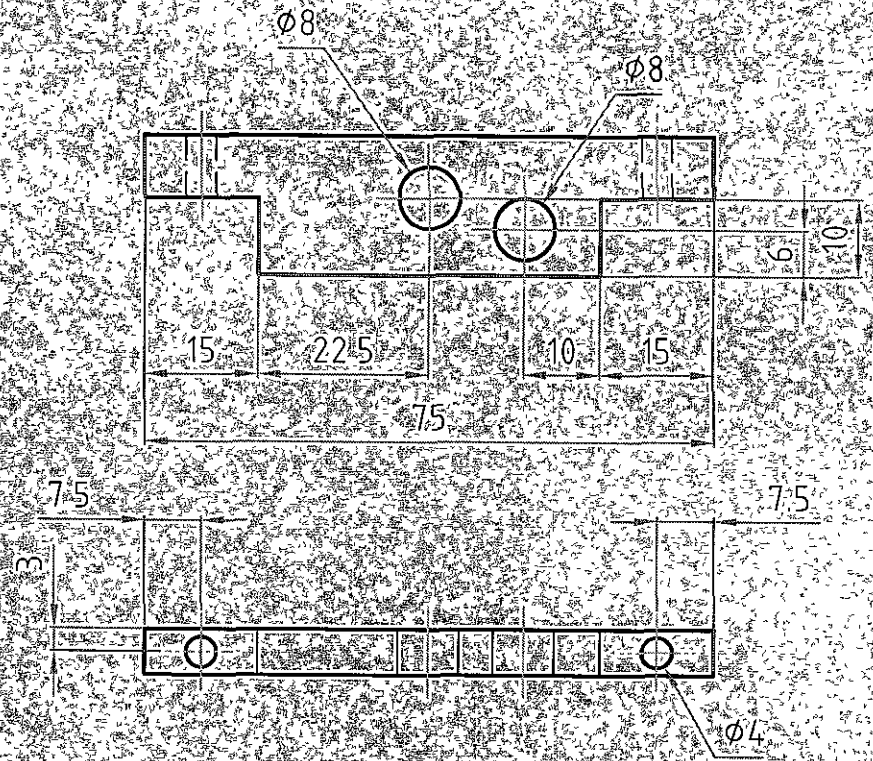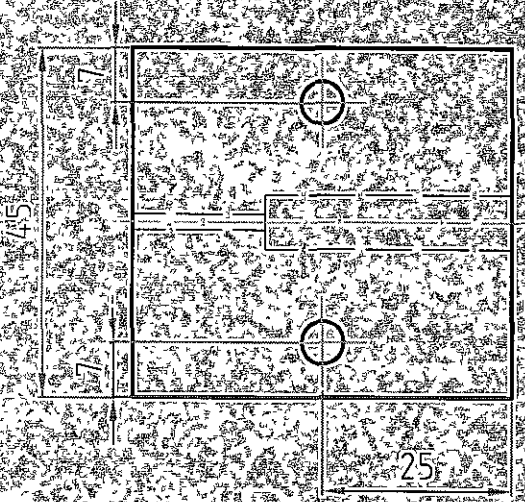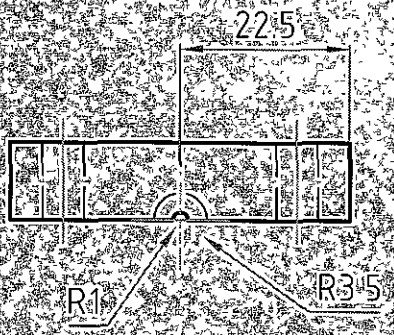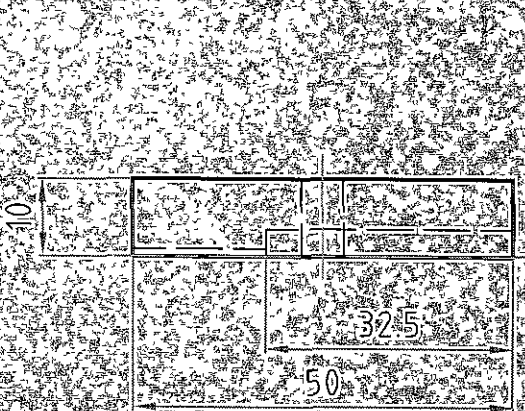
22·5

R1   R3·5

10

32·5

50

Ø8   Ø8

15   22·5   10   15

75

6   10

7

7·5   7·5

3

7·5

7·5

15·5

7

Ø4

25

R0.8

10

100

22.5

⌀5.5

20

45

7

Channel to control wire waveguide movement

Holds tip of laser sensor
on same axis as wire waveguide

Holes for M8 screws
to hold pieces in position

Holds micrometer for controlling
distance between laser sensor tip
and wire waveguide
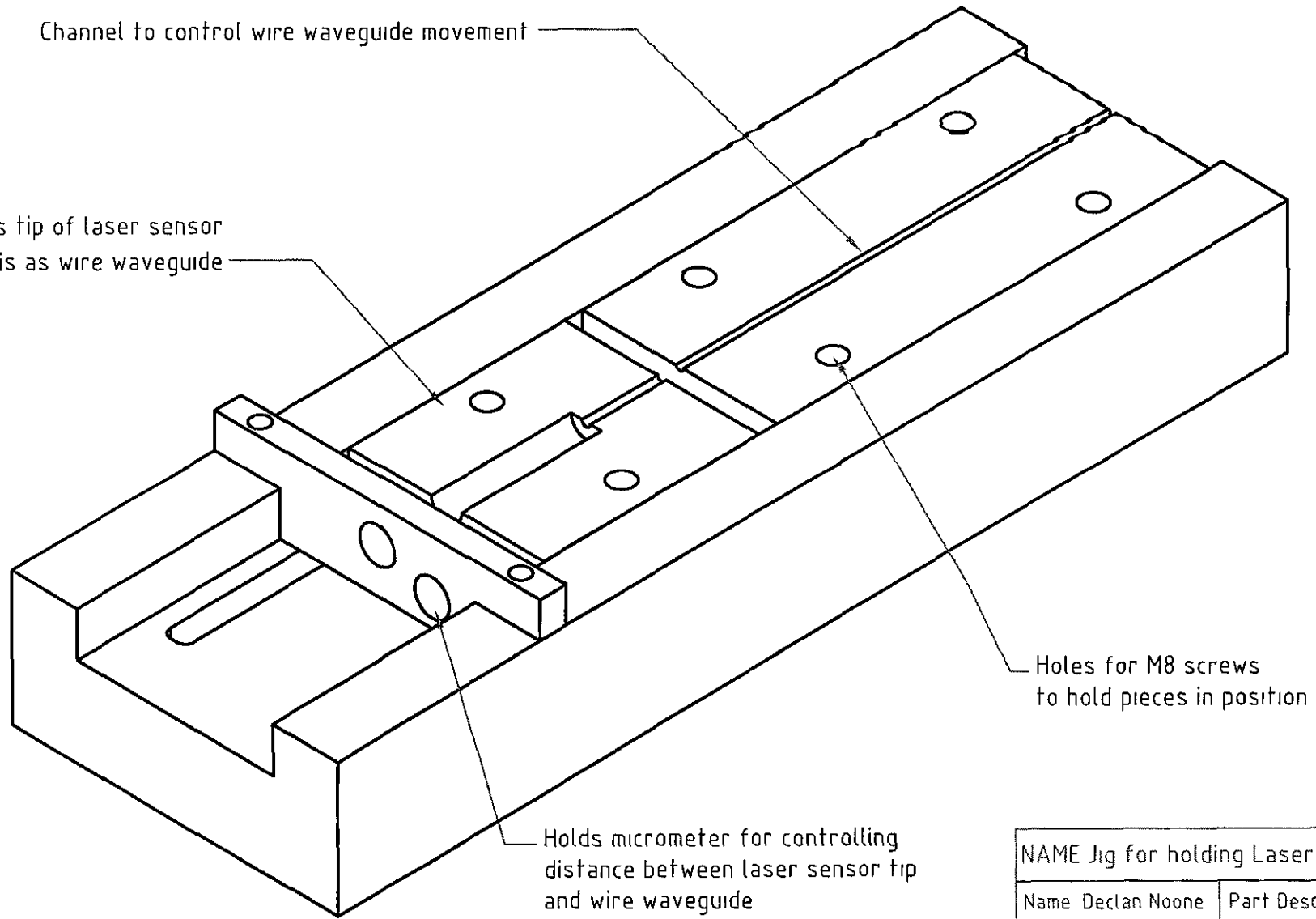
NAME Jig for holding Laser Sensor	
Name Declan Noone	Part Descriptions Isometric view of jig for holding laser sensor, micrometer and wire waveguide without top pieces
Student No·99036797	
Tolerance ±0 01	
Drawing 5 of 5	

Appendix C
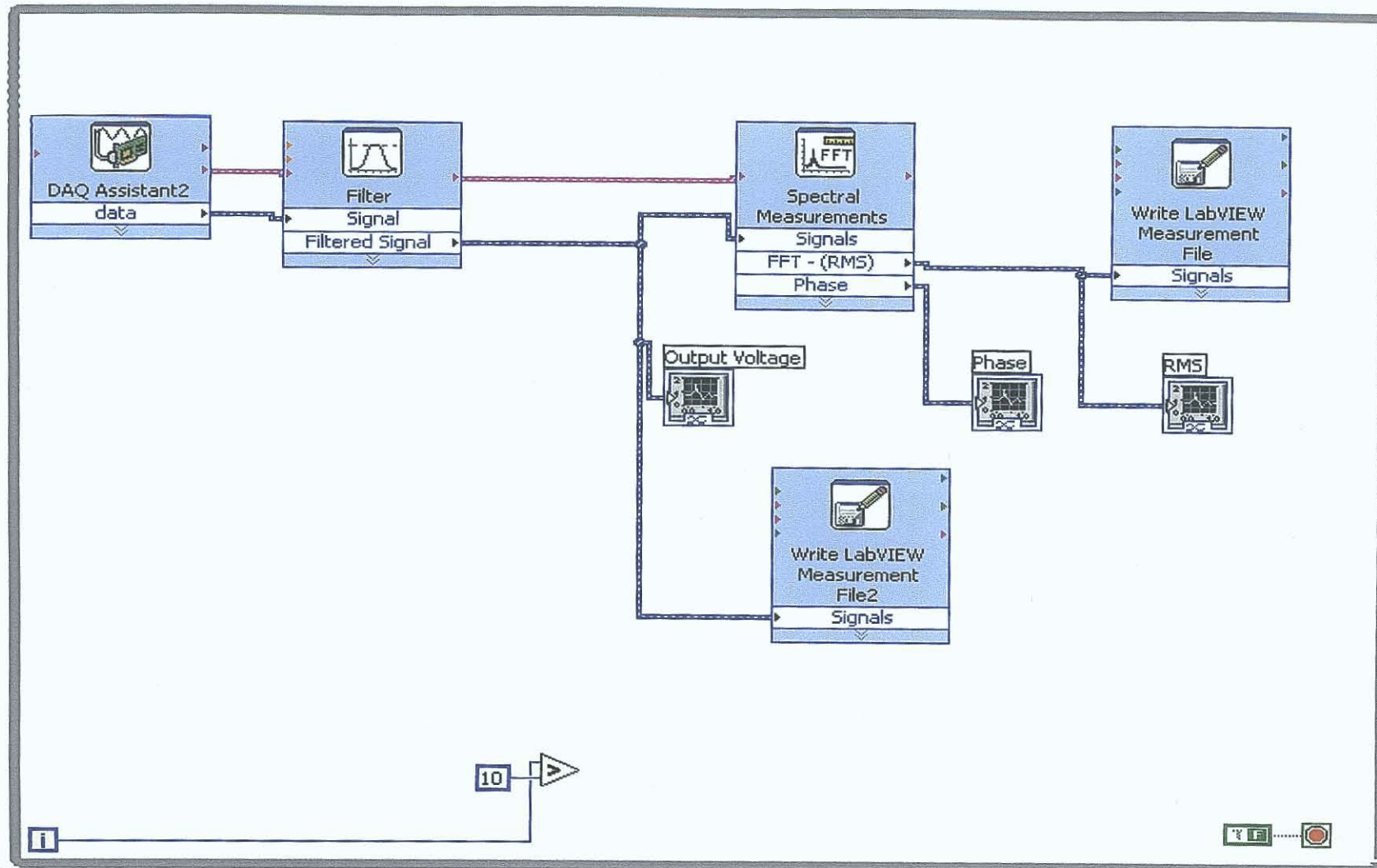
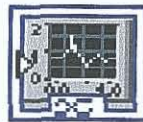Connection wiring between elements of the program for main signal

Connection wiring between elements of the program for errors in the individual components
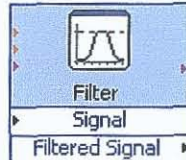
LabVIEW connection to data acquisition card for laser sensor input
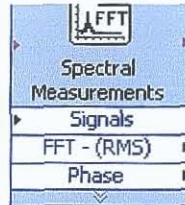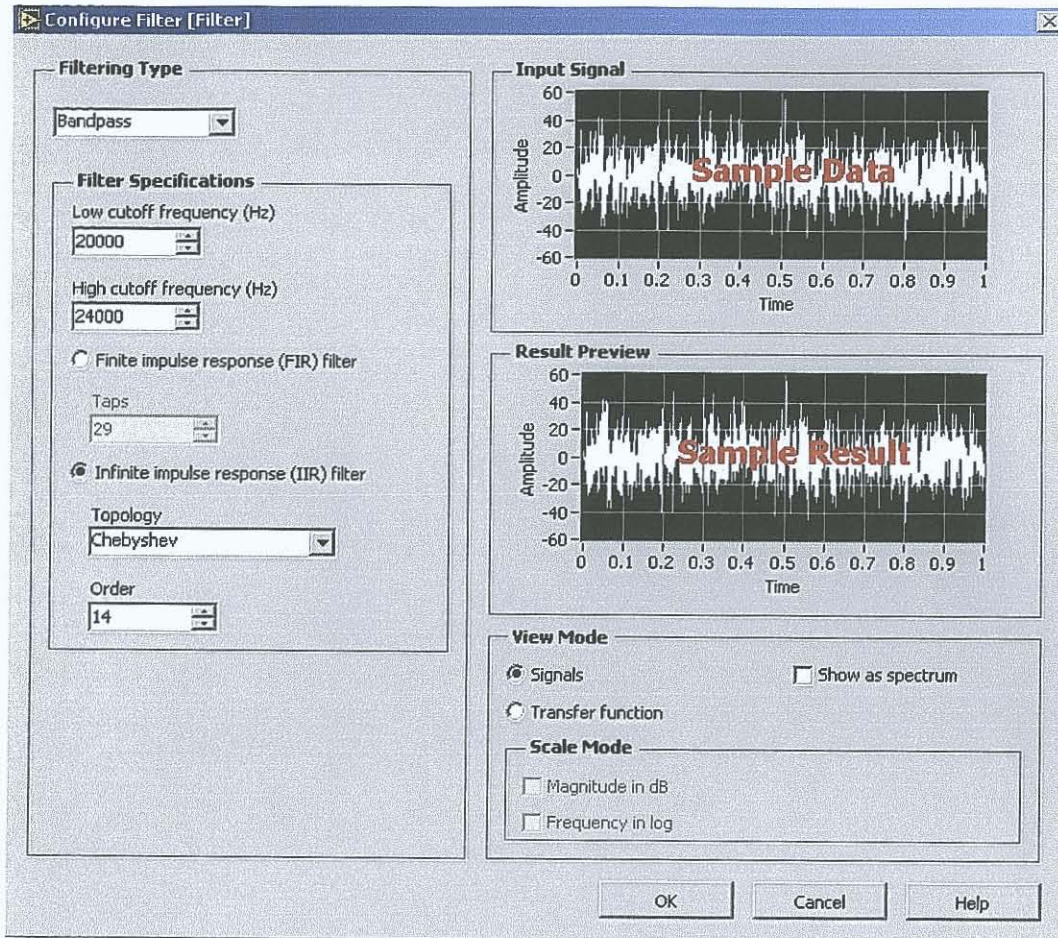

Sends input data to .txt file for storage and analysis

Displays time signal in real time

Filter for raw laser sensor data. Options chosen were an infinite impulse response
(IIR) Chebyshev bandpass filter between 20000Hz and 24000Hz. The order of the
filter was 14

Write LabVIEW
Measurement
File
Signals

Converts filtered signal for time domain to frequency domain. Options chosen was a spectral measurement of the magnitude of the signal using root mean square (RMS). A Hanning window was applied again with RMS with an exponential weighting after 100 averages.
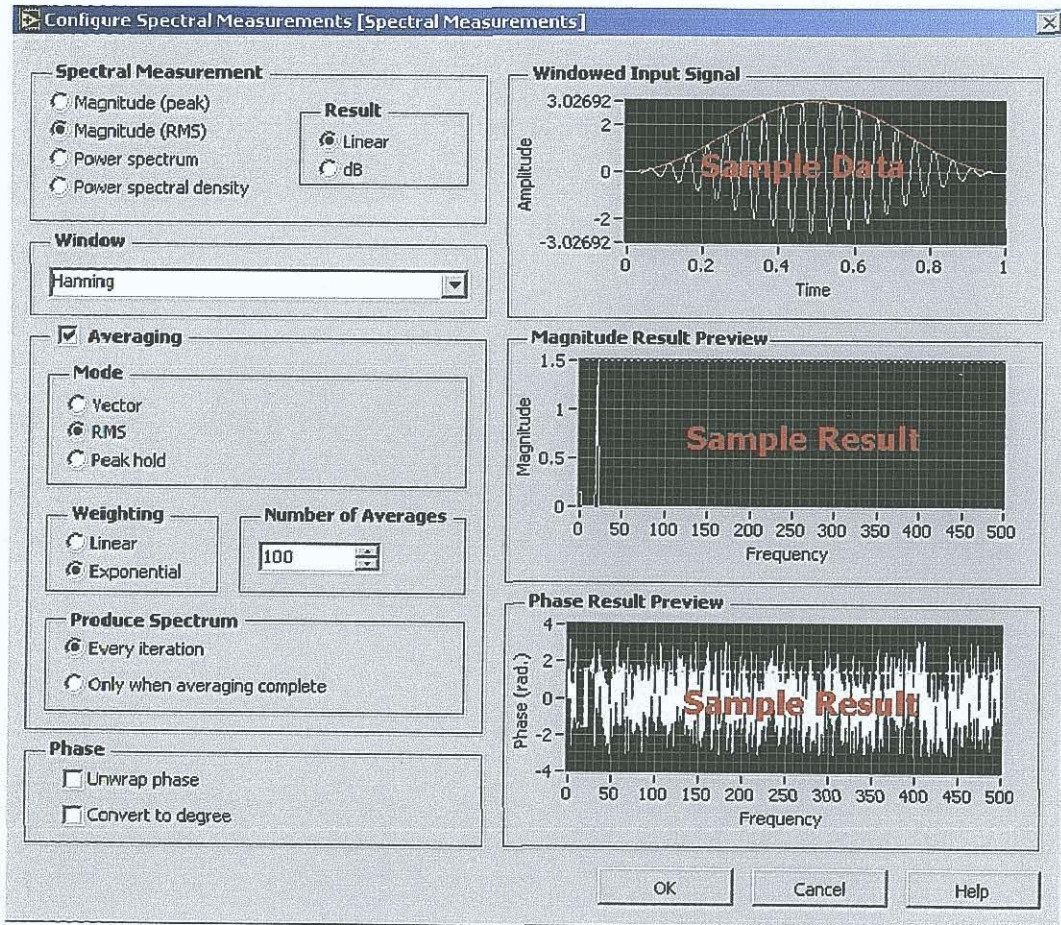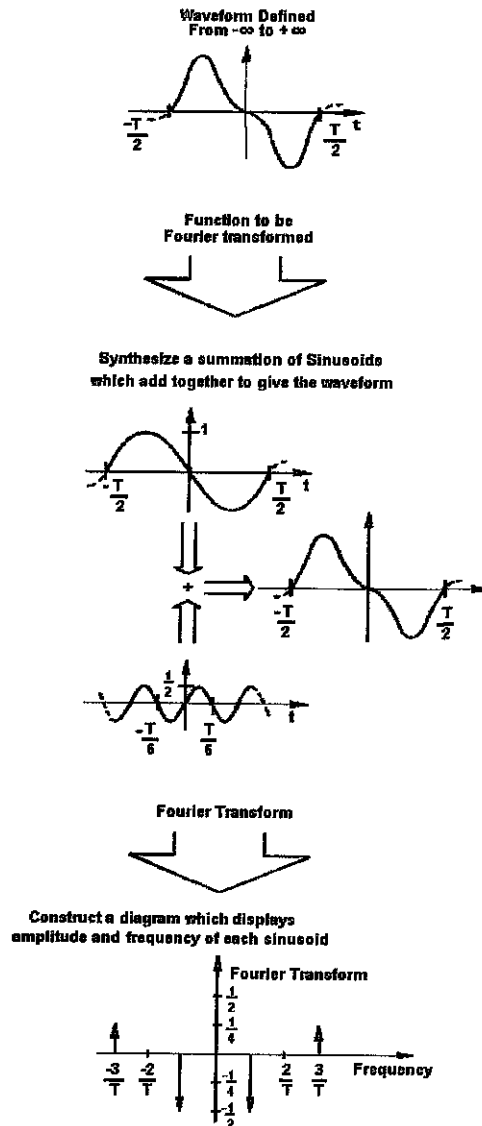
Fast Fourier Transform

The figure below shows a waveform that is separated into two sinusoidal waves with different magnitudes and frequencies that when added together will form the original waveform. This is mathematically represented:

$$S(f) = \int_{-\infty}^{\infty} s(t) e^{-j2\pi f t} dt \qquad\qquad [3.2]$$

Where $s(t)$ is the waveform to be decomposed into a sum of sinusoids and $S(f)$ is the Fourier Transform of $s(t)$. The fast Fourier Transform (FFT) is a member of the Fourier Transform family that uses diagonal matrices to change the signal from the time domain to the frequency domain with the most efficiency.


Interpretation of Fourier Transform [Bingham]

Window Functions

The FFT analysis is based on a finite set of data, the FFT assumes that the finite data set is one period of a periodic signal. When the signal is periodic and an integer number of periods fill the acquisition time interval, the FFT works the most efficiently. However if the number of periods in the signal is not an integer, the endpoints are discontinuous. This is known as spectral leakage. Windowing is a technique used to shape the time portion of the measurement data in order to minimize these discontinuities in the signal to reduce the effects of spectral leakage in the FFT spectrum.

The window function consists of a main lobe and side lobes shown below. Applying a window function reduces the side lobe responses, at the expense of the width of the main lobe. In order to minimize the effects of this the window function is applied that makes the endpoints of the waveform meet smoothly which results in a continuous waveform without sharp transitions.
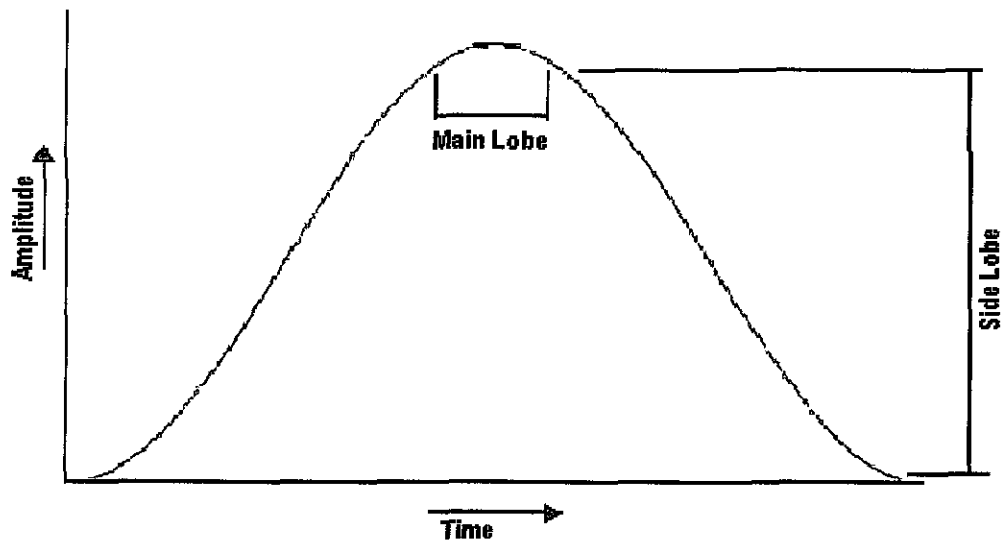
Schematic of the positions of main and side lobes in a window function.

Reference
▫ Brigham EO. Chapter 1: Introduction, In: The Fast Fourier Transform and its Applications. Prentice Hall Publishers, 1988